UNIVERSITY OF ROME

"TOR VERGATA"

The Energy Budget of Cosmic Baryons

by

Andrea Lapi

A Thesis submitted in partial fulfillment of the requirements for the degree of Philosophiae Doctor in Astrophysics.

Ph.D. Thesis supervisor:

Prof. A. Cavaliere

Chair of Ph.D. course:

Prof. R. Buonanno

UNIVERSITY OF ROME

"TOR VERGATA"

This is to certify that I have examined this copy of a Ph.D. Thesis by

Andrea Lapi

and I have found that it is complete and satisfactory in all respects,
and that any and all the revisions required by the final
examining committee have been made.

Chair of Ph.D. Course:

_____

Prof. R. Buonanno

Reading Committee:

_____

Prof. P. de Bernardis

_____

Prof. L. Danese

_____

Prof. A. Righini

Date: _____

In presenting this Thesis in partial fulfillment of the requirements for the Ph.D. degree at the University of Rome "Tor Vergata", I agree that the Library shall make its copy freely available for inspection. I further agree that extensive copying of this Thesis is allowable only for scholarly purposes. Requests for copying or reproduction of this Thesis may be refereed to the author himself, which owns the rights to reproduce and sell microfilmed, electronic and paper copies of this manuscript.

*Signature*_____

*Date*_____

To My Family.

Abstract

I describe everything exactly
As it took place,
Constraining my mind not to wander
From the task.

- Charles Dickens: *A Tale of Two Cities* –

Clusters, groups, and many single galaxies shine in X-rays because they contain large masses of hot, diffuse baryons that radiate strong luminosities by thermal bremsstrahlung and line emission. Such baryons may be also probed in the μwave and submm bands through the Sunyaev-Zel'dovich effect, which provides a direct measure of their large thermal energy content.

Simple conditions are found to prevail in rich clusters. They emit copious X-ray powers $L_X \sim 10^{45}$ erg s^{-1} integrated over Mpc sizes. The temperatures $kT \gtrsim 4$ keV are close to the virial values in the gravitational potential wells provided by dark masses of order $10^{15}\,M_\odot$. The gas densities around 1 particle per liter are consistent with baryonic fractions close to 1/5, the universal value.

But groups and galaxies are found to be *underluminous* in X-rays when compared to clusters; they emit far less than expected from the simple scaling law $L_X \propto T^2$, that would hold if the baryon to dark matter ratio stayed put at the universal value. In other words, the diffuse medium in groups is considerably *underdense* for its observed temperatures. How this may come about constitutes a complex and hotly debated issue.

Our proposal centers on the substantial energies fed back to the baryons, when part of them condense into massive stars then exploding as supernovae, or accrete onto supermassive black holes energizing the activity of quasars. Such energy inputs deplete the baryon density in the shallower potential wells by causing thermal *outflow* and dynamical *blowout* from inside the structures; they also *preheat* the gas exterior to the newly forming systems, hindering its flow into the latter.

Since the complexity of these processes drives state-of-the-art numerical simu-

lations beyond the limits of present supercomputing, in this Thesis we mainly use (semi-)analytic modeling. Our main aim is to investigate if and how the energy feedback from supernovae and quasars can dominantly affect the amount, distribution, and overall energetics of the baryons.

We conclude that the recent X-ray data require active galactic nuclei to substantially preheat the gas before it falls into clusters, and also the quasars to blow some gas out of groups and galaxies. We compute the resulting correlation between X-ray luminosity and temperature, and find it as *steep* as $L_X \propto T^3$ in clusters and even more in groups, if the quasar outputs are coupled to the ambient baryons at fractional levels around 5% (as also independently gauged from recent X-ray observations by Chandra and XMM); shape and (wide) scatter remarkably agree with the data.

Relatedly, we compute the Sunyaev-Zel'dovich *depressions* caused by the same mass ejection. On the other hand, we show the feedback from powerful quasars to yield transient Sunyaev-Zel'dovich *enhancements* in early galaxies and groups. We calculate such signals to have amplitudes of several tens μK if observed at $1'$ resolution, and more at $10''$ resolutions; we discuss their detectability with present and future instrumentation.

Finally, we link the behavior of the X-ray and the μwave/submm observables to the parallel effects of the quasar feedback on the equilibrium of the gas in the host galaxy; we find that these effects also yield the *steep* correlation $M_\bullet \propto \sigma_\star^4$ observed in the optical band between the central black hole masses and the galaxian velocity dispersions.

Curriculum Vitae

What gods notice, they destroy.
Be humble and you will escape
The jealousy of the great.

- Philip K. Dick: *The Man in the High Castle* –

Personal Data

Title:	Dr.
First Name:	Andrea
Last Name:	Lapi
Date of birth:	August, 3rd 1976
Place of birth:	Florence, Italy
Gender:	Male
Citizenship:	Italian

Present position:	Research Contract
Institution:	Astrophysics, Dept. of Physics, Univ. of Rome "Tor Vergata"
Address:	Via della Ricerca Scientifica, 1 - 00133 Rome, Italy
Phone:	+39 06 7259 4566
Fax:	+39 06 202 3507
E-mail:	lapi@roma2.infn.it
Website:	`http://www.  ...//`

Area of Research:	Theoretical modeling for extragalactic astrophysics and cosmology.

Curriculum Studiorum

1990 - 1995:	High School studies @ Liceo Scientifico Statale "A. Landi", Velletri (RM), Italy.
Diploma:	Maturitá Scientifica, 60/60.
Date:	July, 17^{th} 1995.
Other Certificates:	• Preliminary English Test (PET), March 1993. • First Certificate in English (FCE), June 1994.
1995 - 2000:	Undergraduate studies in Physics @ Univ. "Tor Vergata", Rome (RM), Italy.
Degree:	Laurea in Physics, Magna Cum Laude.
Date:	July, 17^{th} 2000.
Advisor:	Prof. Alfonso Cavaliere.
Co-Advisor:	Dr. Nicola Menci.
Thesis:	Un Modello per l' evoluzione cosmologica della SFR. (Modeling the Cosmological Evolution of the Star Formation Rate).
Other Skills Acquired:	• Knowledge of operating systems: VMS, Windows$^{\text{TM}}$, Lindows$^{\text{TM}}$. • Experience of programming in Fortran77.
2000 - 2004:	Ph.D. training @ Univ. "Tor Vergata", Rome (RM), Italy.
Degree:	Doctor of Philosophy.
Date:	April, 15^{th} 2004.
Supervisor:	Prof. Alfonso Cavaliere.
Thesis:	The Energy Budget of Cosmic Baryons.
Graduate Schools:	• Italian National School of Astrophysics, "Turbulence in Space Plasmas-Galaxies and Galaxy Systems", June 3^{rd}-7^{th} 2002, Cetraro (CS), Italy. • Italian National School of Astrophysics, "Cosmology - Relativistic Astrophysics", September 8^{th} -14^{th} 2002, Asiago (PD), Italy. • SIGRAV International School on Contemporary Relativity and Gravitational Physics (V Edition), "Joint Evolution of Black Holes and Galaxies", May 5^{th} -10^{th} 2003, Como (CO), Italy.

Publications

- Cavaliere, A., **Lapi**, **A.**, and Menci, N. 2002, "Probing Scale-Variance from Clusters to Groups of Galaxies", in ASP Conf. Ser. 253, Chemical Enrichment of Intracluster and Intergalactic Medium, eds. F. Matteucci and R. Fusco-Femiano (San Francisco: ASP), 407.
- Cavaliere, A., **Lapi**, **A.**, and Menci, N. 2002, "The Thermal State of the ICM Probed with the SZ Effect", in ASP Conf. Ser. 268, Tracing Cosmic Evolution with Galaxy Clusters, eds. S. Borgani, M. Mezzetti, and R. Valdarnini (San Francisco: ASP), 240.
- Menci, N., Cavaliere, A., and **Lapi**, **A.** 2002, "Dark Matter and Baryons in Groups and Cluster of galaxies", in Dark Matter in Astro- and Particle Physics, DARK 2002, eds. H.V. Klapdor-Kleingrothaus, and R.D. Viollier (Berlin: Springer), 53.
- Cavaliere, A., **Lapi**, **A.**, and Menci, N. 2002, "Quasar Feedback on the Intracluster Medium", ApJ, 581, L1.
- Cavaliere, A., Bardelli, S., Boschin, W., **Lapi**, **A.**, and Tormen, G. 2003, "CoFin2001. Clusters and Groups of Galaxies: the Interplay between Dark and Baryonic Matter", Mem. SAIt, 74, 335.
- **Lapi, A.**, Cavaliere, A., and De Zotti, G., 2003, "Sunyaev-Zel'dovich Effects from Quasars in Galaxies and Groups", ApJ, 597, L93.
- **Lapi**, **A.**, Cavaliere, A., De Zotti, G., and Menci, N. 2004, "Probing the AGN Feedback on the ICM with the Sunyaev-Zel'dovich Effect", Carnegie Observatories Astrophysics Series, Vol. 3: Clusters of Galaxies: Probes of Cosmological Structure and Galaxy Evolution, ed. J. S. Mulchaey, A. Dressler, and A. Oemler (2004, Pasadena: Carnegie Observatories), `http://www.ociw.edu/ociw/symposia/series/symposium3/proceedings.htm/`.
- De Zotti, G., Burigana, C., Cavaliere, A., Danese, L., Granato, G.L., **Lapi, A.**, Platania, P., and Silva, L., 2004, "The Sunyaev-Zel'dovich Effect as a Probe of the Galaxy Formation Process", in AIP Conf. Proc. 703, *Plasmas in the Laboratory and in the Universe: New Insights and New Challenges*, eds. G. Bertin, D. Farina and R. Pozzoli (New York: AIP), 375.
- **Lapi, A.**, Cavaliere, A., and De Zotti, G., 2004, "The IntraCluster Plasma: Probing its Amount and Thermal State in X-rays and in μwaves", in AIP Conf. Proc. 703, *Plasmas in the Laboratory and in the Universe: New Insights and New Challenges*, eds. G. Bertin, D. Farina and R. Pozzoli (New York: AIP), 355.
- **Lapi, A.**, and Cavaliere, A., 2004, "Intracluster Entropy from Quasar Activity", in IAU Conf. Proc. 195, *Outskirts of Galaxy Clusters: Intense Life in the Suburbs*, ed. A. Diaferio (Cambridge: Cambridge Univ. Press), 299.
- **Lapi, A.**, Cavaliere, A., and Menci, N., 2005, "Intracluster and Intragroup

Entropy from Quasar Activity", ApJ, in press.

Workshops and Conferences

- Meeting CRoNA01, November, 7^{th} 2001, Roma (RM), Italy.
- II CMBNet General Meeting, December, 13^{th}-14^{th} 2001, Monteporzio Catone (RM), Italy.
- CoFin01: Coordination Meeting, April, 9^{th} 2002, Padova (PD), Italy.
- XLVI SAIt National Workshop, April 10^{th} -12^{th} 2002, Padova (PD), Italy.
- Meeting CRoNA02, April, 22^{nd} 2002, Roma (RM), Italy.
- VII National Workshop on Cosmology, November 5^{th} - 8^{th} 2002, Monteporzio Catone (RM), Italy.
- "TEXAS in Tuscany" - XXI Symposium on Relativistic Astrophysics, December 9^{th} -13^{th} 2002, Firenze (FI), Italy.
- Carnegie Observatories Centennial Symposium - "Clusters of Galaxies: Probes of Cosmological Structures and Galaxy Evolution", January 27^{th} -31^{st} 2003, Pasadena (CA), USA.
- International Symposium "Plasmas in the Laboratory and in the Universe: New Insights and New Challenges", Semptember 16^{th} - 19^{th} 2003, Como (CO), Italy.
- International Workshop "Modelling the Intergalactic and Intracluster Media", October 1^{st} - 5^{th} 2003, Vulcano (ME), Italy.
- "Baryons in Cosmic Structures: A Meeting in Honour of A. Cavaliere", October, 20^{th} - 21^{st} 2003, Monteporzio Catone (RM), Italy.
- CoFin01: Final Meeting, December, 4^{th} - 5^{th} 2003, Bologna (BO), Italy.
- IAU Colloquium 195 "Outskirts of Galaxy Clusters: Intense Life in the Suburbs", March, 12^{th} - 16^{th} 2004, Torino (TO), Italy.
- XLVIII SAIt National Workshop, April 19^{th} -23^{rd} 2004, Milano (MI), Italy.

Talks and Posters

- **A. Lapi**, "La Connessione tra Gruppi/Ammassi di Galassie e Nuclei Galattici Attivi (The Connection between Groups/Clusters of Galaxies and Active Galactic Nuclei)", November, 6^{th} 2001, talk at the Meeting CRoNA01, Roma, Italy.
- A. Cavaliere, V. D' Elia, **A. Lapi**, F. Vagnetti, and V. Vittorini, "Strutture Cosmiche (Cosmic Structures)", poster presentation at the "Settimana della Scienza", Roma, Italy.

- **A. Lapi**, "La Storia dei Barioni Cosmici (The History of Cosmic Baryons)", March, $12^{\rm th}$ 2002, Ph.D. journal club, Roma, Italy.
- **A. Lapi**, "Feedback from SNae and AGNs onto the Intracluster Medium", Aprile, $9^{\rm th}$ 2002, talk at the Coordination Meeting CoFin01, Padova, Italy.
- **A. Lapi**, "Lo Stato Termico del Mezzo Intracluster (The Thermal State of the Intracluster Medium)", April, $12^{\rm th}$ 2002, talk at the XLVI SAIt National Workshop, Padova, Italy.
- **A. Lapi**, and V. Vittorini, "The Thermal History of the ICM: Feedback from SNae or AGNs?", April, $10^{\rm th}$-$12^{\rm th}$ 2002, poster presentation at the XLVI SAIt National Workshop, Padova, Italy.
- **A. Lapi**, "Feedback from AGNs: the Blastwave Approach", April, $22^{\rm nd}$ 2002, talk at the Meeting CRoNA02, Roma, Italy.
- **A. Lapi**, "Feedback da SN e AGN sul Mezzo Intracluster (Feedback from SN and AGN onto the Intracluster Medium)", June, $6^{\rm th}$ 2002, talk at the National School of Astrophysics, Cetraro (CS), Italy.
- **A. Lapi**, "Feedback da AGN in Galassie e Gruppi (AGN Feedback on Galaxies and Groups)", October, $4^{\rm th}$ 2002, invited seminar at the Padova Astronomic Observatory, Padova, Italy.
- **A. Lapi**, A. Cavaliere, and G. De Zotti, "Probing the AGN Feedback with the Sunyaev-Zel'dovich Effect", January, $28^{\rm th}$-$31^{\rm st}$ 2003, poster presentation at the Carnegie Observatories Centennial Symposium, Pasadena (CA), USA.
- **A. Lapi**, "Il Mezzo Intergalattico in Ammassi: Raffreddamento vs. Riscaldamento da SNae ed AGNs (The Intracluster Medium: Cooling vs. Heating from SNae and AGNs)", February, $25^{\rm th}$ 2003, invited seminar at the Univ. of Torino, Torino, Italy.
- **A. Lapi**, "Feedback da AGNs in Galassie, Gruppi ed Ammassi (Feedback from AGNs in Galaxies, Groups and Clusters)", March, $12^{\rm th}$ 2003, S.A.S. seminar at the Rome Astronomical Observatory, Monteporzio Catone (RM), Italy.
- **A. Lapi**, "Enhanced SZ Effects in Galaxies from AGN Feedback", May, $7^{\rm th}$ 2003, talk at the SIGRAV School 2003, Como (CO), Italy.
- **A. Lapi**, "The IntraCluster Plasma: Probing its Amount and Thermal State in X-rays and in μwaves", September, $19^{\rm th}$ 2003, talk at the International Symposium "Plasmas in the Laboratory and in the Universe: New Insights and New Challenges", Como (CO), Italy.
- **A. Lapi**, "Iniezioni di Energia da SNae e AGNs sui Barioni Diffusi (Energy Injections by SNae and AGNs on the Diffuse Baryons)", December, $4^{\rm th}$ 2003, talk at the Final Meeting CoFin01, Bologna (BO), Italy.
- **A. Lapi**, "Intracluster Entropy from Quasars", poster presentation at the IAU Colloquium 195, March, $12^{\rm th}$ - $16^{\rm th}$ 2004, Torino (TO), Italy.
- **A. Lapi**, "Sondare il Feedback dei Quasar Tramite l' Effetto Sunyaev-

Zel'dovich (Probing the Quasar Feedback with the Sunyaev-Zel'dovich Effect)", talk at the XLVIII SAIt National Workshop, Milano (MI), Italy.

N.B.: This Curriculum Vitae is updated to April 15^{th}, 2004.

Acknowledgements

O brave new world
That has such people in't!

- William Shakespeare: *Hamlet, Act I, Scene 5* –

I would like to thank my supervisor, Prof. Alfonso Cavaliere, for his suggestions, advices, and patience. This manuscript has greatly improved after his critical reading. I also enjoyed very much the stimulating discussions we had together about several topics in contemporary physics and cosmology.

I would like to thank Prof. Roberto Buonanno (INAF, Rome Astronomical Observatory), chairman of this Ph.D. course, for having stimulated my attendance to graduate courses, schools and seminars that have widely extended my background in astronomy and astrophysics.

I would also like to acknowledge Dr. Gianfranco De Zotti (INAF, Padua Astronomical Observatory) and Dr. Nicola Menci (INAF, Rome Astronomical Observatory); many of the results presented in this Thesis are due to fruitful collaborations with them both.

Finally, I extend out thanks to my friends and colleagues Francesco Shankar and Valerio Vittorini for enlightening discussions, and for having shared with me some results of their work before publication; Valerio is also acknowledged for having partially typos-corrected this manuscript.

This Thesis research was carried on at the Dept. of Physics, Univ. of Rome "Tor Vergata" from November, 1st 2000 to February, 14th 2004, and has benefitted from the M.I.U.R. grant COFIN2001028932 in the context of the project "Clusters and Groups of Galaxies: The Interplay between Dark and Baryonic Matter".

Contents

Introduction

Make up your mind to act decidedly
And take the consequences.
No good is ever done in this
World by hesitation.

- Thomas H. Huxley: *Evidences on Man's Place in Nature* –

This Thesis is aimed at investigating how the energy budget of cosmic baryons is originated, and in particular what is the role played by the energy inputs from astrophysical sources like supernovae and quasars.

This field of research has been boosted to a large and still growing chapter of astrophysics and cosmology since the early 1970s by the pioneering proposal [34] that powerful X-ray emissions were generally associated with clusters and groups of galaxies, due to thermal bremsstrahlung from gas virialized at keV energies contained by all such systems. Indeed, spectral data soon showed the characteristic continuum shape and the high-excitation emission lines (due to "metals") consistent with such a framework.

Such discoveries nailed down the notion that these galaxy aggregations do constitute real and stable condensations, and dispelled a lingering suspicion that they might be simple superpositions of galaxies or even exploding systems. Thus the high velocity dispersions around 10^3 km s^{-1} observed for both the member galaxies and the diffuse baryonic component indicated large amounts $10^{15}\,M_\odot$ of non-baryonic dark matter to be present.

On this basis the hierarchical clustering picture grew up, and envisaged the dark matter structures to evolve through continuous merging of smaller into larger units. The baryons are thought to have falled into the gravitational potential wells provided by the dark mass, both as cool gas condensing into substructures [207], and in the form of a hot phase pervading the wells to constitute the intracluster medium [35]. Soon it became clear that the latter, observed in X-rays and also in the μwave/submm band through the induced tilt in the spectrum of the cosmic back-

ground radiation (the Sunyaev-Zel'dovich effect, see [187]; [13]), could highlight and probe the dynamical processes driven by the dark matter out to Mpc scales. During the recent years, thanks to the Chandra and XMM-Newton satellites many groups and clusters are being observed out to redshifts $z \gtrsim 1$, when they are presumably young or still forming. So the study of clusters in X-rays is constituting a mine of information concerning both the astrophysics of the baryons and the dynamic evolution of cosmic structures out to substantial redshifts.

Further points became into focus meanwhile. In the 1990s it was convincingly argued [209] that the intracluster medium comprises a major fraction of a cluster's baryonic content, and that it reliably samples the universal baryon fraction. Thus the increasingly large number of galaxy clusters discovered in the nearby and distant Universe with and after the ROSAT mission has even allowed us to use them as cosmological probes, complementary to the observations of high-redshift type-Ia supernovae and of the cosmic μwave background radiation (for a review, see [170]).

All that has driven an explosion of activity both on the observational and on the theoretical front. The developing picture seeks to unite the evolution of galaxies and of their systems in terms of a competition between two processes (e.g., [130]). One is constituted by the gravitational drive of the dark matter, which tends to build up structures nearly invariant with the mass scale. The other half of the story is the active response of the baryons to the dark matter's fatal attraction, that strives away from scale-invariance (see, e.g., [46]).

In fact, the diffuse baryons in groups appear to be underluminous and hence underdense than in clusters, much more than expected on considering the different temperatures, sizes and formation epochs of such structures. On the observational side, the issue stands out in the X-ray luminosity vs. temperature correlation, which is much steeper than expected if the gas had been "gravitationally" heated up by shocks when it fell into the dark matter potential wells ([92]; [142]). The issue is reinforced by the fact that the entropy of the diffuse baryons is enhanced relative to what is expected from gravitational heating alone [144], implying that energy additions or losses occurred during the formation of groups and clusters.

An intriguingly simple interpretation is just in terms of extensive radiative cooling ([30]; [203]); if this acts over a Hubble time on supergalactic scales, it would selectively remove low-entropy gas from the dense centers of clusters and especially of groups. However, while within galaxies cooling has certainly a leading role in triggering the observed star formation, in such an extended form it would cause too many, unseen stars to form, and in any case it still falls short of producing the required entropy levels (see, e.g., [134]; [194]; [205]).

Alternatively, energy inputs additional to that of gravitational origin may be responsible for the lack of self-similarity between groups and clusters. By the way, extra-heating of stellar origin is necessary in all hierarchical models to avoid an early catastrophic cooling of the gas [14]; in fact, the supernova explosions following the galaxian star formation drive superwinds that can eject part of the cool gas from

the disks, so regulating the stellar mass fraction itself. In addition, such feedback actions providing initial energies of some 10^{-1} keV per particle can affect the diffuse baryons, particularly in the shallower wells of poor clusters and groups; there the ratio of baryonic to dark mass is limited to values smaller than the cosmic one and the X-ray luminosity (entropy) is correspondingly suppressed (enhanced), see [39], [24]. However, in the recent years several authors have argued that supernovae alone cannot provide the energy budget required to closely reproduce the X-ray data (see, e.g., [103]; [154]); this claim comes also from studies of the metal content as a diagnostic for the number of supernovae exploded and/or for the coupling of their energy feedback to the baryons within galaxies and groups.

Additional energy inputs and extra heating may be provided by the quasars that turn on in forming galaxies, and are rekindled in galaxies as members of condensing groups ([201]; [210]; [45]). The related energy outputs are very large, but the fraction actually coupled to the surrounding diffuse baryons is more uncertain than for supernovae, ranging between 10^{-2} and 10^{-1} with large variance. Thus it is still unclear whether this process can provide effective non gravitational heating to explain the X-ray observations.

To address these open problems is the main aim and goal we will pursue throughout this Thesis; we will mainly resort to (semi-)analytic modeling, because the complexities of the processes involved drive even state-of-the-art numerical simulations to, or beyond the limits of present supercomputing [20].

The structure of the Thesis is as follows. Chapter 1 is designed to introduce the reader to the standard cosmological and cosmogonical scenarios. In particular, § 1.1 briefly describes the kinematics and dynamics of the Universe; § 1.2 offers an overview of the hierarchical clustering picture for structure formation.

Chapter 2 discusses the complex interplay between dark and baryonic matter in cosmic structures. Specifically, § 2.1 deals with the dark component, and highlights its closely scale-invariant evolution; § 2.2 is instead centered on the baryons, emphasizing how their much more complex behavior may be traced back to energy injections by astrophysical sources.

Chapter 3 is devoted to stellar feedback. In § 3.1 a model for the preheating by supernovae is elaborated, and the impact on the X-ray observables at the scales of galaxy groups and clusters is investigated. But § 3.2 points out the intrinsic drawbacks of this approach, and critically discusses possible alternatives.

Chapter 4 is focused on the energy feedback from quasars. In particular, § 4.1 covers some basic aspects of quasar astrophysics that are of interest for our discussion; then the preheating (§ 4.2) and the internal feedback (§ 4.3) from quasars are modeled, and their results are compared with the most recent data in various observational bands at the scales of galaxies, groups and clusters.

Finally, our original results and clear-cut predictions are summarized and discussed in the Conclusions.

Chapter 1

Cosmology and Cosmogony

To see a World in a Grain of Sand
And a Heaven in a Wild Flower,
Hold Infinity in the palm of your hand
And Eternity in a hour.

- William Blake: *Auguries of Innocence* –

This introductory Chapter deals with the standard cosmological and cosmogonical scenarios. We adopt the usual terminology, according to which the *cosmology* describes the geometrical and dynamical properties of our Universe, while the *cosmogony* refers to the formation and evolution of cosmic structures within such a background. Here our aim is not to be exhaustive, rather to recall some well-known concepts and tools that will be extensively used in the next Chapters.

1.1 The cosmological model

The standard cosmological model relies on two basic assumptions: The *cosmological principle*, i.e., the isotropy and homogeneity of the matter distribution at sufficiently large scales (see Fig. 1.1; [55]); and the validity of Einstein's general relativity to describe the gravitational interactions and hence the global structure of the Universe [206].

1.1.1 *The Robertson-Walker metric*

The tenet of homogeneity and isotropy is expressed by requiring the metric of the Universe to have the *Robertson-Walker* form

$$\mathrm{d}s^2 = dt^2 - a^2(t)\left\{\frac{dr^2}{1-k\,r^2} + r^2\left[d\vartheta^2 + \sin^2\vartheta\, d\varphi^2\right]\right\} \tag{1.1}$$

in a suitable set of dimensionless coordinates (r, ϑ, φ), named the comoving frame; here $a = a(t)$ is the time-dependent *expansion factor*, and $k = 0, \pm 1$.

Defining the new spatial coordinate $\chi = (r, \sin^{-1} r, \sinh^{-1} r)$ for $k = (0, +1, -1)$ and the conformal time $\tau = \int^t dx/a(x)$ turns the line element (1.1) into the form

$$\mathrm{ds}^2 = a^2(t) \left\{ d\tau^2 - d\chi^2 - S_k^2(\chi) \left[d\vartheta^2 + \sin^2 \vartheta \, d\varphi^2 \right] \right\} \ , \tag{1.2}$$

in terms of the function $S_k(\chi) = (\chi, \sin\chi, \sinh\chi)$ for $k = (0, +1, -1)$. From the above expression it is immediately seen that k determines the geometry of space, the latter being Euclidean, elliptic or hyperbolic if $k = 0, +1, -1$, respectively.

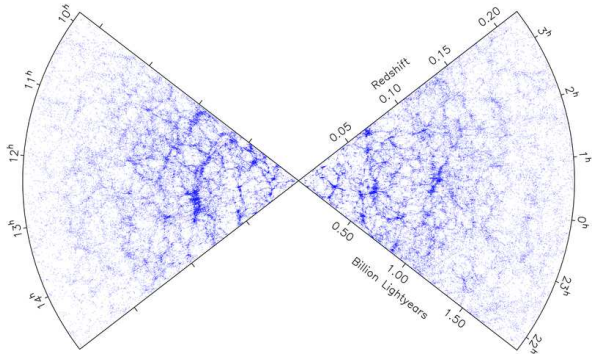

Fig. 1.1 The redshift-cone plot from the 2dFGRS shows that our Universe is rather homogeneous on scales larger than 100 Mpc. Figure taken from [55].

Since cosmological observations very often rely on radiation emitted by distant astrophysical sources, let us consider some kinematical properties of photons that depend on the metric (1.1) but not on the explicit form of $a(t)$. While travelling to us through an expanding background photons suffer a stretching of their wavelengths $\lambda \propto a(t)$, which results in the shift of emission/absorption lines to a redder section of the spectrum. This effect is quantified by the *redshift* z, defined through the relation $(1 + z) \equiv a_0/a(t)$ with a_0 the current value of the expansion factor. In any range of epochs during which $a(t)$ is monotonic, the redshift z is a good time coordinate since $dt = -dz/(1 + z)\, H(z)$, with the *Hubble parameter* $H = \dot{a}/a$ measuring the expansion rate of the Universe.

The redshift is related to other distances commonly used in cosmology. The *proper distance* that photons emitted at redshift z should cover to reach the observer at $z = 0$ is simply obtained on setting $\mathrm{ds}^2 = 0$ in Eq. (1.2), and reads

$$d_p(z) \equiv S_k(\alpha) \ , \quad \alpha = \int_0^z dx \, \frac{1}{a_0 \, H(x)} \ . \tag{1.3}$$

The *luminosity distance* is defined in terms of the radiative flux $\mathcal{F}$ received from a

source of intrinsic luminosity L through

$$d_L(z) \equiv \sqrt{\frac{\mathcal{F}}{4\,\pi\,L}} = a_0\,d_p(z)\,(1+z)\ . \tag{1.4}$$

The *angular diameter distance* $d_A \equiv \delta\,D$ concerns the physical size D of an object subtending a small angle δ to the observer. These three distance modules are related by

$$d_A(z) = a_0\,d_p(z)/(1+z) = d_L(z)/(1+z)^2\ . \tag{1.5}$$

1.1.2 *The Friedman equations*

The essence of Einstein's general relativity is that the geometric structure of space-time is determined by the matter-energy distribution, and viceversa. The cosmological principle ensures the latter to be isotropic and homogeneous (at least for a comoving observer), so that the global dynamics of the Universe is governed by the *Friedman equations*:

$$\frac{d(\rho_i\,a^3)}{da} = -3\,a^2\,p_i\quad,\quad\forall i \tag{1.6}$$

$$\left(\frac{\dot{a}}{a}\right)^2 = \frac{8\,\pi\,G}{3}\sum_i\,\rho_i - \frac{k}{a^2} \tag{1.7}$$

where ρ_i and p_i are the energy density and pressure of the i-eth species. The first set of equations yields the evolution of the energy densities

$$\rho_i = \rho_i(a_0)\,\left(\frac{a_0}{a}\right)^3\,\exp\left[-3\int_{a_0}^{a}\frac{dx}{x}\,w_i(x)\right]\ , \tag{1.8}$$

after the *equations of state* $w_i = p_i/\rho_i$ have been specified. From now on we will restrict to the simple case of constant w_i, so that $\rho_i(a) \propto a^{-3\,(1+w_i)} \propto (1+z)^{3\,(1+w_i)}$ obtains; e.g., for radiation $w = 1/3$ and $\rho \propto a^{-4} \propto (1+z)^4$ holds.

Once the functions ρ_i, $\forall i$ are known, the expansion factor $a(t)$ is determined by the remaining Friedman equation. This may be recast as

$$\left(\frac{\dot{a}}{a}\right)^2 = H_0^2\,\sum_i\,\Omega_i\,\left(\frac{a_0}{a}\right)^{3\,(1+w_i)} - \frac{k}{a^2}\ ; \tag{1.9}$$

here $H_0 = 100\,h$ Km s^{-1} Mpc^{-1} is the Hubble constant today, and we have introduced the quantities $\Omega_i \equiv \rho_i(a_0)/\rho_c = 8\,\pi\,G\,\rho_i(a_0)/3\,H_0^2$ in terms of the *critical density* for flatness $\rho_c \equiv 3\,H_0^2/8\,\pi\,G \approx 2.8\times10^{11}\,h^2\,M_\odot$ Mpc^{-3}. The couple of values H_0, $\Omega \equiv \sum_i\,\Omega_i$ constitutes a valid initial condition to integrate the Friedman equations. In fact, evaluating Eq. (1.9) at the present epoch yields $k/a_0^2 = H_0^2\,(\Omega-1)$ and so enables us to fix the values of a_0 and $\dot{a}_0 = H_0\,a_0$ for $\Omega \neq 1$; if $\Omega = 1$, it is conventional to take $a_0 = 1$ and $\dot{a}_0 = H_0$ since these may be rescaled arbitrarily.

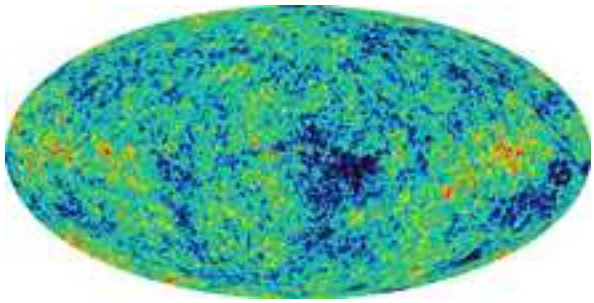

Fig. 1.2 The cosmic μwave background radiation as observed by the WMAP satellite. Figure taken from [10].

To obtain an accurate value of H_0 was one of the main motivations for building the Hubble Space Telescope. In particular the H_0-Key Project had its ultimate goal in measuring the Hubble parameter basing on a Cepheid calibration and a number of secondary distance indicators; its final determination was [80]

$$h = 0.72 \pm 0.08 \ . \tag{1.10}$$

Concerning the geometry of our spacetime, the observations of the cosmic μwave background performed by the WMAP ([10]; see Fig. 1.2) mission have confirmed the previous findings of the high-altitude balloon experiments MAXIMA [6] and BOOMERanG [61]. The total energy density is found to be

$$\Omega \approx 1.02 \pm 0.02 \ , \tag{1.11}$$

therefore our Universe is very close to spatial flatness ($k = 0$). However, detailed analysis of the WMAP data revealed a lack of correlation across the μwave sky on angular scales wider than about 60°. This may constitute evidence in favor of a complex topology and/or a slightly positive curvature of the Universe, whose finite size would impose a natural cutoff on the largest waves (space is simply not big enough to support them; [68], also [116]). The upcoming Planck mission will determine Ω up to a 1% accuracy and is expected to settle the issue.

1.1.3 *The standard Universe*

The simplest solutions of the Friedman equations obtain whenever any one component dominates over the others; in that case $a \propto t^{2/[3\,(1+w)]}$ for $w > -1$ and $a(t) \propto \exp(\alpha\, t)$ with $\alpha = \text{const}$ for $w = -1$.

To proceed further we need to know what the main components of the Universe are, and how their equation of state looks like; there have recently been noticeable progress on this issue owing to the detections and the follow-up of high-redshift type-Ia supernovae (SNae; [168], [152]; [102]). In Table 1.1 we present such a cosmic inventory of energy densities; it is quite stunning that ordinary matter,

Table 1.1 Cosmic inventory of energy densities.

i-eth Component	$\mathbf{w_i}$	$\mathbf{\Omega_i}$	$\rho_\mathbf{i} \propto (\mathbf{1+z})^\mathbf{x}$
Photons	1/3	$\sim 5 \times 10^{-5}$	4
Baryons	0	0.044 ± 0.004	3
Neutrinos	1/3	< 0.015	4
Dark matter	0	0.23 ± 0.04	3
Curvature	-1/3	0.02 ± 0.02	2
Dark energy	≈ -1 (< -0.78)	0.73 ± 0.04	≈ 0 (< 0.66)

i.e., radiation and baryons contribute only a minor fraction to the actual content of the Universe. Indeed, the latter is constituted for about 1/3 by pressureless ($w = 0$), non baryonic *dark matter* (DM) and for the remaining 2/3 by some exotic form of *dark energy* with $w \approx -1$. This set of parameters defines the so called *Concordance Cosmology*, the name recalling that it satisfies the constraints from the complementary observations of the cosmic background radiation (CMBR), of type-Ia SNae, and of matter abundances in clusters and large scale structures (see Fig. 1.3; also discussion by [185]).

Looking at the redshift dependence of the energy density for the various components, we may identify some important epochs in the dynamical history of the Universe. The first one is the time of *equidensity* $1+z_{\rm eq} = (\Omega_M/\Omega_\gamma) \approx 3.9\times10^4\,(\Omega_M\,h^2)$ at which the energy densities of the radiation Ω_γ and of the non-relativistic matter (DM + baryons) $\Omega_M \equiv \Omega_{DM} + \Omega_B$ were equal. Around $z_{\rm eq}$ the Friedman equation has the solution

$$H_{\rm eq}\,t = \frac{2\sqrt{2}}{3}\,\left[\left(\frac{a}{a_{\rm eq}} - 2\right)\,\left(\frac{a}{a_{\rm eq}} + 1\right)^{1/2} + 2\right]\;; \tag{1.12}$$

for $t >> t_{\rm eq}$ matter dominates and $a/a_{\rm eq} \simeq (3/2\sqrt{2})^{2/3}\,(H_{\rm eq}\,t)^{2/3}$, while for $t << t_{\rm eq}$ radiation prevails and $a/a_{\rm eq} \simeq (3/\sqrt{2})^{1/2}\,(H_{\rm eq}\,t)^{1/2}$. Extrapolating backwards in time, the expansion factor is smaller in the past and becomes null at a definite time. Actually this singularity, which is often referred to as the *big-bang*, is only a feature of the simple Friedman treatment; owing to the dominance of quantum gravitational effects (see, e.g., [88]), the Einstein equations did no longer hold when the spacetime had size comparable to the fundamental *Planck length* $(G\,\hbar/c^3)^{1/2} \approx 10^{-33}$ cm.

A second relevant epoch marks the *decoupling* of baryons from photons. Today the background radiation has a very low temperature $T_\gamma \approx 2.725 \pm 0.002$ K, but it was much higher in the past since scales as $(\Omega_\gamma/a^4)^{1/4} \propto (1+z)$; e.g., at the equidensity the corresponding specific energies amounted to about $9.2\,(\Omega\,h^2)$ eV. Thus at early times the Universe was in a state of so high energy to forbid the formation of bound atomic structures. Baryons, photons and electrons were tightly coupled by scattering and collisional processes, while the high number of free electrons maintained the Universe opaque to radiation. When at a redshift $z_{\rm dec} \approx 1100$

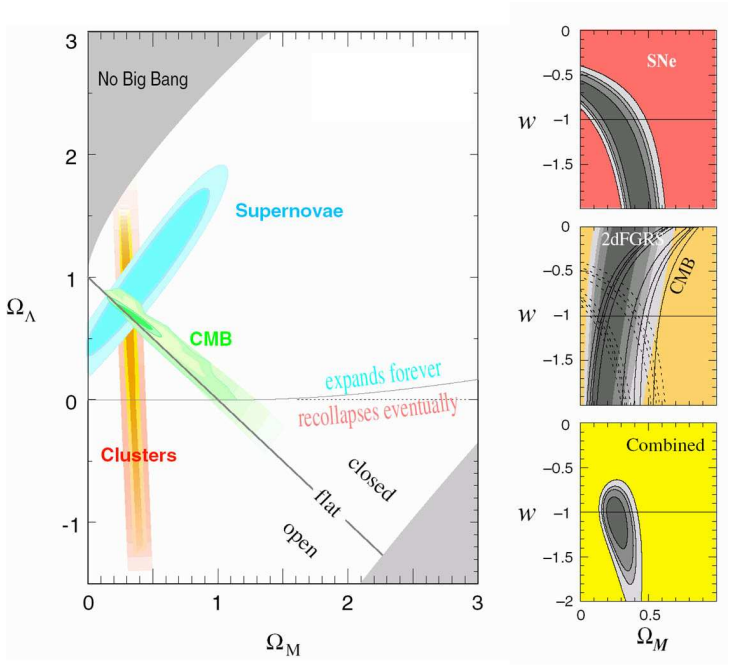

Fig. 1.3 The constraints in the $\Omega_\Lambda - \Omega_M$ and in the $w_\Lambda - \Omega_M$ planes provided by the observations of the CMBR, of type-Ia SNae and of matter abundances in clusters of galaxies and large-scale structures. Figure taken from [102].

the temperature dropped below 10^3 K because of the expansion, neutral atomic systems formed by recombination processes and photons decoupled from matter, originating as a fossil record the background radiation we now observe in μwaves.

The last, but not the least, important epoch is the transition between a dark matter and a dark energy (density Ω_Λ) dominated Universe, occurring at $1 + z_\Lambda = (\Omega_\Lambda/\Omega_M)^{1/3}$, i.e., close to the present. The standard tenet assumes for the dark energy an equation of state $w_\Lambda = -1$ (the so called *cosmological constant*); in this case the Friedman equation integrates to [151]

$$\frac{a}{a_0} = \left(\frac{\Omega_M}{\Omega_\Lambda}\right)^{1/3} \sinh^{2/3}\left(\frac{3}{2}\sqrt{\Omega_\Lambda}\, H_0\, t\right) \ . \tag{1.13}$$

The Universe is currently accelerating under the anti-gravitational push of the dark energy component, a behavior which will conceivably continue forever. Since asymptotically the expansion factor $a(t) \propto \exp(H_0\sqrt{\Omega_\Lambda}\, t)$ will grow even more rapidly than the horizon scale $c\,t$, galaxies will disappear from each other's view and the Universe will become increasingly cold and empty.

However, let us remark that the future evolution of our Universe is quite uncertain because it sensitively depends on the exact value of the state parameter w_Λ

(see Fig. 1.3). For example, an intriguing possibility not yet excluded by the current data is $w_\Lambda < -1$ (the so called *phantom energy*); in this case the expansion factor $a \propto (t - t_{\rm rip})^{-2/3\,|1+w_\Lambda|}$ will diverge at a finite time $t_{\rm rip} \sim 40$ Gyr. Moreover, while with the cosmological constant the dark energy density does not depend on time and structures already bound by gravity will survive the background expansion, the phantom energy density $\rho_\Lambda \propto (1+z)^{-3\,|1+w_\Lambda|}$ will increase in the future, to the effect of progressively ripping apart galaxies, stellar systems, planets, and ultimately molecules, atoms, and even nuclei just before the final cosmic doomsday [32].

1.2 The cosmogonical scenario

The standard cosmogonical paradigm assumes that the cosmic structures we see today had their origin in the early Universe from quantum-generated energy density perturbations subsequently grown by *gravitational instability* (see, e.g., [148], [146]).

1.2.1 *Linear growth of perturbations*

The basic quantities to describe the growth of a perturbation are its physical size λ and its *density contrast* $\delta \equiv (\rho - \bar\rho)/\bar\rho$ relative to the background $\bar\rho$.

The initial evolutionary stages of perturbations are driven by general relativistic effects, as their size λ is bigger than the Hubble radius $d_H \equiv (\dot a/a)^{-1}$ at sufficiently large redshifts; this is because $\lambda = \lambda_0\,(1+z)^{-1} \propto a$ while $d_H \propto a^2$ in the radiation-dominated or $d_H \propto a^{3/2}$ in the matter-dominated era. In this regime ($\lambda >> d_H$) a perturbation with density $\bar\rho\,(1+\delta)$ behaves as a $k \neq 0$ universe embedded in a $k = 0$ one of background density $\bar\rho$. Comparing the Friedman equations for the inner and outer regions

$$H^2 = \frac{8\,\pi\,G}{3}\,\bar\rho \qquad\qquad H^2 + \frac{k}{a^2} = \frac{8\,\pi\,G}{3}\,\bar\rho\,(1+\delta)\ , \tag{1.14}$$

shows their density difference to be accommodated by the addition of the spatial curvature term. If this condition is to be maintained at all times, one must have

$$\delta \propto \frac{1}{\bar\rho\,a^2}\ . \tag{1.15}$$

As δ is small, $a(t)$ would not differ too much from that of an unperturbed universe, so $\delta \propto a^2$ in the radiation-dominated phase and $\delta \propto a$ in the matter-dominated era.

At a subsequent time $t_{\rm enter} \propto \lambda\,a_{\rm enter}$ the perturbation enters the Hubble radius; if $\lambda \approx \lambda_{\rm eq} \equiv 14\,(\Omega_M\,h^2)^{-1}$ Mpc this occurs at the time of equidensity. The scales with $\lambda < \lambda_{\rm eq}$ enter the Hubble radius in the radiation-dominated era at a time $1+z_{\rm enter} \approx 4.6\times10^5\,(\lambda_0/1\,{\rm Mpc})^{-1}$, while the scales with $\lambda > \lambda_{\rm eq}$ enter in the matter-dominated phase at $1 + z_{\rm enter} \approx 900\,(\Omega_M\,h^2)^{-1}\,(\lambda_0/100\,{\rm Mpc})^{-2}$. The evolution of the perturbation can now be treated in the Newtonian approximation, basing on

the continuity, Euler and Poisson equations for a fluid embedded in an expanding background, i.e.,

$$\begin{aligned} & a\,\partial_t\delta + \vec{\nabla}_x\left[(1+\delta)\,\vec{u}\right] = 0 \\ & \partial_t(a\,\vec{u}) + (\vec{u}\cdot\vec{\nabla}_x)\,\vec{u} = -\frac{1}{\rho}\,\vec{\nabla}_x p - \vec{\nabla}_x\phi \\ & \nabla_x^2\phi = 4\,\pi\,G\,a^2\,\rho\ ; \end{aligned} \tag{1.16}$$

here x is the comoving coordinate, $\vec{u}$ is the peculiar velocity (subtracted of the Hubble flow), and ϕ is the gravitational potential. As $\delta << 1$ we can linearize and combine the previous equations to get

$$\ddot{\delta}_{DM} + 2\,H\,\dot{\delta}_{DM} = 4\,\pi\,G\,\bar{\rho}\,\delta_{DM}\ , \tag{1.17}$$

for the pressureless DM component. In the radiation dominated phase the previous equation may be recast in the form

$$\frac{d^2\delta_{DM}}{d^2y} + \frac{2+3\,y}{2\,y\,(1+y)}\,\frac{d\delta_{DM}}{dy} - \frac{3\,\delta_{DM}}{2\,y\,(1+y)} = 0 \tag{1.18}$$

by introducing the variable $y = a/a_{\rm eq} \lesssim 1$. The two leading-order solutions are found by inspection to be $\delta_{DM} \simeq 1+3\,y/2$ and $\delta_{DM} \simeq \ln(4/y)$. Therefore δ_{DM} stays nearly constant (actually it increases only logarithmically) before the equidensity epoch; this is the well-known *Meszaros effect*.

After equidensity, Eq. (1.17) has to be integrated taking into account the contribution of DM and dark energy to the background density. The result ($w_\Lambda = -1$) reads

$$\delta_{DM} = D(z) \equiv \frac{5}{2}\,\Omega_M\,H(a)\int_0^a dx\,\frac{1}{x^3\,H^3(x)} \tag{1.19}$$

with $H(x) = [\Omega_M\,x^{-3} + \Omega_\Lambda]$. An accurate fit to the above expression is given by [105]

$$D(z) \simeq \frac{5}{2}\,\frac{\Omega_z}{1+z}\left(\frac{1}{70} + \frac{209\,\Omega_z}{140} - \frac{\Omega_z^2}{140} + \Omega_z^{4/7}\right)^{-1}\ , \tag{1.20}$$

where $\Omega_z = \Omega_M\,(1+z)^3/[\Omega_\Lambda + (1+z)^3\,\Omega_M]$, see Fig. 1.4. Note that the growth of perturbations is halted for $1+z \lesssim (\Omega_\Lambda/\Omega_M)^{1/3}$ by the rapid expansion of the Universe.

Now we repeat the previous analysis for the baryons. Since they are tightly coupled to photons until the recombination epoch at $z \approx 10^3$, we cannot neglect the pressure support. It is convenient to work with the Fourier modes $\delta^{(k)}$ of the

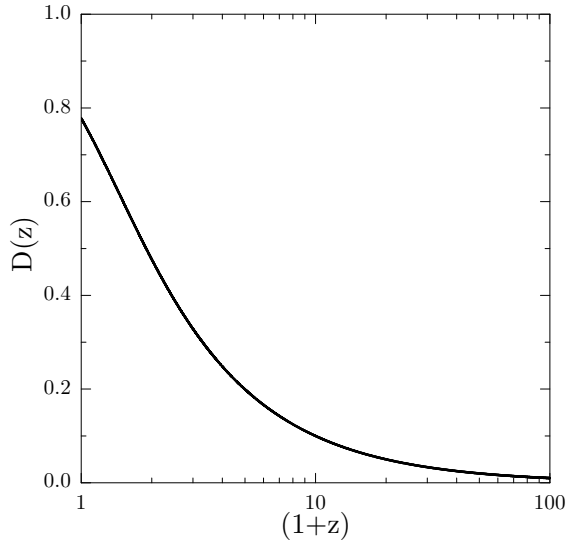

Fig. 1.4 The growth function in the Concordance Cosmology.

density contrast, defined through

$$\delta(\vec{x},t) = \int \frac{d^3k}{(2\,\pi)^3} \delta^{(k)}\, e^{i\,k\,x}\ ; \tag{1.21}$$

the expansion in plane waves is allowed by the (nearly exact) flatness of the Universe. Then each Fourier mode of the baryonic density contrast satisfies the equation

$$\ddot{\delta}_B^{(k)} + 2\,H\,\dot{\delta}_B^{(k)} + \left(\frac{k^2\,c_s^2}{a^2} - 4\,\pi\,G\,\bar{\rho}_B\right)\,\delta_B^{(k)} = 4\,\pi\,G\,\bar{\rho}_{DM}\,\delta_{DM}^{(k)}\ , \tag{1.22}$$

where $c_s \equiv \sqrt{\delta p/\delta\rho}$ is the sound speed. The nature of the solutions is determined essentially by the comparison between the physical size of the perturbation $\lambda = (2\,\pi/k)\,a(t)$ and the *Jeans length*

$$\lambda_J \equiv \left(\frac{\pi\,c_s^2}{G\,\bar{\rho}}\right)^{1/2}\ ; \tag{1.23}$$

only modes with $\lambda > \lambda_J$ can grow because for them gravity overcomes the pressure support.

It is useful to reconsider this issue in terms of the *Jeans mass* $M_J \propto (c_s^3/\bar{\rho}_B^{1/2})$ defined as the amount of baryonic matter contained within a sphere of radius $\lambda_J/2$. Between the equidensity and the recombination epoch $c_s \approx 1/3$ and $M_J \propto a^{3/2}$ holds. After decoupling, baryons expands adiabatically, so $c_s \propto a^{-1}$ and $M_J \propto a^{-3/2}$ obtains; moreover, the support provided by the photons vanishes, and baryons

can only resist gravity by normal gas pressure. Hence around the recombination epoch the Jeans mass drops from values $M_J^{(bd)} \approx 10^{16}\, M_\odot\, (\Omega_B/\Omega)\, (\Omega\, h^2)^{-1/2}$ down to $M_J^{(ad)} \approx 10^4\, M_\odot\, (\Omega_B/\Omega)\, (\Omega\, h^2)^{-1/2}$.

Modes with $M > M_J^{(bd)}$ always grow, but are not of much astrophysical interest; modes with $M_J^{(ad)} < M < M_J^{(bd)}$ do not grow until well after decoupling. Finally, consider perturbations of scale $M < M_J^{(ad)}$. For $z \gtrsim 10^2$ the temperature of matter is not too different from that of radiation, so we may assume $c_s^2 \simeq (k_B\, T_\gamma/m_p)\, (1/a)$. Introducing the variable $y = (a/a_0)^{1/2}$ the baryonic perturbation equation becomes

$$\frac{1}{y^2}\,\frac{d}{dy}\left(y^2\,\frac{d\,\delta_B^{(k)}}{dy}\right) + \frac{\omega^2\,\delta_B^{(k)}}{y^2} = 0\ , \tag{1.24}$$

in terms of the constant $\omega^2 = (4\,k^2/H^2a^3)\,(k_B\,T_\gamma/m_p)$. Since we are considering modes for which $\lambda \ll d_H$, then $\omega \gg 1$ and the solutions oscillate while decaying with time as

$$\delta_B^{(k)} \simeq t^{-1/6 \pm i\,\omega/3}\ . \tag{1.25}$$

After decoupling, however, the baryons will feel the gravitational attraction of the DM perturbations that had already been growing since the equidensity epoch.

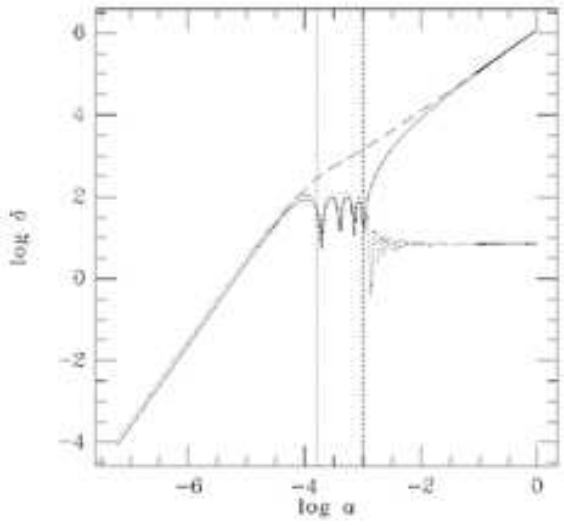

Fig. 1.5 The time evolution of baryonic (*solid*), cold DM (*dashed*), and photonic (*dotted* line) perturbations with $k = 10^{-1}$ Mpc^{-1}. The vertical lines mark equidensity and decoupling. Figure kindly provided by A. Balbi (Univ. of Rome "Tor Vergata").

Eq. (1.22) now becomes

$$\ddot{\delta}_B^{(k)} + \frac{4}{3\,t}\,\dot{\delta}_B^{(k)} + \left(\frac{k_B\,T}{m_p}\right)\,\frac{k^2}{a^2}\,\delta_B^{(k)} = \frac{2}{3}\,\frac{\delta_{DM}^{(k)}}{t^2}\ , \tag{1.26}$$

and easily integrates to

$$\delta_B^{(k)}(t) = \frac{\delta_{DM}^{(k)}(t)}{1 + A\,k^2} \tag{1.27}$$

in terms of the constant $A = (3/2)\,(k_B\,T_0/m_p)\,(t^2/a^3) \approx 1.5 \times 10^{-6}\,h^{-2}$ Mpc^2. In conclusion, at large scales the DM induces corresponding perturbations in the baryons, while at small scales the latter are suppressed because of pressure support (see Fig. 1.5).

1.2.2 *Statistical indicators*

Acquired the results of the previous section, we are now able to evolve the DM fluctuation field in the linear regime, i.e., until $\delta_{DM}(\vec{x},t) \approx 1$; however, we are not so interested in its exact form, but rather in its statistical properties. If the initial density inhomogeneities have Gaussian distribution, the Fourier modes $\delta_{DM}^{(k)}$ are uncorrelated and satisfy

$$\langle \delta_{DM}^{(k)}(t_i), \delta_{DM}^{(p)}(t_i) \rangle = (2\,\pi)^3\,P(k,t_i)\,\delta_D(k-p) \tag{1.28}$$

at some initial instant t_i. The *power spectrum* $P(k,t_i)$ contains the complete statistical information of the Gaussian random field; sometimes it is convenient to use the power per unit logarithmic interval in wavenumber, defined as $\Delta_k^2 \equiv k^3\,P(k)/2\,\pi^2$.

The recent results from the WMAP mission indicate the initial power spectrum to be scale-free, i.e., of the form

$$P(k,t_i) \propto k^{n_p}\ , \tag{1.29}$$

with nearly constant primordial *spectral index* $n_p \approx 0.99 \pm 0.04$.

On the other hand, the evolution until the end of the linear regime for each mode of the fluctuation field is parameterized as $\delta_{DM}^{(k)}(t) = T_k(t_i,t)\,\delta_{DM}^{(k)}(t_i)$ in terms of the *transfer function* T; correspondingly, the power spectrum evolves as $P(k,t) = P(k,t_i)\,T_k^2(t_i,t)$. We will now discuss the shape of such a transfer function, which depends on the nature of the DM particles and on the dynamics of the perturbation field.

The mass m_{DM} of the DM particles sets the time $t_{NR}(< t_{\rm eq})$ at which they become non-relativistic. At time $t << t_{NR}$ the DM particles cross the horizon within the expansion timescale, so that density perturbations with $\lambda \lesssim \lambda_{FS}$ are washed out. The *free-streaming* wavelength λ_{FS} may be estimated as [145]

$$\lambda_{FS} \approx \left(\frac{a}{a_0}\right)\,(2\,t_{NR})\,\left(\frac{5}{2} + \ln\frac{a_{eq}}{a_{NR}}\right) \approx 28\left(\frac{m_{DM}}{30\,\mathrm{eV}}\right)^{-2}\ \mathrm{Mpc}\ , \tag{1.30}$$

corresponding to a mass $M_{FS} \approx 4 \times 10^{15}\,(m_{DM}/30\,\mathrm{eV})^{-2}\,M_\odot$. This process produces a transfer function $T \propto \exp[-4.6\,(\lambda_{FS}/\lambda)^{3/2}]$ exponentially cut off at low wavelengths [17].

If the DM were made of low-mass particle (*hot dark matter*), there would be very little power at small scales; the first structures to form would have been pancakes of several Mpcs radius, and the galaxies we now observe would have been formed by the latter's fragmentation. This *top-bottom scenario* scenario is not plausible because we observe small structures at high redshift and very massive objects only in the local Universe. Therefore we now reliably know that the DM is *cold*, in the sense it is constituted by massive particles with $m_{DM} \gtrsim \mathrm{keV}$. The resulting cosmogony is a *bottom-up* scenario in which larger and larger structures form progressively by *hierarchical clustering* of smaller units.

Now we turn to analyze the effect of the dynamics on the power spectrum. We start from the modes entering the Hubble radius in the radiation-dominated era. These grow logarithmically of a factor $L(k) \simeq 5\,\ln(k/k_{\mathrm{eq}})$ before equidensity and are proportional to the scale factor just after it, so $\delta(t) = L\,\delta(t_{\mathrm{enter}})\,(a/a_{\mathrm{eq}})$. The modes with $\lambda_{\mathrm{eq}} < \lambda$ enter the Hubble radius in the matter-dominated era and grow proportional to a afterwards, so $\delta(t) = \delta(t_{\mathrm{enter}})\,(a_{\mathrm{eq}}/a_{\mathrm{enter}})\,(a/a_{\mathrm{eq}})$ holds; but $t_{\mathrm{enter}} \propto k^{-3}$ implies $\delta(t) = \delta(t_{\mathrm{enter}})\,(a/a_{\mathrm{eq}})\,(k/k_{\mathrm{eq}})^2$. The amplitude at late times is completely fixed by the behavior of the modes when they entered the Hubble radius. The power spectrum has the approximate behavior

$$\Delta_k^2 \simeq \begin{cases} L^2(k)\,\Delta_k^2(t_{\mathrm{enter}})\,(a/a_{\mathrm{eq}})^2 & \text{if } \; k_{\mathrm{eq}} << k \\ \\ \Delta_k^2(t_{\mathrm{enter}})\,(a/a_{\mathrm{eq}})^2\,(k/k_{\mathrm{eq}})^4 & \text{if } \; k_{\mathrm{eq}} >> k \end{cases} . \tag{1.31}$$

If initially $\Delta_k^2 \propto k^{n_p+3}$ then $\Delta_k^2(t_{\mathrm{enter}}) \propto a_{\mathrm{enter}}^4\,k^{n_p+3} \propto k^{n_p-1}$ for the short wavelength modes and again $\Delta_k^2(t_{\mathrm{enter}}) \propto a_{\mathrm{eq}}^2\,a_{\mathrm{enter}}^2\,k^{n_p+3} \propto k^{n_p-1}$ for the long wavelength ones. Note that the value $n_p = 1$ is special, as in this case all the modes enter the Hubble radius with the same amplitude (*Harrison-Zel'dovich hypothesis*). Finally, putting the previous results together yields

$$\Delta_k^2 \simeq \begin{cases} L^2(k)\,k^{n_p-1}\,(a/a_{\mathrm{eq}})^2 & \text{if } \; k_{\mathrm{eq}} << k \\ \\ k^{n_p+3}\,(a/a_{\mathrm{eq}})^2 & \text{if } \; k_{\mathrm{eq}} >> k \end{cases} . \tag{1.32}$$

Thus we have obtained with simple reasoning the asymptotic expressions of the transfer function and of the power spectrum; for more detailed results we have to integrate the perturbation equation numerically (see Fig. 1.6). A very good fitting formula for the exact cold DM power spectrum in the Concordance Cosmology is given by [111]

$$\Delta_k^2(z) = \left(\frac{c\,k}{H_0}\right)^{3+n_p}\,\delta_H^2\,T^2(k)\,\frac{D^2(z)}{D^2(0)}\;, \tag{1.33}$$

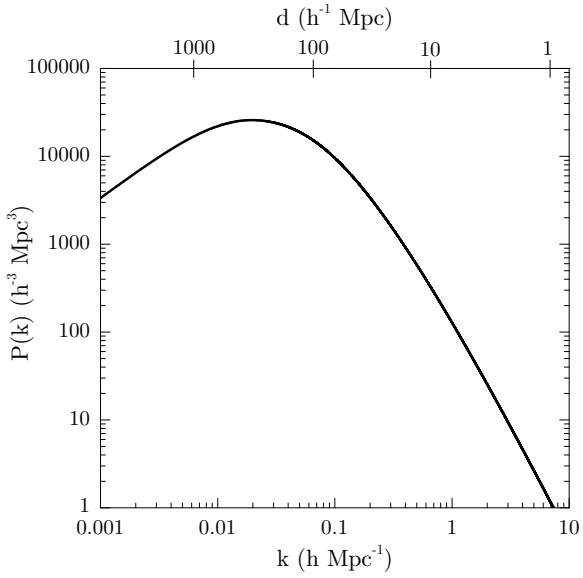

Fig. 1.6 The cold DM power spectrum at $z = 0$; normalization according to Eq. (1.33).

in terms of the normalization $\delta_H = 1.94 \times 10^{-5} \exp[-0.95\,(n_p - 1) - 0.169\,(n_p - 1)^2]$ and of the transfer function [9]

$$T(q) = \frac{\ln(1 + 2.34\,q)}{2.34\,q}\,[1 + 3.89\,q + (16.1\,q)^2 + (5.46\,q)^3\,(6.71\,q)^4]^{-1/4}\ ; \qquad (1.34)$$

here $q \equiv k/h\,\Gamma$ and $\Gamma \equiv \Omega_M\,h\,\exp(-\Omega_B - \sqrt{2\,h}\,\Omega_B/\Omega_M)$ specify how the baryons affect the detailed shape of the spectrum [186].

We conclude this § by discussing another important statistical indicator of the Gaussian fluctuation field, i.e., the *variance* $\sigma \equiv \langle\delta^2\rangle^{1/2}$ (remember that $\langle\delta\rangle = 0$). In particular, to compare with observations it is useful to smooth it out over some scale R,

$$\sigma^2(R) = \int \frac{dk}{2\,\pi^2}\,k^2\,P(k)\,W(k\,R) = \int d\ln k\ \Delta_k^2\,W(k\,R)\ . \qquad (1.35)$$

The result depends on the *window function* adopted; a widely used one is the top-hat $W(x) \equiv (3/x^3)\,(\sin x - x\,\cos x)$ because it allows to relate simply the size of the averaged region to the mass contained within it as $M \equiv (4\,\pi/3)\,\bar{\rho}\,R^3$.

Given the asymptotic expression of the power spectrum Eq. (1.32), we can easily work out the related behaviors of the variance

$$\sigma(M, z) \propto D(z)\,\begin{cases} M^{(1-n_p)/6}\,L^{-1/3} & \text{if}\ \ M << M_{\rm eq} \\ \\ M^{-(n_p+3)/6} & \text{if}\ \ M >> M_{\rm eq} \end{cases}\ , \qquad (1.36)$$

in terms of the mass $M_{\rm eq}$ corresponding to $k_{\rm eq}$.

An analytical fit to the exact σ (and to its derivative $d\sigma/dM$, see Fig. 1.7) is given by [100]

$$\sigma \propto D(z)\,\left(1+2.208\,m^{p}-0.7668\,m^{2\,p}+0.7949\,m^{3\,p}\right)^{-2/9\,p}\ , \tag{1.37}$$

where $p=0.0873$ and $m\equiv M\,(\Gamma\,h)^2/10^{12}\,M_\odot$; the accuracy is within a few percent in the range $10^{-7}\le m\le 10^{5}$.

The normalization of the variance is derived from the observations of the galaxy correlation function, which imply $\sigma(8\,h^{-1}\,{\rm Mpc},t_0)=1$. However, galaxies are likely to have formed on the high-density peaks of the fluctuation field, which are more correlated than the Gaussian field itself. As a result, we may expect the observational value of σ on galactic scales not to be a good estimate of the true variance. Thus the latter's normalization is usually written as $\sigma(8\,h^{-1}\,{\rm Mpc},t_0)=1/b$ in terms of the *bias* parameter b; the observations of large scale structures currently favor values $1/b\approx 0.84\pm 0.04$.

Very often the cold DM power spectrum after decoupling is approximated in a limited range of scales by a power law $P(k)\propto k^n$ in terms of an effective index n slowly dependent on mass. The values of n ranges from -1.2 at the scales of rich clusters to -2.2 in dwarf galaxies, and the variance is correspondingly approximated by $\sigma(M,z)\propto D(z)\,M^{-(n+3)/6}$.

Finally, the mass variance offers the opportunity to have a first look at the non-

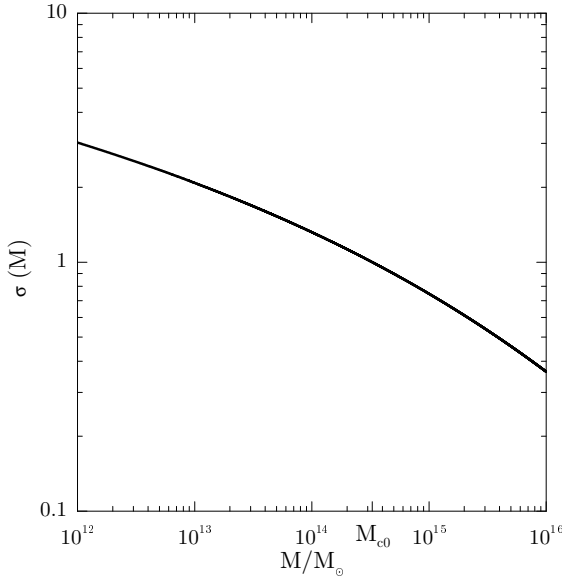

Fig. 1.7 The mass variance at $z=0$, normalized to unity on a scale of $8\,h^{-1}$ Mpc.

linear regime we are going to investigate more fully in the next §. Since the quantity σ represents the typical density contrast, one may regard the condition $\sigma \approx 1$ as to set the transition between the linear and non-linear regimes. This implicitly defines the *characteristic mass* $M_c(t) = M_{c0}\,[D(t)/D(t_0)]^{6/(n+3)}$ that is to collapse at a given epoch, being $M_{c0} \approx 6 \times 10^{14}\,\Omega_M\,h^{-1}\,M_\odot$ the present value. A rather good fit to $M_c(t)$ is provided by [117]

$$M_c(t) = M_{c0} \left[\frac{1 + 3\,\alpha^2\,\dfrac{\Omega_\Lambda}{\Omega_M}}{\left(\dfrac{t_0}{t}\right)^2 + 3\,\alpha^2\,\dfrac{\Omega_\Lambda}{\Omega_M}} \right]^{\frac{2}{n+3}} , \tag{1.38}$$

where $\alpha \equiv 2\,\sqrt{\Omega_M}/\pi\,H_0\,t_0$. From Eq. (1.38) it is easily seen that the characteristic mass has (for $t \gg t_0$) the limiting value $M_{c0}\,\left[1 + (\pi\,H_0\,t_0)^2/(12\,\Omega_\Lambda)\right]^{2/(n+3)}$, that amounts to $1.2 \times 10^{15}\,M_\odot$ in the concordance cosmology; the formation of very massive structures is being frozen out by the currently accelerated cosmic expansion.

1.2.3 *Non linear collapse and mass functions*

In the non-linear regime ($\delta \gtrsim 1$) it is not possible to solve exactly Eqs. (1.16); however, some advance can be made on restricting the analysis to a very symmetric case, the so called *spherical top-hat*. Consider at some initial time a spherical, slightly overdense region. This will obviously expand more slowly than the rest of the Universe; at a certain *turn around* epoch it will reach a maximum radius, then it will collapse and eventually virialize to form a gravitationally bound object.

The radius $R(t)$ of such a region will evolve according to

$$\ddot{R} = -\frac{G\,M_{DM}}{R^2} - \frac{4\,\pi\,G}{3}\,\bar{\rho}_\Lambda\,(1 + 3\,w_\Lambda)\,R\ , \tag{1.39}$$

where we have separated the contribution of DM and dark energy.

Let us first quote the solution of the previous equation in a pure matter-dominated Universe, where $\ddot{R} = -G\,M_{DM}/R^2$. The non-linear density contrast as a function of the redshift is implicitly given by [150]

$$\begin{aligned} (1+z) &= \left(\frac{5}{3}\right)\,\left(\frac{4}{3}\right)^{2/3}\,\frac{\delta_0}{(\theta - \sin\theta)^{2/3}} \\ \delta &= \frac{9}{2}\,\frac{(\theta - \sin\theta)^2}{(1 - \cos\theta)^3} - 1 \end{aligned} \tag{1.40}$$

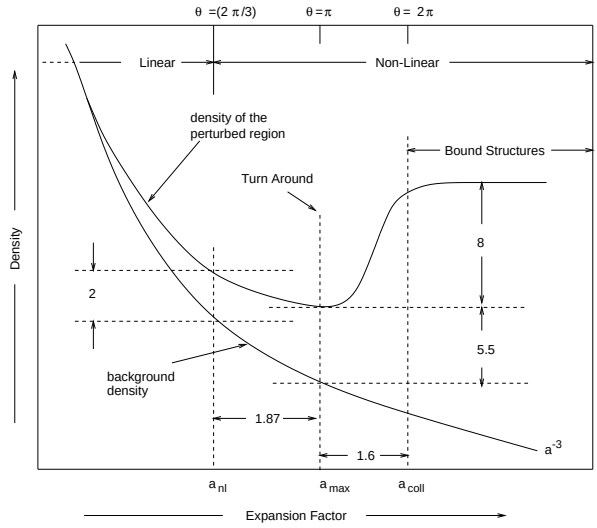

Fig. 1.8 The spherical top-hat model of non-linear collapse. Figure taken from [146].

where δ_0 is the density contrast at present if it were evolved by the linear approximation. The linear density contrast at a given epoch is in general

$$\delta_L = \frac{3}{5}\left(\frac{3}{4}\right)^{2/3}(\theta - \sin\theta)^{2/3} \ . \tag{1.41}$$

Now the evolution of the perturbation is straightforward (see Fig. 1.8): The transition to non-linearity ($\delta \approx 1$) occurs for $\theta = 2\,\pi/3$ when $\delta_L \approx 0.57$, i.e., at redshift $1 + z_{\rm nl} \approx \delta_0/0.57$; the turn-around occurs when $\delta = 4.6$ and $\delta_L \approx 1.063$, i.e., at redshift $1 + z_{\rm ta} \approx \delta_0/1.063$; finally at $\theta = 2\,\pi$ all the mass will be collapsed to a point. However, long before this happens the analysis based on Eq. (1.39) breaks down because the random velocities of DM particles are no longer small. The DM will relax to a virialized configuration in a time which is essentially that corresponding to $\theta = 2\,\pi$. So virialization occurs when $\delta \equiv \Delta_{\rm vir} \approx 18\,\pi^2 \approx 180$ and $\delta_L \equiv \delta_c \approx 1.686$, i.e., at redshift $1 + z_{\rm vir} \approx \delta_0/1.686$.

In presence of dark-energy, the second term in Eq. (1.39) cannot be neglected and the related solution is only numeric. However, the critical threshold for collapse does not depend very much on cosmology; for $w_\Lambda = -1$ it is well fitted by [136]

$$\delta_c \simeq \frac{3\,(12\,\pi)^{2/3}}{20}\left[1 + 0.0123\,\log_{10}\Omega_M\right] \ . \tag{1.42}$$

The overdensity at virialization has to be larger than in a matter-dominated Universe owing to the anti-gravitational action of the dark energy that counteracts the collapse. Moreover, it is found that $\Delta_{\rm vir}$ slowly depends on cosmic time; a good fit

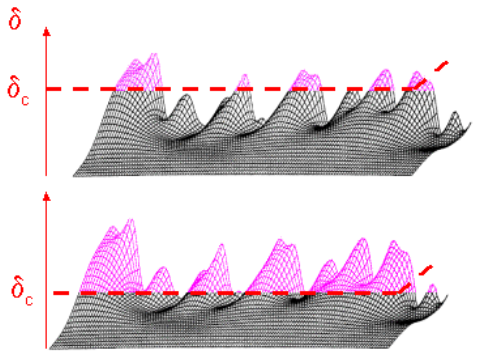

Fig. 1.9 A realization of the fluctuation field; the highlighted peaks correspond to objects above the threshold for collapse. Note how their scales increase with time, determining the hierarchical clustering picture of structure formation.

($w_\Lambda = -1$) is provided by [69]

$$\Delta_{\rm vir}(z) \simeq 18\,\pi^2 + 82\,(\Omega_z - 1) - 39\,(\Omega_z - 1)^2 \ . \tag{1.43}$$

The relevance of the latter quantities emerges from the fact that they can be used to describe the statistics of virialized DM structures in the Universe. This is done through the *mass function* $N(M, z)$, which we are now going to discuss. Firstly, we are interested in computing the number of bound DM structures with mass between M and $M + dM$ at a given redshift; this is provided by the Press & Schechter [160] formula. In deriving its expression it is convenient to reason along the following lines [18].

Given the power spectrum, imagine to construct the corresponding fluctuation field (see Fig. 1.9). Now filter it in a point through a very large effective radius R; the corresponding resolution is $S \equiv \sigma^2(R)$. While lowering the filtering radius, the overdensity δ of the chosen point will determine a random walk $\delta(S)$. If a top-hat window function is used to smooth out the fluctuation field, at every step ΔS the increment $\Delta\delta$ will be uncorrelated from the previous ones, i.e., $\delta(S)$ will be a *Markovian* random walk.

Now consider an absorbing barrier at $\delta_c(z) \equiv \delta_c\, D(0)/D(z)$. When the random walk will upcross the barrier for the first time, identify an object collapsed on scale M at resolution S. The probability $P(\delta|S)$ that δ upcrossed the threshold at the resolution S is the solution of the diffusion equation

$$\frac{\partial}{\partial S}\,P(\delta|S) = \frac{1}{2}\,\frac{\partial^2}{\partial\delta^2}\,P(\delta|S)\ , \tag{1.44}$$

supplemented of the boundary condition $P(\delta_c|S) = 0$. By straightforward integra-

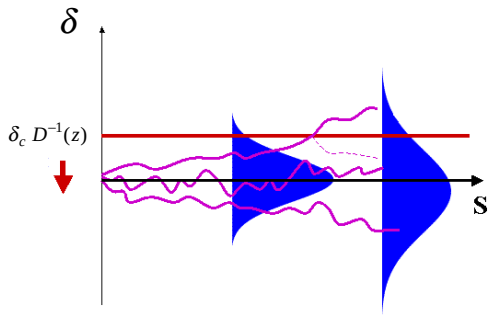

Fig. 1.10 A schematic representation of the absorbing barrier problem, used to derive the Press & Schechter mass function (see main text).

tion one finds

$$P(\delta|S) = \frac{1}{\sqrt{2\,\pi\,S}}\,\left[e^{-\delta^2/S} - e^{-(2\,\delta_c-\delta)^2/S}\right]; \tag{1.45}$$

the second term highlights that each trajectory upcrossing the barrier has a specular one in respect to δ_c (see Fig. 1.10).

Finally, integrating the probability $P(\delta|S)$ over all the trajectories that have upcrossed the barrier and reconverting to physical variables yield the mass function

$$N(M,z) = \bar{\rho}\sqrt{\frac{2}{\pi}}\,\frac{\delta_c(z)}{M_{c0}^2}\,\left|\frac{d\ln\sigma}{d\ln m}\right|\,\frac{m^{-2}}{\sigma(m)}\,\exp\left[-\frac{\delta_c^2(z)}{2\,\sigma^2(m)}\right]\;; \tag{1.46}$$

here both the mass and the variance are normalized to the respective values on a scale of $8\,h^{-1}$ Mpc, i.e., $m = M/M_{c0}$ and the dependence on the bias parameter b is implicit. The main features of the Press & Schechter mass function are a power-law behavior at the low-mass end and an exponential cutoff at high masses (see Fig. 1.11). At larger z the cutoff recedes while the power-law at the lower end steepens, so that the total collapsed mass is conserved; in this sense the evolution is self-similar, a feature that fits in the hierarchical clustering framework.

Although in the sequel we will mainly use the Press & Schechter mass function, here it is worth mentioning one of its main drawback. In fact, high resolution N-body simulations (see, e.g., [93]) show the Press & Schechter formula to provide acceptable results at the high mass end, but to largely overpredict the number of small objects. This discrepancy can be substantially reduced on considering that a realistic collapse is likely to be ellipsoidal, rather than spherical. Even in this case it is possible to work out an approximate expression of the mass function, which

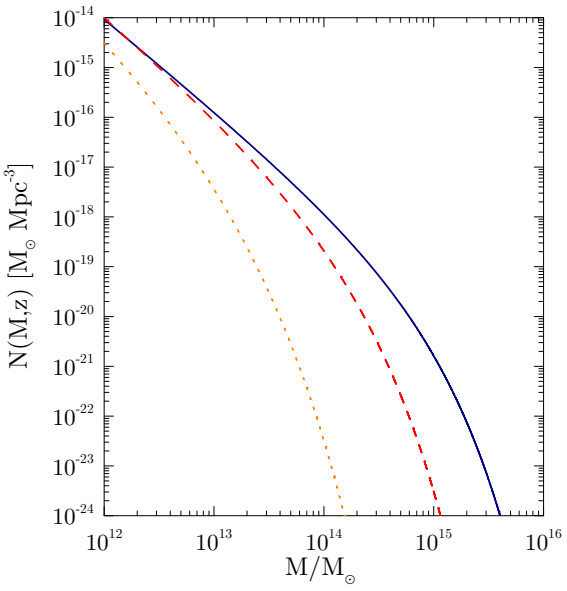

Fig. 1.11 The Press & Schechter mass function at $z = 0$ (*solid* line), at $z = 1$ (*dashed* line) and at $z = 3$ (*dotted* line); evolution computed in the Concordance Cosmology.

reads [179]

$$N(M,z) = A\,\bar{\rho}\sqrt{\frac{2\,a}{\pi}}\,\frac{\delta_c(z)}{M_{c0}^2}\left|\frac{d\ln\sigma}{d\ln m}\right|\,\frac{m^{-2}}{\sigma(m)}\,\left[1+\left(\frac{\sigma^2}{a\,\delta_c^2(z)}\right)^p\right]\times$$

$$\times\,\exp\left[-a\,\frac{\delta_c^2(z)}{2\,\sigma^2(m)}\right]\,. \tag{1.47}$$

The average values of the fitting coefficients $A = 0.3222$, $a = 0.707$ and $p = 0.3$ are obtained from comparison with N-body simulations [178].

Now we move to extend the above results to compute the *conditional probability* distribution $dP(m', z'|m, z)/dm'$ that an object with mass m at a given redshift z had a progenitor of mass m' at z'. The solution is easily found on considering that in terms of Markovian random walks nothing changes in respect to the previous situation but the source of trajectories, which is now moved from the origin to the point $[\delta_c(z'), S' = \sigma^2(m')]$. The result comes to [104]

$$\frac{dP}{dm'}(m', z'|m, z) = \frac{1}{\sqrt{2\,\pi}}\,\frac{\delta_c(z') - \delta_c(z)}{[\sigma^2(m') - \sigma^2(m)]^{3/2}}\,\frac{m}{m'}\,\times$$

$$\times\left|\frac{d\sigma^2}{dm'}(m')\right|\,\exp\left\{-\frac{1}{2}\,\frac{[\delta_c(z') - \delta_c(z)]^2}{\sigma^2(m') - \sigma^2(m)}\right\}\,. \tag{1.48}$$

In turn, this is easily related by the Bayes theorem to the probability distribution

per unit time that at a given epoch z a progenitor increases its mass m' by a merging event with a lump of mass Δm to produce a final object of mass $m = m' + \Delta m$. Such a *merging rate* writes down as [22]

$$\frac{d^2P}{d\Delta m\, dz}(m' \to m) = \sqrt{\frac{2}{\pi}} \left| \frac{d\ln D(z)}{dz} \right| \left| \frac{d\ln \sigma}{dm}(m) \right| \times$$
$$\times \frac{\delta_c(z)}{\sigma(m)} \frac{1}{[1-\sigma^2(m)/\sigma^2(m')]^{3/2}} \times$$
$$\times \exp\left\{ -\frac{\delta_c^2(z)}{2} \left[\frac{1}{\sigma^2(m)} - \frac{1}{\sigma^2(m')} \right] \right\} . \qquad (1.49)$$

Strictly linked to Eq. (1.48) is also the statistical distribution of formation epochs; this may be defined as the probability for an object of mass m at redshift z to have had a mass $m/2$ for the first time at redshift z_f. A very good fitting formula of such a distribution is given by [100]

$$\frac{\partial P}{\partial z_f}(m, z_f, z) = \frac{\partial \omega_f}{\partial z_f} \left[\frac{A(\alpha)}{1 + C(\alpha)\,\omega_f} e^{-5\,\omega_f^2} + 2\,B(\alpha)\,\omega_f\, \mathrm{erfc}\left(\frac{\omega_f}{\sqrt{2}} \right) \right] \qquad (1.50)$$

in terms of the parameters

$$\omega_f = \frac{\delta_c(z_f) - \delta_c(z)}{\sqrt{\sigma^2(m/2) - \sigma^2(m)}}$$
$$\alpha = n\,(0.6268 + 0.3058\,n) , \qquad (1.51)$$

and of the fitting functions

$$A(\alpha) = \sqrt{\frac{8}{\pi}}\,(1-\alpha)\,(0.0107 + 0.0163\,\alpha)$$
$$B(\alpha) = 1 - \frac{1-\alpha}{25}$$
$$C(\alpha) = \frac{2}{A(\alpha)} \left[B(\alpha) - \frac{2^\alpha - 1}{\alpha} \right] . \qquad (1.52)$$

The main consequences of the above expressions may be summarized as follows: (i) the minor merging events (those between two structures quite different in mass) are more numerous than major merging ones; (ii) the mass accretion rate is equally contributed from minor and major merging events; specifically half the final mass M of a given object is provided by the main progenitor, and half by lumps with masses in the range from $M/20$ to $M/3$; (iii) large objects (compared to the characteristic mass) survive for a limited time, about half the age of the Universe at the time

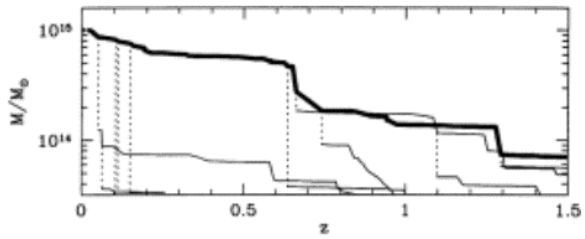

Fig. 1.12 A merging tree for a final object of $10^{15}\, M_\odot$. Figure taken from [38].

of formation; (iv) small objects have widely distributed survival times, so that a relevant number of them can survive for several Hubble times.

The expressions (1.48), (1.49) and (1.50) may be implemented in Montecarlo schemes to build merging trees (see [98]; [52]), i.e., numerical realizations of the *merging histories* undergone by virialized DM condensations; an example is illustrated in Fig. 1.12.

Chapter 2

Cosmic Structures

So, Nat'ralists observe, a Flea
Hath smaller Fleas that on him prey;
And these have smaller still to bite 'em;
And so proceed ad infinitum.

- Jonathan Swift: *On Poetry: A Rhapsody* –

This Chapter is devoted to discuss some properties of the DM and baryonic content framing the cosmic structures that populate our Universe. We will show that the DM is closely *scale-invariant*, while the baryons are found to behave quite differently at the various scales owing to their "strongly collisional" nature.

2.1 Dark matter: closely scale invariant

Cosmic structures are gravitationally dominated by relatively high amounts of (cold) DM, which drives their hierarchical formation and evolution. Random initial perturbations condense and virialize under the action of self-gravity over progressively larger scales. Once formed these DM *halos* do not remain secluded, rather grow in size and mass by continuous merging events with comparable clumps and accretion of much external matter. As in this process only *weak gravity* is active, nearly scale-invariant features and closely self-similar profiles are expected.

2.1.1 *Scaling laws*

The scale-invariant nature of DM may be highlighted on considering how the characteristic quantities of a halo scale with mass and redshift. For example, the DM density ρ_{DM} is a merely amplified copy of the background's $\bar{\rho} = \rho_c\,(\Omega_M/\Omega_z)\,(1+z)^3$, or

$$\rho_{DM} = \Delta_{\rm vir}\,\bar{\rho} \approx 4.97\times 10^{13}\,h^2\,\frac{M_\odot}{{\rm Mpc}^3}\,\left(\frac{\Delta_{\rm vir}(z)}{18\,\pi^2}\,\frac{\Omega_M}{\Omega_z}\right)\,(1+z)^3\ ; \qquad (2.1)$$

note that the dependence on the redshift slightly differs from $(1+z)^3$ in the Concordance Cosmology, owing to the presence of the dark energy. The latter actually causes a minor breaking of the DM scale-invariance, because it becomes important only for $z \lesssim 1$.

The halo spatial extent is specified by the *virial radius*, which is trivially related to the mass by the geometric relation $R_v = (3\,M_{DM}/4\,\pi\,\rho_{DM})^{1/3}$ and reads

$$R_v \approx 1.7\,h^{-1}\,\mathrm{Mpc}\,\left(\frac{M_{DM}}{10^{15}\,h^{-1}\,M_\odot}\right)^{1/3}\,\left(\frac{\Delta_{\rm vir}(z)}{18\,\pi^2}\,\frac{\Omega_M}{\Omega_z}\right)^{-1/3}\,(1+z)^{-1}\ . \qquad (2.2)$$

The *circular velocity* $v_v \equiv \sqrt{G\,M_{DM}/R_v}$ is defined through the centrifugal-force balance equation and scales as

$$v_v \approx 1620\,\frac{\mathrm{km}}{\mathrm{s}}\,\left(\frac{M_{DM}}{10^{15}\,h^{-1}\,M_\odot}\right)^{1/3}\,\left(\frac{\Delta_{\rm vir}(z)}{18\,\pi^2}\,\frac{\Omega_M}{\Omega_z}\right)^{1/6}\,(1+z)^{1/2}\ . \qquad (2.3)$$

We will often have occasion to use the DM 1-D *velocity dispersion* σ_v, defined in a such way that the total kinetic energy of the system is $3\,M_{DM}\,\sigma_v^2/2$. The relation between σ_v and v_v depends on the detailed shape of the profile, that we are going to discuss in the next §; here we just note that $v_v = \sqrt{2}\,\sigma_v$ holds in the simple case $\rho_{DM}(r) \propto r^{-2}$.

Finally, the halo *dynamical timescale* $t_{\rm dyn} \equiv R_v/v_v$ takes on values

$$t_{\rm dyn} \approx 1\,h^{-1}\,\mathrm{Gyr}\,\left(\frac{\Delta_{\rm vir}(z)}{18\,\pi^2}\,\frac{\Omega_M}{\Omega_z}\right)^{-1/2}\,(1+z)^{-3/2}\ . \qquad (2.4)$$

2.1.2 *Radial profiles*

As anticipated at the beginning of the §, the DM halos have nearly self-similar radial profiles, differing from each other only via a global rescaling. Many numerical works support this statement (see Fig. 2.1); in fact, they provide evidence for an apparent *universality* of the DM profiles, valid over several orders of magnitude in mass.

We will focus on the widely used, analytical expression of the DM density profile proposed by Navarro, Frenk & White (NFW, [138]) on the basis of their numerical simulations. It reads

$$\rho_{DM}(r) \equiv \frac{\rho_s}{\dfrac{r}{r_s}\left(1+\dfrac{r}{r_s}\right)^2}\ , \qquad (2.5)$$

in terms of the characteristic density ρ_s and of the scale radius r_s. Introducing the *concentration* parameter $c \equiv R_v/r_s$, the NFW profile may be recast as

$$\rho_{DM}(r) = \rho_c\,\frac{\Delta_{\rm vir}}{3}\,\frac{c^2\,g(c)}{s\,(1+cs)^2}\ , \qquad (2.6)$$

Fig. 2.1 The optical emissions (*top*) and the rescaled DM skeletons (*bottom*) of a Milky-way like galaxy (*right*) and a Coma-like cluster of galaxies (*left*), as extracted from a numerical simulation. The picture is intended to show the closely scale-invariant behavior of DM structures. Credit: B. Moore, `http://www.nbody.net`

in terms of the adimensionalized radial coordinate $s \equiv r/R_v$ and of the shorthand

$$g(c) \equiv \left[\ln(1+c) - \frac{c}{1+c}\right]^{-1} \quad . \tag{2.7}$$

Note that the logarithmic slope $-(1+3\,cs)/(1+cs)$ is equal to -2 at $r = r_s$.

The concentration parameter c describing the shape of the density profile introduces another minor deviation from scale-invariance because it depends inversely on the DM mass; this is because on average smaller structures have formed at earlier epochs, when the density of the Universe was higher. The recent cosmological simulations suggest [31]

$$c \approx \frac{9}{1+z}\left(\frac{M_{DM}}{10^{13}\,h^{-1}\,M_\odot}\right)^{-0.13} \quad ; \tag{2.8}$$

note that the scatter around the mean is quite wide already at the 1-sigma level (see Fig. 2.2).

The mass enclosed within a sphere of radius r is found by straightforward integration to read

$$\frac{M_{DM}(<r)}{M_{DM}} = g(c)\,\left[\ln(1+cs) - \frac{cs}{1+cs}\right] \ , \tag{2.9}$$

in terms of the virial value M_{DM}. The gravitational potential corresponding to that

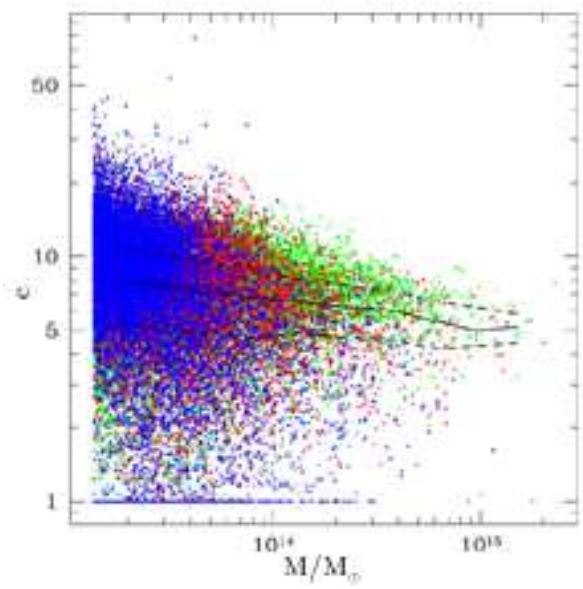

Fig. 2.2 The concentration parameter as a function of halo mass. Figure kindly provided by G. Tormen (INAF, Padua Astronomical Observatory).

mass distribution is

$$\Phi(r) = -v_v^2\, g(c)\, \frac{\ln(1+cs)}{s}\ ; \tag{2.10}$$

hence we see that at the center $\Phi(0) = -c\, g(c)\, v_v^2$ is finite (see Fig. 2.3).

From the previous expression it is also easy to compute the circular velocity profile, that obeys

$$\frac{v^2(r)}{v_v^2} = \frac{g(c)}{s}\ \left[\ln\left(1+cs\right) - \frac{cs}{1+cs}\right]\ . \tag{2.11}$$

The 1-D velocity dispersion profile can be found on solving the *Jeans equation*

$$\frac{1}{\rho}\frac{d}{dr}(\rho\,\sigma_r^2) + \frac{2}{r}\,(\sigma_r^2 - \sigma_\theta^2) = -\frac{d}{dr}\,\Phi\ , \tag{2.12}$$

supplemented by the boundary condition $\sigma(r) \to 0$ for $s \to \infty$. For isotropic orbits with equal tangential (σ_θ) and radial (σ_r) dispersions, the result is [115]

$$\frac{\sigma^2(r)}{v_v^2} = \frac{1}{2}c^2\, g(c)\, s\,(1+cs)^2\ \left[\pi^2 - \ln(cs) - \frac{1}{cs} - \frac{1}{(1+cs)^2} - \frac{6}{1+cs} + \left(1 - \frac{4}{cs} + \right.\right.$$
$$\left.\left. +\ \frac{1}{c^2\, s^2} - \frac{2}{1+c\,s}\right)\ \ln(1+cs) + 3\ln^2(1+cs) + 6\,\mathrm{Li}_2(-cs)\right] \tag{2.13}$$

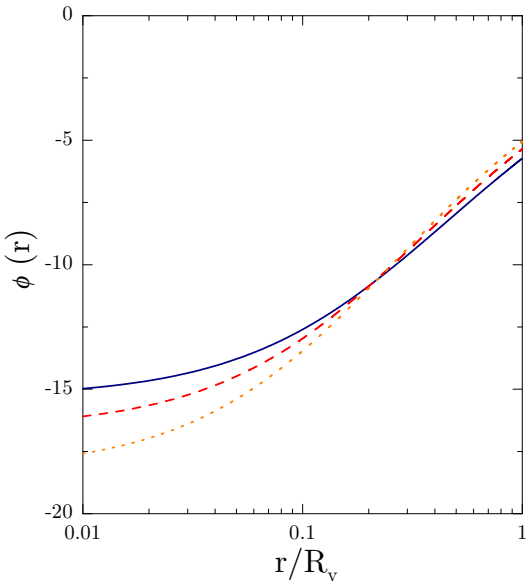

Fig. 2.3 The NFW potential normalized to σ_v^2 for a rich cluster of $k_B T_v = 8$ keV (*solid* line), a poor cluster of $k_B T_v = 2$ keV (*dashed* line) and a group with $k_B T_v = 0.5$ keV (*dotted* line).

in terms of the special function (the dilogarithm)

$$\mathrm{Li}_2(x) = \int_x^0 dt\, \frac{\ln(1-t)}{t} \simeq x \left[1 + 10^{-0.5}(-x)^{0.62/0.7}\right]^{-0.7} \quad ; \qquad (2.14)$$

the last approximation is accurate to better than 1.5% in the range $-100 < x < 0$. At the virial radius one has $v_v^2 \approx 2.7\,\sigma_v^2$, even if the exact coefficient depends slowly on the concentration parameter [53].

2.2 Baryons ≠ scale-invariant!

At a first glance, one would expect the baryons to evolve passively following the gravitationally dominant DM component, and so to be scale-invariant. But several observations in the X-ray, optical and radio/submm bands show this not to be true. The reason is that during/after the fall into the DM potential wells the baryons are driven away from scale-invariance by many *non-adiabatic* processes, such as radiative cooling, condensation into stars or black holes, and heating by astrophysical sources or by gravitationally-driven shocks.

2.2.1 *Diffuse baryons*

Cosmic structures contain large masses $f_{\rm gas}\, M_{DM} \lesssim (\Omega_b/\Omega_M)\, M_{DM} \approx 0.15\, M_{DM}$ of diffuse baryons. The latter constitute a hot, highly ionized "plasma" phase often referred to as the *intracluster medium* (ICM; see Fig. 2.4).

Such gaseous baryons reside in approximate virial equilibrium within the DM potential well, at specific energies close to the virial values

$$k_B T_v \approx 5.3\,{\rm keV} \left(\frac{M_{DM}}{10^{15}\, h^{-1}\, M_\odot}\right)^{2/3} \left(\frac{\Delta_{\rm vir}(z)}{18\,\pi^2}\,\frac{\Omega_M}{\Omega_z}\right)^{1/3} (1+z)\ . \tag{2.15}$$

These are good measures of the DM well depths, since the equipartition of energy states $k_B T_v = \mu m_p\, \sigma_v^2$, with $\mu \approx 0.6$ the mean molecular weight for a plasma of nearly cosmic composition.

In fact, the ICM is settled to *hydrostatic equilibrium* within the DM potential wells, and its steady distribution may be obtained from the Euler equation

$$\frac{1}{m_p\, n}\,\frac{dp}{dr} = -\frac{d\Phi}{dr}\ , \tag{2.16}$$

supplemented by the boundary condition $n(R_v) = n_2$. The gas number density n, the pressure p and the actual temperature T are not independent, rather are related by the Boyle's law $p = n\, k_B T/\mu$. But to close the differential Eq. (2.16) a further local relation between $n(r)$ and $T(r)$ is needed.

The simplest assumption states the gas to be *isothermal*, i.e., $T(r) \approx$ const; then the density runs as

$$n(r) = n_2\, e^{\beta\, \Delta\phi(r)}\ . \tag{2.17}$$

Here $\Delta\phi(r) = [\Phi(R_v) - \Phi(r)]/\sigma_v^2$ is the adimensionalized potential difference and

$$\beta \equiv \frac{\mu m_p\, \sigma_v^2}{k_B T} = \frac{T_v}{T} \tag{2.18}$$

is the ratio between the plasma and the DM scale heights [94]. If the DM is also distributed with constant $\sigma(r) = \sigma_v$, then from the Jeans equation $\rho_{DM}(r) \propto e^{\Delta\phi}$ holds and the standard β-model $n(r) \propto \rho_{DM}^{\beta}(r)$ obtains [35]. This is not the case with the NFW potential, for which the equilibrium reads [121]

$$\frac{n(r)}{n_2} = \left[\frac{(1+cs)^{1/s}}{1+c}\right]^{v_v^2\, \beta\, g(c)/\sigma_v^2}\ . \tag{2.19}$$

Although X-ray observations indicate the intragroup medium to be closely isothermal ([157]; [162]), a slow decrease of temperature with radius in clusters has been observed both in the sky (e.g., [66]; [123]; [70]; [62]) and in the simulations (see, e.g., [29]; [81] and references therein). This may be described by a *polytropic* assumption $p(r) \propto n^\Gamma(r)$ in terms of the macroscopic adiabatic index Γ; the latter has to be in the range $1 \le \Gamma \le 5/3$, otherwise the gas temperature would rise with

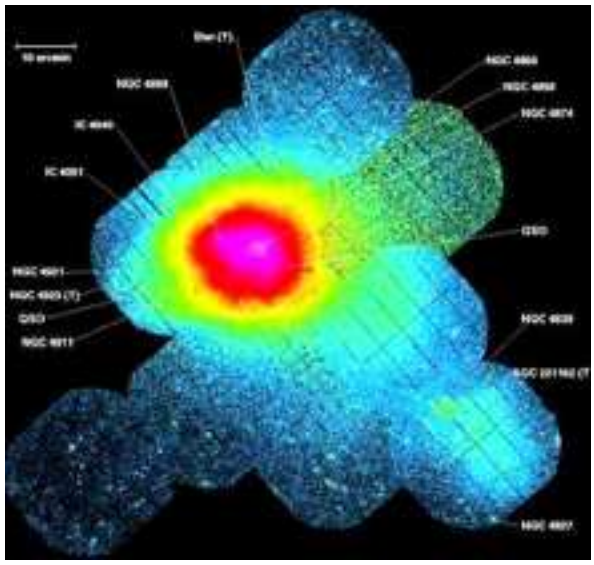

Fig. 2.4 The Coma cluster and an infalling group as seen in X-rays by XMM-Newton. Credit: ESA/U. Briel.

radius ($\Gamma < 1$) or the plasma would not be stable to convection ($\Gamma > 5/3$). In fact, the observations mentioned above indicate $\Gamma \approx 1.1$ up to 1.2 in hot clusters; the corresponding equilibrium follows

$$\frac{n(r)}{n_2} = \left[\frac{T(r)}{T_2}\right]^{1/(\Gamma-1)} = \left[1 + \frac{\Gamma-1}{\Gamma}\,\beta\,\Delta\phi(r)\right]^{1/(\Gamma-1)} , \tag{2.20}$$

where $\beta = T_v/T_2$ is now written in terms of the temperature T_2 at R_v.

The behavior of the gas density run for $r \to 0$ may be found from Eq. (2.16) basing on the corresponding asymptotic slope of the DM profile. Concerning this issue it is worthwhile to retain generality because some recent, high-resolution numerical works have shown that the halo core was not completely resolved in the NFW simulations [84]. Suppose that $\rho_{DM}(r) \propto r^{-\alpha}$ for $r \to 0$. Then the gas density profile at the center is regular for $\alpha \geq -1$; in particular, it is flat for $\alpha > -1$, and angled for $\alpha = -1$ (the NFW case). For $\alpha \leq -1$ it progressively takes on a more singular behavior, showing a cusp (finite value but infinite derivative) for $-2 < \alpha < -1$, and a vertical asymptote for $\alpha \leq -2$.

The diffuse baryonic component pervading galaxies, groups and clusters may be efficiently probed by its copious X-ray emission, mainly originated by *thermal bremsstrahlung* for $k_B T_v \gtrsim 2$ keV, but with an increasing contribution from *emission lines* toward cooler systems. The full form of the cooling function at every T is well

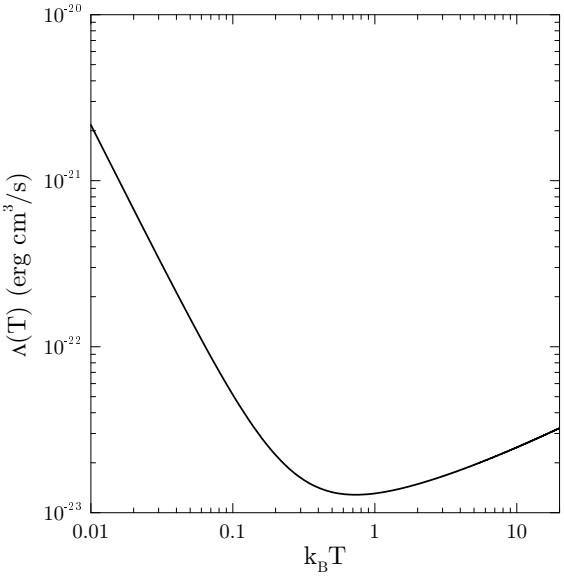

Fig. 2.5 The cooling function for a plasma of 0.3-solar metallicity.

fitted by [189]

$$\Lambda(T) \approx 10^{-22} \, \frac{\mathrm{erg\ cm^3}}{\mathrm{s}} \, \left[C_1 \left(\frac{k_B T}{\mathrm{keV}} \right)^a + C_2 \left(\frac{k_B T}{\mathrm{keV}} \right)^b + C_3 \right] \tag{2.21}$$

with parameters:

$$a = -1.7 \qquad b = 0.5 \qquad C_1 = 8.6 \times 10^{-3} \qquad C_2 = 5.8 \times 10^{-2} \qquad C_3 = 6.4 \times 10^{-2} \ .$$

This behaves as $\Lambda(T) \propto T^\epsilon$ with $\epsilon \approx 1/2$ for $k_B T \gtrsim 1$ keV, $\epsilon \approx 0$ for $k_B T \sim 1$ keV, $\epsilon \approx -1/2$ for $0.1 \lesssim k_B T \lesssim 1$ keV, and $\epsilon \approx -1$ for very low $k_B T \lesssim 0.1$ keV (see also Fig. 2.5).

The corresponding X-ray luminosity reads [175]

$$L_X = 4\pi \int_0^{R_v} dr \, r^2 \, n^2(r) \, \Lambda[T(r)] \ ; \tag{2.22}$$

in clusters with sizes $R_v \sim 2$ Mpc and temperatures $k_B T \sim 5$ keV, the X-ray power attains $L_X \sim 10^{45 \pm 1}$ erg s^{-1}. The inferred average densities are around $n \sim 10^{-3}$ cm^{-3}, implying that: (i) The ICM is the best *plasma* ever in the Universe, because the condition $k_B T / e^2 n^{1/3} \gg 1$ is satisfied by a factor 10^{11}, even larger than for the primordial medium pervading the cosmo before the recombination epoch; (ii) the thermal energy $E \sim n \, T \, R^3 \sim 10^{62}$ ergs of the ICM is so huge that, despite

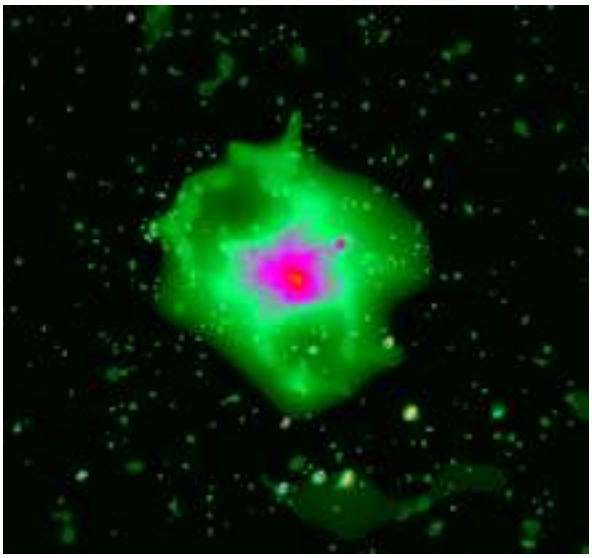

Fig. 2.6 The compact group of galaxies HCG62 as seen in X-rays by CHANDRA. Credit: NASA/CfA/J. Vrtilek.

the strong luminosities emitted, the cooling time $t_{\rm cool} \sim E/L_X \gtrsim t_H$ is on average longer than the age of the Universe $t_H \sim 13.7$ Gyr.

But then one question naturally arises: How did the diffuse baryons acquire their thermal state? A simple answer is provided by the scale-invariant framework [96], which traces the origin of the gas temperature T_2 back to the process of hierarchical buildup. In fact, the baryonic content of merging DM halos undergoes strong shocks and is heated up while supersonically falling into the forming potential wells, taking on densities $n_2 = 4\, n_1 = 4\, f_{\rm gas}\, (\rho_{DM}/m_p)$ proportional to the background's $\bar{\rho}_{DM}$.

Assuming negligible pressure of the accreting gas and efficient conversion of the infall kinetic energy into heat provides the gas temperature

$$k_B T_2 = \frac{1}{3}\, \mu m_p\, v_1^2 \tag{2.23}$$

in terms of the infall velocity v_1. This is in turn determined by the DM gravitational potential through energy conservation, which yields

$$v_1 = \sqrt{-2\, \xi\, \Phi(R_v)}\ ; \tag{2.24}$$

the parameter $\xi = 1 - R_v/R_f$ expresses our ignorance on the exact position of the radius $R_f \gtrsim R_v$ at which nearly free fall begins. The upper bound $\xi \approx 0.7$ is obtained by equating the Hubble-flow to the free-fall velocity, while the lower limit $\xi \approx 0.3$ is found on imposing the accretion to begin at the turnaround radius (see

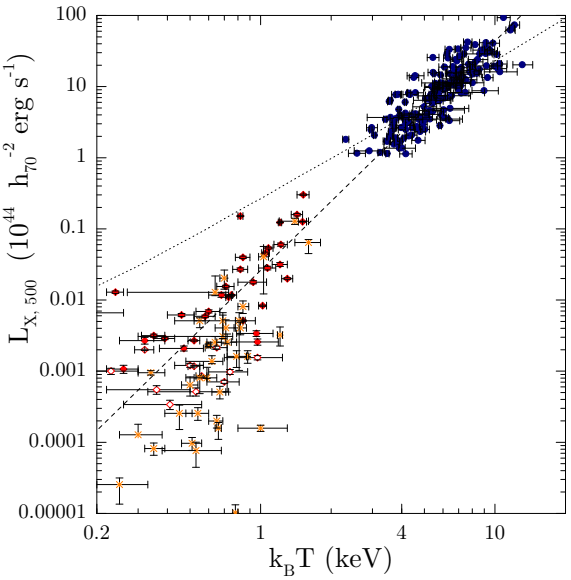

Fig. 2.7 The integrated X-ray luminosity (out to $\sim 2\,R_v/3$) vs. X-ray temperature. Data for clusters (*circles*) are from [92]. Data for groups are from [142]: *Filled diamonds* mark X-ray emission from a group potential and *open diamonds* from a galactic halo. Data for early-type galaxies (*stars*) are from [144]. The *dotted line* is the gravitational scaling, while the *dashed line* is the best fit correlation to the cluster and group data.

also [11]). Collecting the previous results together leads to

$$k_B T_2 = k_B T_v \, \frac{-2\,\xi}{3} \, \phi(R_v) \; , \tag{2.25}$$

with $\phi = \Phi/\sigma_v^2$. Therefore in this scenario the temperature of the diffuse baryons $k_B T_2 \propto k_B T_v$ would be determined by the deepening of the DM potential wells during the hierarchical buildup. The observations of the ICM in rich clusters indicate $\beta = T_v/T_2 \approx 0.7$, while we predict $\beta \approx 0.26/\xi$, because with $c \approx 5$ the NFW potential at the virial radius reads $-\phi(R_v) \approx 5.7$. Pleasingly, the resulting value $\xi \approx 0.37$ is within the bounds given above.

On the other hand, the observations of X-ray surface brightness profiles [156] show that in moving toward poor groups (see, e.g., Fig. 2.6) and galaxies β decreases down to values around 1/2; such a trend can not be understood within the scale-invariant picture, because $-\phi(R_v)$ decreases slowly for increasing concentration and β would be, if anything, slightly higher in the smaller (and earlier) objects.

Furthermore, under scale-invariant conditions the X-ray luminosity is expected to follow the *gravitational scaling* law [97]

$$L_{\rm grav} \propto n^2 \, R_v^3 \, T^\epsilon \propto \left(\frac{\Delta_{\rm vir}(z)}{18\,\pi^2} \, \frac{\Omega_M}{\Omega_z} \right)^{1/2} (1+z)^{3/2} \, T_v^{\epsilon+3/2} \; , \tag{2.26}$$

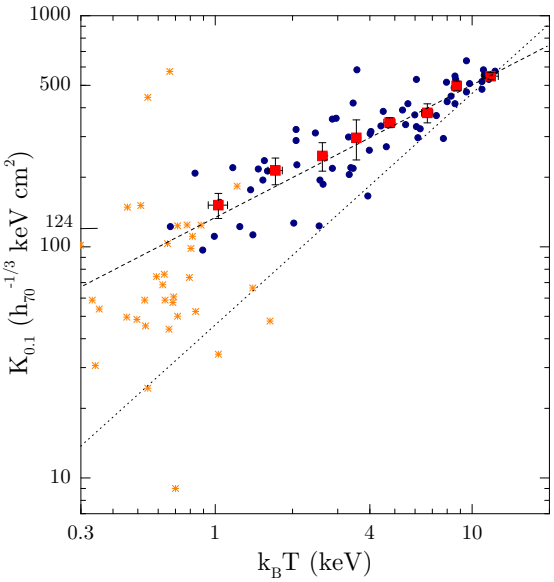

Fig. 2.8 The entropy (measured at $0.1\,R_v$) vs. X-ray temperature. Data for clusters and groups (*circles*: individuals without error bars, *squares*: binned) are from [157], and data (without errors) for early-type galaxies (*stars*) are from [144]. The *dotted line* is the gravitational scaling, while the *dashed line* is the best fit correlation to the binned data in clusters and groups.

i.e., $L_{\rm grav} \propto T_v^2$ for brems-dominated and $L_{\rm grav} \propto T_v$ for line-dominated emission. The above stems on assuming $n/\rho_{DM} \approx$ const., $T \approx T_v$ and

$$R \approx R_v \propto \left(\frac{\Delta_{\rm vir}(z)}{18\,\pi^2}\,\frac{\Omega_M}{\Omega_z}\right)^{-1/2} (1+z)^{-3/2}\,T_v^{1/2}\ . \tag{2.27}$$

But the envisaged trend contrasts with the observed $L_X - T$ correlation, which has a shape like $L_X \propto T^3$ already at the scales of richness 1 clusters (see Fig. 2.7; [124], [4], [92]). In groups pioneering works by [90] claimed that $L_X \propto T_v^{4.5}$ would steepen further; these have been superseded by more recent data (see [142]) that show the correlation to be consistent with a single slope $L_X \propto T_v^{3.3}$ throughout the relevant temperature range, but with a widening, intrinsic scatter of non-Gaussian nature toward smaller scales [144].

The very same X-ray observations may be recast in terms of a more physically appealing quantity, namely, the gas *specific entropy* s. As it has become customary in this context, we will use the *adiabat*

$$K \equiv \frac{k_B T}{n^{2/3}} \equiv \frac{h^2}{2\pi\,\mu m_p}\,\exp\left(\frac{2}{3}\,\frac{s}{k_B} - \frac{5}{3}\right) \tag{2.28}$$

as a measure of the thermodynamic entropy [23]. This is the only combination of n and T that is invariant under adiabatic transformations of the gas.

According to the scale-invariant picture, the quantity K should follow

$$K_{\rm grav} \propto \left(\frac{\Delta_{\rm vir}(z)}{18\,\pi^2}\,\frac{\Omega_M}{\Omega_z}\right)^{-2/3} (1+z)^{-2}\,T_v\ . \tag{2.29}$$

But the X-ray observations indicate that the entropy (measured at $R_v/10$) scales as $K_{0.1} \propto T^{0.57}$, and hence in groups attains values largely exceeding those predicted by Eq. (2.30), see also Fig. 2.8. Some authors addressed the possibility of an *entropy floor*, i.e., a lower limit around $k_B T/n^{2/3} \approx 124\,h_{70}^{-1/3}$ keV cm^2 to the entropy a collapsed system can have [113]; this notion appears not to be confirmed by the most recent data [157]. In any case, the entropy excess requires a density deficit at constant or increased T/T_v, and constitutes clear evidence for the action of strongly *non-adiabatic* processes on the diffuse baryonic component. Remarkably, the X-ray luminosity deficit and entropy excess can be linked by the *model-independent* relation [43]

$$\frac{K}{K_{\rm grav}} \propto \left(\frac{L_X}{L_{\rm grav}}\right)^{-1/3} \left(\frac{T}{T_v}\right)^{1+\epsilon/3}\ , \tag{2.30}$$

obtained on eliminating n from the standard definitions; in the above we have neglected slowly T-dependent shape factors.

On the other hand, large observational uncertainties at the scales of groups and

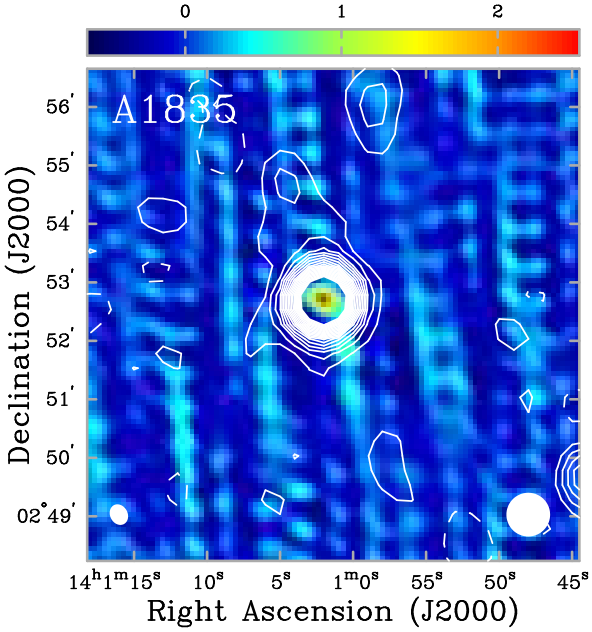

Fig. 2.9 The cluster Abell 1835 mapped in SZ by BIMA. Figure taken from [163].

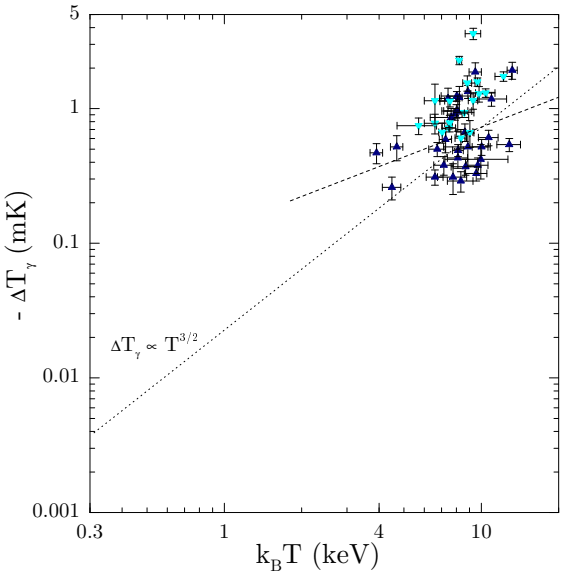

Fig. 2.10 The central SZ decrement as measured in clusters of galaxies. Data (*triangles*) are from [215] and from [163]. The *dashed line* is the best fit to the existing data, while the *dotted line* is the gravitational scaling.

galaxies, systematics concerning especially single galaxy subtractions, and selection effects, have all been stressed several times by many authors (e.g., [120], [171]). Thus, observationally independent probes of the same physics are welcome; we consider an intriguing one to be constituted by the thermal *Sunyaev-Zel'dovich* (SZ) effect [187].

This is originated when the hot ICM electrons inverse Compton scatter some CMBR photons crossing the structure, and tilt the pure black-body spectrum of the cosmic radiation toward higher energies. For non-relativistic electrons, the relative temperature change of the CMBR photons reads [188]

$$\left(\frac{\Delta T}{T}\right)_\gamma = \frac{x^2\, e^x}{(e^x-1)^2}\left[x\,\coth\left(\frac{x}{2}\right)-4\right]\, y\ , \tag{2.31}$$

where $x = h\nu/k_B T_\gamma$ is a dimensionless measure of the frequency ν. The intensity of the SZ effect is quantified by the *Comptonization parameter*

$$y = 2\,\frac{\sigma_T}{m_e c^2}\int d\ell\, p_e(r)\ , \tag{2.32}$$

defined in terms of the electron pressure $p_e = n\, k_B T$ integrated along a line of sight, and so evenly contributed by the density n and temperature T. At μwave frequencies the result translates into an apparent temperature diminution $\Delta T_\gamma \approx -5.5\, y$ K,

proportional to $y \propto n\,T\,R$. To now, SZ signals have been measured in many clusters at levels $y \approx 10^{-4}$ or $\Delta T_\gamma \approx -0.5$ mK (see Fig. 2.9; [166], [12], [215], [163]).

Scale-invariance would imply the gravitational scaling [51]

$$y_{\rm grav} \propto \left(\frac{\Delta_{\rm vir}(z)}{18\,\pi^2}\,\frac{\Omega_M}{\Omega_z}\right)^{1/2} (1+z)^{3/2}\,T_v^{3/2}\ ; \tag{2.33}$$

will this behavior be retained in poor clusters and groups? Measures at these mass scales are challenging at present, and still missing (see Fig. 2.10).

Nevertheless, the levels of y in groups may be anticipated under equilibrium conditions, on using the information (mainly on n) provided by the X-ray observations of the diffuse baryons. Model-independently, the Compton parameter and the gas entropy in equilibrium are linked by [41]

$$\frac{y}{y_{\rm grav}} \propto \left(\frac{K}{K_{\rm grav}}\right)^{-3/2} \left(\frac{T}{T_v}\right)^{5/2}\ ; \tag{2.34}$$

so for structures where $K \gtrsim K_{\rm grav}$ holds, one may expect also some deficit in y to occur [65].

2.2.2 *Condensed baryons*

The diffuse baryonic component may cool owing to several processes. In principle, one way is through the same mechanism that originates the SZ effect. The Compton cooling timescale reads [173]

$$t_{\rm Comp} = \frac{3\,m_e\,m_p\,(1+z)^4}{8\,\mu\,\sigma_T\,\Omega_\gamma\,\rho_c} \approx 2.1\times 10^{12}\,(1+z)^{-4}\,{\rm yr}\ , \tag{2.35}$$

and its ratio to the dynamical time $t_{\rm dyn}$ is

$$\frac{t_{\rm Comp}}{t_{\rm dyn}} \approx 2\times 10^2\,(1+z)^{-5/2}\ . \tag{2.36}$$

This kind of cooling is efficient only at high redshifts $z \gtrsim 7$, independently of the halo mass; so it is not of much relevance for our discussion.

At the lower z we are interested in here, cooling is mainly due to the same X-ray radiation we have discussed in the previous §. It occurs on timescales

$$t_{\rm cool} \equiv \frac{3\,k_B T}{2\,\mu\,n\,\Lambda(T)}\ , \tag{2.37}$$

given by the ratio between the gas thermal energy and the X-ray emissivity. The efficiency of the process is determined by the ratio $t_{\rm cool}/t_{\rm dyn}$ of the cooling timescale $t_{\rm cool} \propto T^{1-\epsilon}/n$ to the dynamical one $t_{\rm dyn} \propto 1/\sqrt{\rho_{DM}}$. If $t_{\rm cool} \lesssim t_{\rm dyn}$ the baryons can cool, condense at the center of the DM potential well, and eventually form stars.

In massive structures where bremsstrahlung dominates the emission, the relevant ratio reads

$$\frac{t_{\rm cool}}{t_{\rm dyn}} \approx \frac{90\,h^{-1}}{1+z}\left(\frac{M_{DM}}{10^{15}\,h^{-1}\,M_\odot}\right)^{1/3}\left(\frac{f_{\rm gas}}{0.15}\right)^{-1}\left(\frac{T}{T_v}\right)^{1/2}\left(\frac{\Delta_{\rm vir}(z)}{18\,\pi^2}\,\frac{\Omega_M}{\Omega_z}\right)^{-1/3}, \tag{2.38}$$

so that cooling is not very efficient in the volume of clusters and groups. An exception concerns the inner regions of these structures where the density is higher and the cooling time shorter. There, the gas should slowly move toward the center constituting a *cooling flow* [71]; the related observational evidence, however, is still highly controversial [64]. It is possible that such a phenomenon is suppressed by the activity of a central radiosource, see also Chapter 4.

On the other hand, in smaller structures where line emission is important one obtains

$$\frac{t_{\rm cool}}{t_{\rm dyn}} \approx \frac{M_{DM}}{10^{12}\,M_\odot}\left(\frac{f_{\rm gas}}{0.15}\right)^{-1}\left(\frac{T}{T_v}\right)^{3/2}. \tag{2.39}$$

This explains why the fraction of condensed baryons is higher in galaxies than in groups and clusters ([59]; see also [171] and [112]).

We conclude from the previous considerations that the action of radiative cooling depends strongly on the mass scale, and certainly contributes to drive galactic structures away from scale-invariance. Its impact on groups and clusters is instead much more limited, but we postpone to the next Chapter the detailed discussion of this issue. Here we just stress that some form of energy input from stars must have been at work to counteract the high efficiency of radiative cooling at early times (when all densities were larger); otherwise, all the diffuse baryons would have condensed long before the present, originating the so called *cooling catastrophe* (see [208]; [14]).

Another evidence for the "scale-variance" of the condensed baryons comes from the giant black holes with masses $M_\bullet \sim 10^6$ up to few $10^9\,M_\odot$ residing in the galactic cores; in a given halo, they contain a baryon fraction of roughly 10^{-4} the DM mass. If such supermassive black holes were scale-invariant, their total mass should passively follow the hierarchical growth of the DM hosts' $M_{DM} \propto \rho_{DM}\,R_v^3$. Then the gravitational scaling law

$$M_{\bullet\,\rm grav} \propto M_{DM} \propto \left(\frac{\Delta_{\rm vir}(z)}{18\,\pi^2}\,\frac{\Omega_M}{\Omega_z}\right)^{-1/2}(1+z)^{-3/2}\,\sigma_v^3 \tag{2.40}$$

should hold; this relation would indicate a scenario in which black holes evolve by binary coalescence in parallel with the merging of their halos [86].

But the recent data show that $M_\bullet \propto \sigma_v^5$, considerably steeper than the above scale-invariant prediction. This result stems from the tight correlation $M_\bullet \propto \sigma_\star^4$ observed between the massive dark objects detected at the centers of many local galaxies and the velocity dispersions $\sigma_\star$ of the host bulges (see Fig. 2.11; [82], [77],

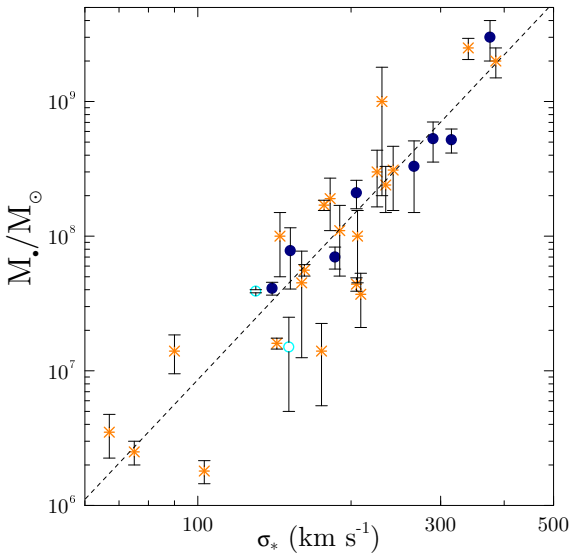

Fig. 2.11 The $M_\bullet - \sigma_\star$ correlation. Data from [197]: masses are obtained from stellar (*stars*), gas (*filled circles*), and maser kinematics (*empty circles*). The *dashed line* is the best fit correlation to the data.

[197]), which in turn are found to correlate $\sigma_\star \propto \sigma_v^{5/4}$ more than linearly [78] with the DM 1-D velocity dispersions.

Chapter 3

Stellar Feedback

No star is ever lost we once
Have seen,
We always may be what we
Might have been.

- Adelaide A. Procter: *Legend of Provence* –

In this chapter we investigate how the diffuse baryons may be driven away from scale invariance by the energy inputs from stars, and in particular from those massive ones which dramatically end their lives exploding as type II supernovae (SNae).

3.1 Feedback from SNae

In the previous Chapter we mentioned that some form of energy input by stars is necessary to avoid the cooling catastrophe. The sources of such a feedback action are naturally identified with the type II SN explosions following the star formation in the galaxy members of groups and clusters. Here we will show that such extra energy inputs provide also steps toward a plausible explanation for the observational features of the intracluster medium.

3.1.1 *Energetics*

Prompt, type II SN explosions canonically release $E_{SN} \approx 10^{51}$ ergs of initial kinetic energy, coupled to the surrounding gas in the form of SN remnants. If isolated the latter are subject to strong radiative losses after some 10^5 yr, but nearly coeval star formation induces galactic superwinds ([25]; [139]; also [153]) and cooperative propagation out to, and beyond the galaxian outskirts ([89]; see Fig. 3.1). However, the issue concerning the effective coupling of the SN energy to the ambient medium is still highly controversial (see, e.g., [192]; [103]); from now on, we will take as our

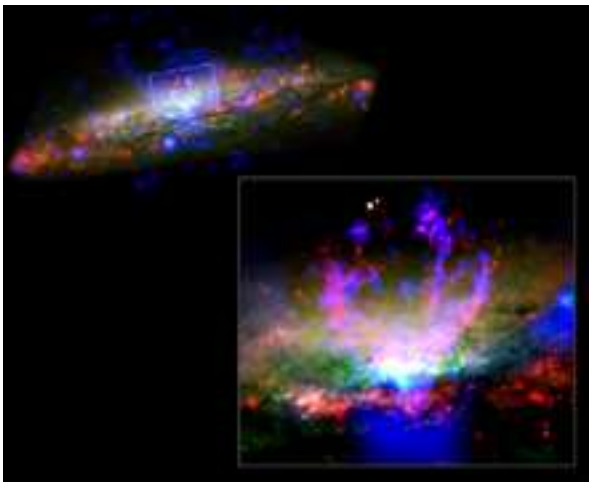

Fig. 3.1 Optical + X-ray image of the spiral galaxy NGC3079. Note the towering filaments of hot gas, originated by a superwind erupting from the galaxy disk. Credit: NASA/CXC/STScI/Univ. North Carolina/G. Cecil.

baseline a maximal coupling efficiency $f_{SN} \lesssim 50\%$.

The energy input from a baryon amount $\Delta m_\star$ converted into stars comes to

$$\Delta E_\star = f_{SN}\, E_{SN}\, \eta_\star\, \Delta m_\star \lesssim 3 \times 10^{48}\, \mathrm{ergs}\, \frac{\Delta m_\star}{M_\odot}\ ; \tag{3.1}$$

here $\eta_\star \lesssim 5 \times 10^{-3}/M_\odot$ represents the standard type II SN occurrence in the initial mass function, and already includes a factor accounting for the contribution of the strong winds from young hot stars [26].

The mechanical action of the feedback is specified by the amount of material Δm_h that can be ejected from the host structure within $t_{\rm dyn}$. Such an ejected mass can be estimated on requiring the actual bulk kinetic energy $q_0\, \Delta E_\star \lesssim 10\%\, \Delta E_\star$ to equal the work $\Delta m_h\, v_v^2/2$ done in moving the gas out of the well. One obtains

$$\Delta m_h = \Delta m_\star \left(\frac{\sigma}{\sigma_h}\right)^{-2}\ , \tag{3.2}$$

where $\sigma_h = q_0\, \eta_\star\, f_{SN}\, E_{SN} \approx 80$ km s^{-1}.

Eq. (3.2) is often used in many numerical works as a phenomenological parameterization (e.g., [184]; [54]; [129]); in the above we have just shown it is physically well motivated (see also [67]). The dynamical effects of SN feedback are not relevant in clusters, groups or even massive galaxies; significant ejected fractions ($\gtrsim 10\%$) are expected only in dwarf galaxies or in smaller objects ([119]; [183]).

However, most of the input fed back from SNae is converted into thermal energy

of the hot gas mass m_h; such an heating amounts to

$$k_B \Delta T_\star = (1 - q_0) \, \frac{\Delta E_\star \, m_p}{3 \, m_h} \approx 0.5 \, \mathrm{keV} \, \frac{\Delta m_\star}{m_h} \ . \tag{3.3}$$

The above temperatures are to be compared with the virial $k_B T_v$. In the way of an average estimate we may substitute the differential quantity $\Delta m_\star$ with the integrated stellar content $m_\star$. Then the SN heating comes to $k_B \Delta T_\star \lesssim 0.25$ keV per particle $\sim k_B T_v$ in groups where $m_\star / m_h \sim 1/2$, and mildly larger values are expected in galaxies; here the heating from SNae can drive the gas to flow out of the potential well.

3.1.2 *Feedback at the 0th order*

Toward modeling, the key question is: How sensitive is the ICM density run to thermal inputs? We discuss the issue at levels of progressively deeper refinement, starting from simple considerations based on hydrostatic equilibrium. Our aim here is to show that the density response to extra-heating undergoes a twofold *deamplification* from clusters to groups. The first stems from the hydrostatics disposition of the plasma in the DM potential well $\Delta\phi$; from § 2.2.1 the density run of an isothermal ICM reads $n(r) = n_2 \, \exp\left[\beta \, \Delta\phi\right]$ in terms of the boundary value n_2 and

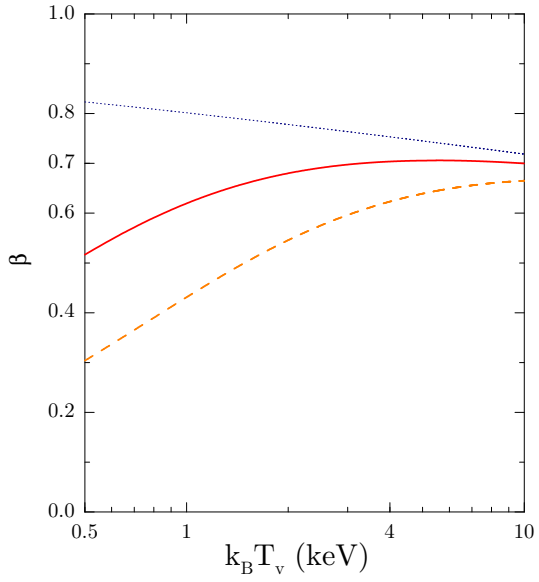

Fig. 3.2 The β parameter as a function of the virial temperature. The *solid* line is for $k_B \, \Delta T = 0.25$ keV and the *dashed* line is for $k_B \, \Delta T = 0.75$ keV. The *dotted* line is the prediction $\beta_{\rm grav}$ of the scale-invariant picture; note the small increase in $\beta_{\rm grav}$ toward smaller structures, due to concentration effects (see § 2.2.1).

of the parameter $\beta = T_v/T_2$.

As shown in § 2.2.1, in absence of whatever energy input $T_2 = T_v/\beta_{\rm grav}$ with $\beta_{\rm grav} \equiv [-2\,\xi\,\phi(R_v)/3]^{-1} \to 0.7$ in rich clusters. Now we expect $T_2 = T_v/\beta_{\rm grav} + \zeta\,\Delta T$ in terms of a thermalization efficiency $\zeta \sim 1$ for the extra heating (see [44]). We will specify ζ in the next §; for the time being, let us note that the ratio between the gas and DM specific energies now reads

$$\beta = \frac{\beta_{\rm grav}}{1 + \beta_{\rm grav}\,\zeta\,\dfrac{\Delta T_\star}{T_v}}\,. \tag{3.4}$$

At the scales of the clusters where $T_v \gg \Delta T$ holds, nearly constant $\beta \approx \beta_{\rm grav}$ applies. Moving toward smaller-T_v structures would reduce β (see Fig. 3.2) and tend to produce flatter density profiles. However, in the cluster range the decrease of β is efficaciously counteracted by the increased values of the concentration, hence of $\Delta\phi$. In practice, the density profiles stay nearly self-similar down to poor clusters (see Figs. 3.3, 3.4), where eventually they flatten because the reduction of β starts to overwhelm the concentration effects.

Such a flattening is more evident for higher values of the non-gravitational energy input, as illustrated in Figs. 3.3, 3.4; we have used the standard $k_B\Delta T = k_B\Delta T_\star =$

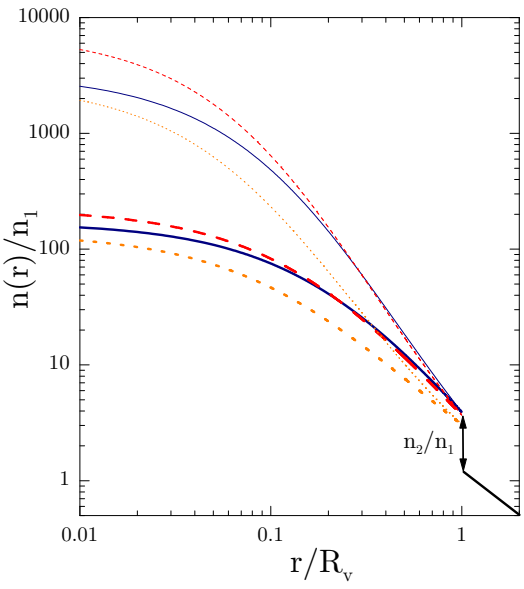

Fig. 3.3 Density profiles for isothermal (*thin* lines) and polytropic ($\Gamma = 1.2$, *thick* lines) ICM in the NFW potential. Non-gravitational heating $k_B\Delta T = 0.25$ keV. The *solid* lines are for a rich cluster with $k_BT_v \approx 8$ keV; the *dashed* lines are for a poor cluster with $k_BT_v = 2$ keV; and the *dotted* lines are for a group with $k_BT_v = 0.5$ keV. Note the density jump n_2/n_1 at the shock near R_v, see § 3.1.3.

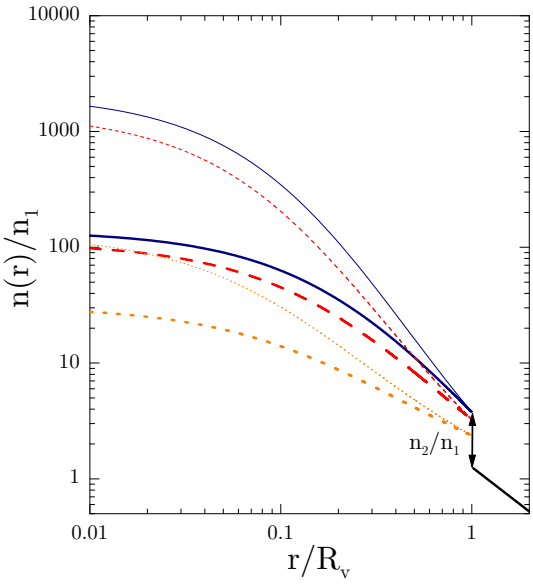

Fig. 3.4 Same as Fig. 3.3, but for non-gravitational heating $k_B\Delta T = 0.75$ keV.

0.25 keV for SNae and a value 3 times higher that is suitable after including the quasar contribution, see Chapter 4. We stress that the non linear (exponential) dependence of the density run amplifies the inverse variation of β with ΔT. In the polytropic case (where T increases with n while $p \propto nT$ is basically set by DM gravity) the inner densities are lower, hence less sensitive to a given energy input (see again Figs. 3.3, 3.4).

The second de-amplification factor is provided by the sensitivity to ΔT of the boundary condition n_2, which sets the normalization of the profile. Next we address the boundary conditions provided by *accretion shocks*.

3.1.3 *Accretion shocks*

Extensive shock transitions are expected to take place when external gas falls supersonically into a deep potential well. Many 1-D and 3-D simulations confirm that shock fronts form at about R_v during the formation of groups and clusters (e.g., [101]; [190]; [83]; [1]); recently, observational evidence is also mounting (see, e.g., [169]; [125]).

As a matter of fact, throughout the merging history of a DM structure smaller lumps and associated gas flow in together; but just inside R_v the smaller and/or less bound gas bunches are stripped away while their entropy is raised (see recent simulations by [193]). This comes about through a complex patchwork of variously-sized shocks, to the overall result of an outer shell with thickness $\Delta/R_v \lesssim 10^{-1}$

wherein most of the entropy jump takes place. This configuration may be rendered with a coherent accretion shock roughly spherical, located at about $r \sim R_v$ ([38]; [205]); then the conservation laws of mass, energy and total stress across such any layer for a perfect, monatomic gas write down as [106]

$$\begin{aligned} &\rho_1\,\tilde{v}_1 = \rho_2\,\tilde{v}_2 \\ &p_1 + \rho_1\,\tilde{v}_1^2 = p_2 + \rho_2\,\tilde{v}_2^2 \\ &\frac{1}{2}\,\rho_1\,\tilde{v}_1^2 + \frac{5}{2}\,p_1 = \frac{1}{2}\,\rho_2\,\tilde{v}_2^2 + \frac{5}{2}\,p_2\ , \end{aligned} \tag{3.5}$$

to within Δ/R_v accuracy. As it is customary we have indicated with the subscripts 1 and 2 the pre- and post-shock variables, respectively; in addition, the tilted v indicates that the velocity is measured in the rest frame of the shock.

From the previous system of equations we can easily work out the temperature jump

$$\frac{T_2}{T_1} = \frac{7}{8} + \frac{3}{16}\,\frac{\mu m_p\,\tilde{v}_1^2}{k_B T_1} - \frac{5}{16}\,\frac{k_B T_1}{\mu m_p\,\tilde{v}_1^2}\ ; \tag{3.6}$$

it is seen that shock heating ($T_2 \geq T_1$) requires the flow to be supersonic in the shock rest frame, i.e., $\tilde{v}_1 \geq c_s = \sqrt{5\,k_B T_1/3\,\mu m_p}$. The corresponding density jump (also called the *compression factor*) reads

$$g \equiv \frac{n_2}{n_1} = \frac{4}{1 + \dfrac{5\,k_B T_1}{\mu m_p\,\tilde{v}_1^2}}\ . \tag{3.7}$$

But now we need to rearrange these expression in terms of the infall velocity v_1 in the center of mass frame (see Fig. 3.5). This is the true physical variable, in turn linked to the virial temperature by $\mu m_p\,v_1^2 = -2\,\xi\,\phi(R_v)\,k_B T_v$ as specified in § 2.2.1. Assuming that the downstream kinetic energy is small (so that the shock speed is close to $-\tilde{v_2}$) as indicated by the numerical simulations, one has

$$\tilde{v}_1 = \frac{2}{3}\,v_1\left[1 + \sqrt{1 + \frac{15}{4}\,\frac{k_B T_1}{\mu m_p\,v_1^2}}\right]\ . \tag{3.8}$$

Introducing the previous expression into Eqs. (3.6) and (3.7) yields

$$\frac{T_2}{T_1} = 1 + \frac{4\,\mu m_p\,v_1^2}{15\,k_B T_1}\left[\frac{1}{4} + \sqrt{1 + \frac{15}{4}\,\frac{k_B T_1}{\mu m_p\,v_1^2}}\right] \tag{3.9}$$

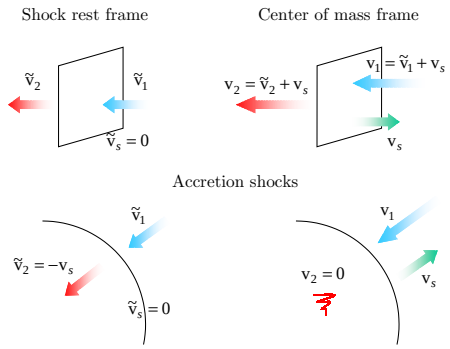

Fig. 3.5 Illustration of the velocity fields near a shock transition, in the shock rest frame and in the center of mass frame. The bottom pictures are specialized to the accretion shocks with $v_2 \approx 0$ as discussed in the main text.

for the temperature jump and

$$g = 1 + \frac{1 + \dfrac{5\,k_B T_1}{\mu m_p\, v_1^2}}{1 + 2\sqrt{1 + \dfrac{15\,k_B T_1}{4\,\mu m_p\, v_1^2}}} \tag{3.10}$$

for the compression factor. Further combining the previous expressions leads to [37]

$$g = 2\left(1 - \frac{T_1}{T_2}\right) + \sqrt{4\left(1 - \frac{T_1}{T_2}\right)^2 + \frac{T_1}{T_2}}\ , \tag{3.11}$$

which is actually independent of the coordinate frame.

Note that for strong shocks with $k_B T_1/\mu m_p\, v_1^2 \ll 1$ that take place in clusters and rich groups, one find the approximation $k_B T_2 \simeq \mu m_p\, v_1^2/3 + 3\,k_B T_1/2$, matching our preliminary expectation Eq. (3.4). Therefore the accretion shocks provide at once the boundary conditions on the density (n_2/n_1, see Fig. 3.3, 3.4) and the thermalization efficiency $\zeta = 3/2$ of the external energy $k_B T_1$. This eventually enables us to fix the $\beta = T_v/T_2$ parameter (see Fig. 3.2) and to set the hydrostatic equilibrium of the ICM (see previous §, and Figs. 3.3, 3.4).

We can now determine the resulting behavior of the X-ray and SZ observables simply by specifying the external T_1. Actually it depends on the detailed accretion history of the structure under consideration and in fact we will take care of this aspect in the next §; here we begin by identifying T_1 with the extra-heating temperature ΔT provided, e.g., by SNae. In this simplified approach, many results can be derived analytically through simple approximations in three different regimes: Strong, intermediate and weak shocks. We will mainly focus on the entropy, as the

corresponding results for the X-ray luminosity and SZ effect easily follow after the model-independent relations Eqs. (2.31) and (2.35).

Strong shocks

The strong shock regime is by far the most interesting one because it concerns the deviations from scale-invariance down to poor clusters. One has

$$\frac{T_1}{T_2} \ll 1 \; ; \qquad \frac{n_2}{n_1} \simeq 4 \left(1 - \frac{15}{16}\,\frac{T_1}{T_2}\right) \; . \tag{3.12}$$

The β parameter and the entropy at the shock expand as

$$\beta \simeq \beta_{\rm grav} \left(1 - \frac{3}{2}\,\frac{T_1}{T_2}\right) \; ; \qquad K_2 \simeq \frac{T_2}{(4\,n_1)^{2/3}} \left(1 + \frac{5}{8}\,\frac{T_1}{T_2}\right) \; . \tag{3.13}$$

In isothermal conditions the entropy run approximates to

$$\frac{K}{K_{\rm grav}} \simeq \left(1 + \frac{5}{8}\,\frac{T_1}{T_2}\right) \exp\left[\beta_{\rm grav}\Delta\phi\,\frac{T_1}{T_2}\right] \simeq 1 + \frac{T_1}{T_2}\,\left[\frac{5}{8} + \beta_{\rm grav}\Delta\phi\right] \; , \tag{3.14}$$

in terms of

$$K_{\rm grav} \equiv \frac{T_2}{(4\,n_1)^{2/3}} \exp\left[-\frac{2}{3}\,\beta_{\rm grav}\,\Delta\phi\right] \; . \tag{3.15}$$

Redoing our analysis for the polytropic case, we obtain

$$\frac{K}{K_{\rm grav}} \simeq \left(1 + \frac{5}{8}\,\frac{T_1}{T_2}\right) \left[1 - \frac{\dfrac{3}{2}\,\dfrac{\Gamma-1}{\Gamma}\,\beta_{\rm grav}\Delta\phi}{1 + \dfrac{\Gamma-1}{\Gamma}\,\beta_{\rm grav}\Delta\phi}\,\frac{T_1}{T_2}\right]^{\dfrac{\Gamma-5/3}{\Gamma-1}} \simeq$$

$$\simeq 1 + \frac{T_1}{T_2}\left[\frac{5}{8} - \frac{\dfrac{3}{2}\,\dfrac{\Gamma-5/3}{\Gamma}\,\beta_{\rm grav}\Delta\phi}{1 + \dfrac{\Gamma-1}{\Gamma}\,\beta_{\rm grav}\Delta\phi}\right] \; , \tag{3.16}$$

in terms of

$$K_{\rm grav} \equiv \frac{T_2}{(4\,n_1)^{2/3}} \left[1 + \frac{\Gamma-1}{\Gamma}\,\beta_{\rm grav}\,\Delta\phi\right]^{\dfrac{\Gamma-5/3}{\Gamma-1}} \; . \tag{3.17}$$

Intermediate shocks

This shock regime holds in poor clusters and groups; we call these shocks intermediate because $g \approx 5/2$ (remember that $1 \leq g \leq 4$).

$$\frac{T_2}{T_1} \to \frac{12}{5} \; ; \qquad \frac{n_2}{n_1} \simeq \frac{5}{2}\left[1 - \frac{15}{64}\left(\frac{12}{5} - \frac{T_2}{T_1}\right)\right] \; . \tag{3.18}$$

The β parameter and the entropy at the shock expand as

$$\beta \simeq \frac{5}{12}\,\beta_{\rm grav}\left[1 - \frac{25}{48}\left(\frac{12}{5} - \frac{T_2}{T_1}\right)\right] \; ; \quad K_2 \simeq \frac{12\,T_1/5}{(5\,n_1/2)^{2/3}}\left[1 - \frac{25}{96}\left(\frac{12}{5} - \frac{T_2}{T_1}\right)\right] \; . \tag{3.19}$$

In isothermal conditions the entropy run approximates to

$$\frac{K}{K_{\rm int}} \simeq 1 - \left(\frac{12}{5} - \frac{T_2}{T_1}\right)\left[\frac{25}{96} - \frac{125}{864}\,\beta_{\rm grav}\Delta\phi\right] \; , \tag{3.20}$$

in terms of

$$K_{\rm int} \equiv \frac{12\,T_1/5}{(5\,n_1/2)^{2/3}}\exp\left[-\frac{5}{18}\,\beta_{\rm grav}\,\Delta\phi\right] \; . \tag{3.21}$$

In the polytropic case we derive

$$\frac{K}{K_{\rm int}} \simeq 1 - \left(\frac{12}{5} - \frac{T_2}{T_1}\right)\left[\frac{25}{96} - \frac{\dfrac{125}{854}\dfrac{\beta_{\rm grav}\Delta\phi}{\Gamma}}{1 + \dfrac{5}{12}\dfrac{\Gamma-1}{\Gamma}\beta_{\rm grav}\Delta\phi/12}\right] \; , \tag{3.22}$$

in terms of

$$K_{\rm int} \equiv \frac{12\,T_1/5}{(5\,n_1/2)^{2/3}}\left[1 + \frac{5}{12}\,\frac{\Gamma-1}{\Gamma}\,\beta_{\rm grav}\,\Delta\phi\right]^{\dfrac{\Gamma-5/3}{\Gamma-1}} \; . \tag{3.23}$$

Weak shocks

This is the adiabatic limit, suitable only for poor groups or smaller lumps. There

$$\frac{T_2}{T_1} \to 1 \; ; \qquad \frac{n_2}{n_1} \simeq 1 + \frac{3}{2}\left(\frac{T_2}{T_1} - 1\right) \; . \tag{3.24}$$

The β parameter goes formally to zero (and so does T_v), while the shock-generated entropy is null up to the third order [106], i.e.,

$$\beta \simeq \frac{15}{12}\,\beta_{\rm grav}\left(\frac{T_2}{T_1} - 1\right)^2 \; ; \qquad K_2 \simeq \frac{T_1}{n_1^{2/3}}\left[1 + \frac{5}{6}\left(\frac{T_2}{T_1} - 1\right)^3\right] \; . \tag{3.25}$$

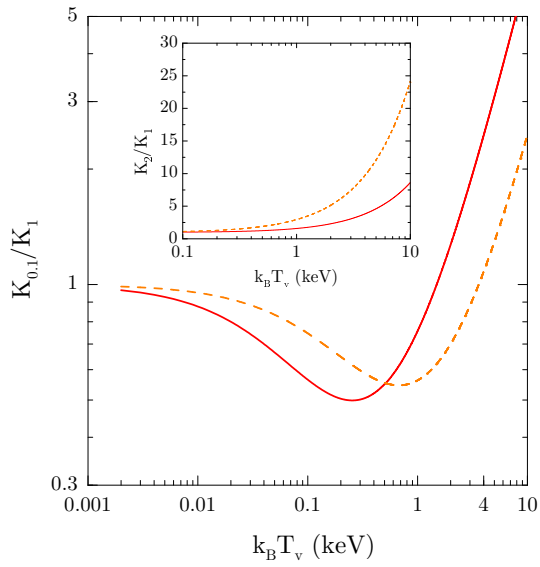

Fig. 3.6 The entropy at $0.1\,R_v$ (normalized to $K_1 = k_B T_1/n_1^{2/3}$) as a function of the virial temperature, computed from the shock model for a fixed $T_1 = \Delta T$. The *solid* line is for $k_B\Delta T = 0.25$ keV and the *dashed* line is for $k_B\Delta T = 0.75$ keV. The inset shows the same for the entropy jump at the shock.

The entropy run approaches

$$K \simeq \frac{T_1}{n_1^{2/3}} \left[1 - \frac{5}{6}\,\frac{\beta_{\rm grav}\Delta\phi}{\Gamma} \left(\frac{T_2}{T_1} - 1\right)^2 + \frac{5}{6} \left(1 - \frac{\beta_{\rm grav}\Delta\phi}{\Gamma}\right) \left(\frac{T_2}{T_1} - 1\right)^3 \right] . \tag{3.26}$$

Note how the term involving $\Delta\phi$ (which is present whenever we consider the entropy at $r < R_v$) introduces a negative contribution going quadratically to zero. The full computation provides the result illustrated in Fig. 3.6.

3.1.4 *Hierarchical preheating from SNae*

The results obtained in the previous sections constitute a relevant starting point, but they need to be substantially refined. One crucial improvement consists in modifying the naïve assumption $T_1 = \Delta T_\star$, which leads to overestimate the compression factor g. In fact, the latter quantity depends not only on the condition of the considered object at formation, but also on its past merging history.

The SN feedback acts while a structure and its gaseous content are built up hierarchically through merging events with a range of partners. In the process, about half the final DM mass in the main progenitor (and half the ICM mass likewise) is contributed by smaller partners with masses M'_{DM} within the *window*

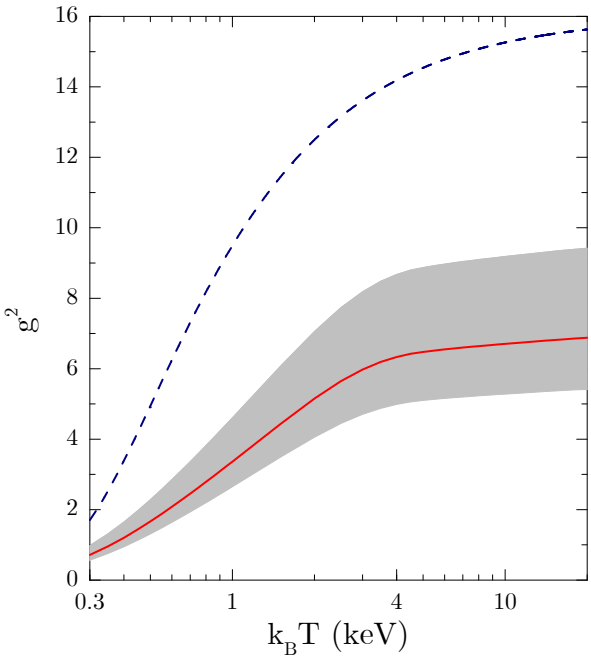

Fig. 3.7 The compression factor (squared) as a function of the X-ray temperature. The *dashed* line is for a fixed $k_B\,\Delta T_\star = 0.25$ keV, while the *solid* line is the mean result after performing the average over the DM merging histories. The shaded region is the statistical uncertainty (at 99% level) induced by the merging stochasticity.

$M_{DM}/3$ to $M_{DM}/20$, corresponding to T_v' from 0.6 down to $0.15\,T_v$ (see [38]).

Each merging event has associated its own *punctual* compression factor g that has to be computed in terms of the external temperature

$$T_1 = \max\left[T_v'\ ,\ \Delta T_\star\right]\ , \tag{3.27}$$

the higher between the virial temperature T_v' of the lump being accreted and the stellar preheating $\Delta T_\star$.

The effective value of $\langle g\rangle$ for a structure of mass M_{DM} at redshift z is the average over its possible merging histories. Specifically, we have to sum over the shocks caused at redshifts $z' \geq z$ in all progenitor of mass M'_{DM} (weighting with their number) by the accreted clumps of mass ΔM_{DM} (weighting with their merging rate). Such an average is performed in terms of the conditional probability and merging rate both given in § 1.2.3, to read

$$\langle g\rangle = \mathcal{N}^{-1}\int_z^\infty dz' \int_0^m dm'\,\frac{dP}{dm'}(m',z'|m,z)\int_0^{m-m'} d\Delta m\,\frac{d^2P}{d\Delta m\,dz}(m'\to m)\,g\ ; \tag{3.28}$$

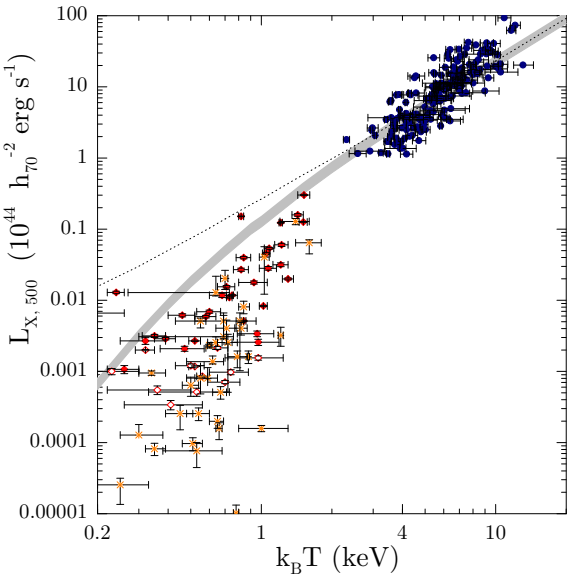

Fig. 3.8 Integrated X-ray luminosity vs. X-ray temperature. Data as in Fig. 2.7. The *shaded strip* is the results from SN feedback, computed according to the hierarchical preheating model.

here all the masses are measured in units of the characteristic mass and

$$\mathcal{N} \equiv \int_z^\infty dz' \int_0^m dm' \, \frac{dP}{dm'}(m', z'|m, z) \int_0^{m-m'} d\Delta m \, \frac{d^2P}{d\Delta m \, dz}(m' \to m) \quad (3.29)$$

is a normalization factor. The stochasticity of the merging process introduces an intrinsic variance given by

$$\delta g = \sqrt{\langle g^2 \rangle - \langle g \rangle^2} \, . \quad (3.30)$$

In Fig. 3.7 we plot $\langle g^2 \rangle$ together with its variance (at 99% confidence level) $\delta g^2 = 2 \langle g \rangle \delta g$ as a function of the final ICM temperature at $z = 0$.

The previous considerations and computations highlight how SNae make optimal use of their energy in that they produce *hierarchical preheating* of the ICM. Virialized clusters or groups possess too large thermal energy in order to be affected substantially by SN feedback from the inside. But the smaller progenitors of such structures have shallower potential wells and host higher ratios of stellar luminosity to mass. So they are more effective both at producing star-related energy, and at using it for heating the associated gas. As the structure hierarchy develops, such preheated gas will be partly hindered from flowing into the forming structures and from contributing to their hot medium [39]; thus lower densities are propagated some steps up the hierarchy.

In Figs. 3.8, 3.9, and 3.10 we plot the resulting X-ray luminosity, entropy, and

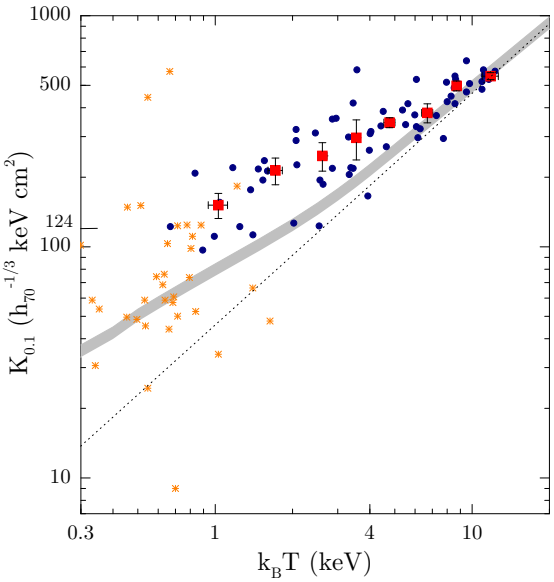

Fig. 3.9 Entropy vs. X-ray temperature. Data as in Fig. 2.8. The *shaded strip* is the result from SN feedback, computed according to the hierarchical preheating model.

SZ decrement as a function of system temperature. The convolutions made to average over the merging histories introduce stochastic variance, which amounts to $\delta L_X/L_X \approx 18\%$, $\delta K/K \approx 6\%$, and $\delta y/y \approx 9\%$ (at 96% confidence level) for L_X, K, and the SZ parameter y, respectively. But the resulting luminosity depressions or entropy enhancements are limited both in amplitude and scatter (see also [21]). Is stronger feedback required?

3.2 Alternatives to SN feedback

In this § we further point out the intrinsic drawbacks of the above scenario, and critically discuss the alternatives to SN feedback that have been proposed in the recent years.

3.2.1 *The crisis: energy budget and entropy profiles*

SNae with their small energetics are likely to preheat the baryons prior to virialization, because it is energetically convenient to move the gas on a higher adiabat when its density is lower. But such an external preheating cannot be spread uniformly among the baryons, lest the Ly$_\alpha$ forest would disappear. The level of preheating consistent with the current observations of the Ly$_\alpha$ clouds at $z \lesssim 3$ is of order few 10^4 K [48], corresponding to entropies at least one order of magnitude below

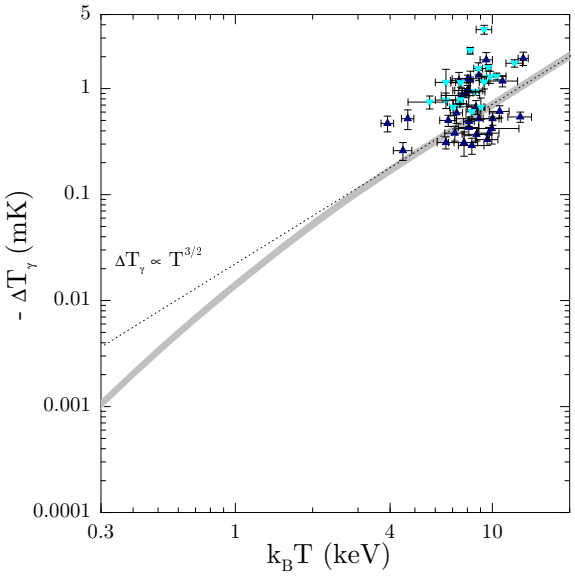

Fig. 3.10 SZ decrement vs. X-ray temperature. Data as in Fig. 2.10. The *shaded strip* is the result from SN feedback, computed according to the hierarchical preheating model.

those required in the cores of groups and clusters. A possible solution is that only the baryons that will end up in virialized structures have been heated by a biased distribution of sources. Observations of the OVI absorption features at low [198] or intermediate [165] redshift are necessary in order to test this hypothesis.

Another wayout is that the baryons have been heated by SNae after collapse, but then levelling the higher-density gas up to a given entropy requires larger energy inputs, around 1 keV per particle (see [27]). Furthermore, the heating efficiency of SNae may be reduced since the thermal energy transferred to a high-density gas component is rapidly radiated away. All these aspects seem to suggest that SNae cannot provide the required energy budget, and a crisis has been "officially" declared [196].

A further problem concerns the entropy profiles predicted by the preheating scenario. They reflect the history of progressive depositions of shocked shells during the hierarchical growth (see also [195]; [205]). In rich clusters where strong shocks dominate, the entropy deposited in the last shell accreted onto the current mass $m \propto M_c(z) \propto (1+z)^{3.17}$ scales as $K \propto T\,(1+z)^{-1.91} \propto m^{2/3}\,(1+z)^{-0.96} \propto m^{0.97}$; for simplicity, here we have power-law approximated Eq. (1.38) to better than 6% for $z \lesssim 10$ in the case of a DM effective spectral index $n \approx -1.2$ and Concordance Cosmology. Setting the gas in hydrostatic equilibrium with such an outer entropy distribution $K \propto m^{0.97}$ yields the outer radial profiles $K \propto r^{1.1}$ and $n(r) \propto r^{-1.86}$; these nicely agree with the data by [157] and the simulations of [19]. The previous

relations also set the local polytropic index Γ through $K \propto n^{\Gamma-5/3}$, which implies $\Gamma \approx 1.08$, again in accord with the observed values (see § 2.2.1).

On the other hand, if preheating has been at work in modulating the accretion shocks during the hierarchical buildup, one would expect most of the mass to have flowed adiabatically into groups, and flat entropy profiles to be originated out to relatively large radii ([7]; [5]; [204]). But several observations indicate that groups do not have large isentropic cores, rather their entropy rises steeply with increasing radius ([159]; [162]).

3.2.2 *Large-scale cooling/heating*

Various alternatives to the standard preheating from SNae have been proposed in the recent years; they can be divided into three main classes: large-scale cooling models, large-scale heating models, and quasar feedback models. Here we discuss the first two kinds, while we defer the analysis of quasar feedback to the next Chapter.

A number of authors ([30]; [149]; [203]; [211]; [58]) addressed the possibility that heating could not be necessarily invoked in order to explain the entropy excess in groups. This is because large-scale, extensive cooling may emulate heating by selectively removing low-entropy gas from the centers of clusters and, more efficiently, of groups where the cooling time is shorter.

The entropy-temperature correlation predicted by cooling models may be found by simple arguments basing on the expression Eq. (2.38) for the cooling time. We recall that the latter scales as $t_{\rm cool} \propto T^{1-\epsilon}/n$ in terms of the emissivity power-law index $\epsilon \approx \pm 1/2$. The adiabat may be written in terms of the cooling time and of the temperature as

$$K \propto \frac{T}{n^{2/3}} \propto T^{(1+2\,\epsilon)/3}\, t_{\rm cool}^{2/3}\ . \tag{3.31}$$

The threshold condition for the gas to cool quasi-statically within a Hubble time at formation reads $t_{\rm cool} \approx 13.7\,{\rm Gyr}\,(1+z)^{-3/2}$, yielding $K \propto T^{2/3}\,(1+z)^{-1}$ in the cluster range ($\epsilon = 1/2$) and $K \propto$ const. ≈ 100 keV cm^2 at the group scales ($\epsilon = -1/2$). Originally, a great boost of interest in this approach came because the predicted values of K in groups were amazingly close to the entropy floor; but the recent observations shade doubts on the reality of such a feature, probably reducing the above consideration to a pure numerical coincidence.

In any case, compared to the most recent data of the core entropy, cooling-based models predict roughly the correct slope of the $K - T$ correlation, but a too low normalization (see Fig. 3.11). Another fundamental problem with such approaches is that large fraction of baryons are expected to condense in absence of some form of energy feedback [8]. Where do such baryons go? The natural answer is that they form stars, but then the very high star formation efficiencies implied [134] are far above the ones observed [174]. In other words, cooling triggers instabilities unless

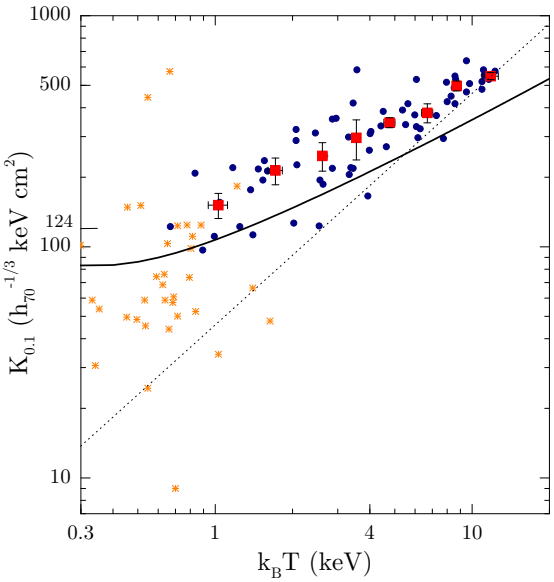

Fig. 3.11 The entropy-temperature correlation from the large-scale cooling model (*thick solid line*). Data as in Fig. 2.8.

closely controlled by other processes feeding energy back to baryons [194]; so energy *additions* are mandatory anyway.

Another class of models consider the large-scale heating that occurs around cosmic filaments or sheets [202] as the basic mechanism to originate the entropy excess. As we have seen in the above, the observed slope of the entropy profile outside the core seems to be consistent with the value predicted from shocked accretion; it is difficult to imagine how shocks cannot contribute in establishing it.

Moreover, cosmological simulations ([47]; [56]) have shown that 30% of present-day baryons do not reside within virialized objects, rather is distributed on large-scale structures as a warm/hot intergalactic medium of temperatures $T \sim 10^6$ K and overdensities $\delta \sim 10$. Thus the idea is that shocks on large-scale filaments or sheets may play a role similar to preheating in preventing cooling of the baryons and further gas accretion during the hierarchical buildup; in principle, this is made possible since the entropy of such a low-density phase can be as large as

$$K = 340 \left(\frac{\delta}{30}\right)^{1/3} \text{ keV cm}^2 \ . \tag{3.32}$$

However, it seems unlikely that such a mechanism could account for the entropy excess in the cores of groups and clusters [141]. This is because the entropy of the warm/hot intergalactic medium generated through such large-scale shocks is expected to decline very steeply with redshift, and it likely was well below the

Table 3.1 Viable interpretations: a quick look

Physical processes	**Affected scales**	**Modus operandi**	**Drawbacks, defects**
Gravitational heating	Groups, Clusters	Accretion shocks	Scale invariant
Radiative cooling	Galaxies, groups	Condensation, star formation	Overcooling problem
Stellar feedback	Galaxies, groups	Heating, outflow	Small energetics
All the above processes cooperate to produce			
Hierarchical pre-heating (by SNae)	Groups, clusters	Preheating in progenitors	Marginal $S(T)$; entropy profiles
Alternatives to SN feedback			
Large-scale cooling	Centers of groups	Removes low-entropy gas	Too much stars; no cooling flows
Large-scale heating	Voids, groups	Heating in filaments/sheets	Not seen in simulations; timing?
Quasar feedback (internal+external)	Galaxies, groups, clusters	Blowout, outflow, preheating	Uncertain coupling

Warning: this overview is not intended to be exhaustive.

threshold for cooling at the epochs when the gas in cluster cores was accreted. In other words, such gas shocked on large-scale filaments or sheets is likely to be re-shocked to the high entropies $K \sim 10^3$ keV cm^2 associated with the outskirts of present-day groups and clusters. This seems to be confirmed by recent high-resolution, 3-D numerical simulations of cluster formation [20], which find closely scale-invariant baryon distribution in absence of any non-gravitational energy input.

In conclusion, the scale-"variance" of cosmic baryons lends itself to several interpretations, which are summarized in Table 3.1 together with the accompanying processes and the intrinsic drawbacks. In our opinion, all seems to point toward a scenario in which the feedback from quasars must have a leading role, as we are now turning to discuss.

Chapter 4

Quasar Feedback

Twinkle, twinkle, quasi-star,
Biggest puzzle from afar.
How unlike the other ones,
Brighter than a billion suns.
Twinkle, twinkle, quasi-star,
How I wonder what you are!

- George Gamow: *Twinkle, Twinkle, Quasi-Star* –

This final chapter is dedicated to investigate the impact of the energy fed by quasars back to the baryons within galaxies, groups and clusters.

4.1 Basics of quasar astrophysics

Active Galactic Nuclei (AGNs) are a wide class of extragalactic sources located at the center of many, generally bright galaxies; at a first optical "sight" when the host is not visible, they appear as pointlike sources not much differing from stars (hence the acronym quasar for quasi-stellar object).

On the other hand, extreme peculiarities emerge when one looks at an AGN spectrum. First of all, the latter shows intense emission lines; the deduced redshifts may even be larger than 6, putting some AGNs among the farthest sources known. Although so distant, they are observable because their optical luminosities can exceed 10^{47} erg s^{-1} - about 10^3 times the luminosity of the Milky Way - and their bolometric outputs can attain 10^{48} erg s^{-1}. The spectrum of all AGNs extends from the far IR to X-rays, but a fraction around 10% is constituted by radio-loud sources, featuring highly-collimated jets of relativistic particles and emitting large powers also in the radio and especially in the γ-ray band (see Fig. 4.1).

The AGNs often show variability of their continuum emission, a feature that is more prominent in the radio-loud sources. The proper timescales of such variability

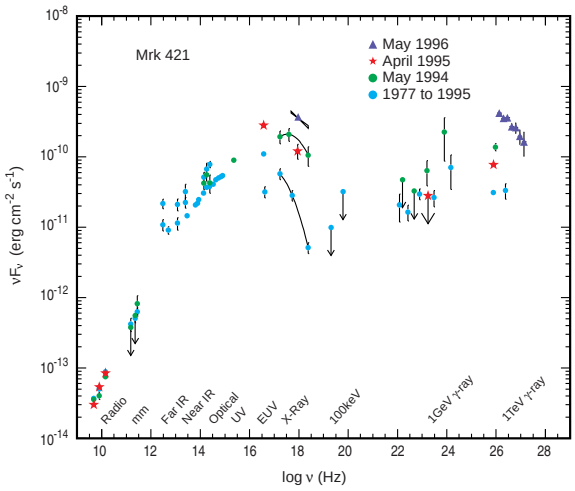

Fig. 4.1 The spectrum of Mkn421. Credit: Univ. Washington/J.H. Buckley.

in some cases is down to $\Delta\tau \sim$ hrs, yielding an upper limit to the linear dimension $R \lesssim c\Delta\tau$ of the source because large luminosity fluctuations require spatial coherence. The inferred limits on the sizes are around $10^{14} \div 10^{15}$ cm, implying that the AGNs emit extraordinary powers up to $10^{14}\, L_\odot$ from a region not larger than the Solar System. To achieve this, a very efficient and compact mechanism for energy production is needed; this suggests that the main origin of the AGN output must be traced back to gravitational contraction rather than thermonuclear burning [118].

The standard paradigm envisages giant black holes (BHs) of masses $M_\bullet \sim 10^6 \div 3{\times}10^9 M_\odot$ as the powerful engines of AGNs; the activity is believed to originate when the gravitational energy of the accreting material is converted into electromagnetic emission. The matter entering the gravitational reach of the BH may be at first subject to strong tidal disruption, then it is constrained to orbit in an accretion disk where progressively loses its angular momentum because of viscous forces; eventually, it falls into the BH horizon from a last stable orbit.

When a baryonic mass drawn from the surrounding structure is accreted on to the BH at a rate $\dot{M}_\bullet$, it originates luminosities of order $L \sim \eta_\bullet \dot{M}_\bullet c^2$. The overall mass-energy conversion efficiency is around $\eta_\bullet \sim 10\%$, much greater than the value provided by thermonuclear processes; note that this quantity actually may range from 6% for a non-rotating Schwarzschild hole up to 42% for a maximally spinning Kerr hole. But there is a maximum luminosity an AGN can emit; this is the *Eddington limit* $L_{\rm Edd}$, attained when the radiation pressure on a test particle balances the gravitational attraction exerted on the latter by the central hole, i.e.,

$$\frac{\sigma_T\, L_{\rm Edd}}{4\pi\, c\, r^2} = \frac{G\, M_\bullet}{r^2}\, m_p \ . \tag{4.1}$$

The resulting luminosity depends only on the BH mass and fundamental constants; it reads

$$L_{\rm Edd} = \frac{4\pi\, G\, M_\bullet\, m_p\, c}{\sigma_T} = 1.3 \times 10^{46}\, {\rm erg\ s^{-1}}\, \frac{M_\bullet}{10^8\, M_\odot}\ . \tag{4.2}$$

Note that a source constantly emitting at the Eddington power e-folds its mass in a *Salpeter time*

$$t_S \equiv \frac{\eta_\bullet\, M_\bullet\, c^2}{L_{\rm Edd}} = \frac{\eta_\bullet\, c\, \sigma_T}{4\pi\, G\, m_p} \approx 0.04\, {\rm Gyr}\ . \tag{4.3}$$

Thus to achieve bolometric luminosities $L \sim 5 \times 10^{46}$ ergs s^{-1}, BH masses $M_\bullet \gtrsim 3 \times 10^8\, M_\odot$ are required. Pleasingly, these are appropriate to a BH with Schwarzschild radius around 10^{14} cm, which is just the size estimated from variability. These masses are also consistent with the recent observations of compact, massive dark objects at the center of many local galaxies [167], which can be understood as the relic BHs having energized past AGNs. All this suggests we have got a consistent picture on involving massive BHs fuelled by accretion.

In this scenario, the continuum component of the AGN spectrum is related to the accretion disk. In particular, the thermal B-UV component comes from the gas near the last stable orbit and is often prominent in the spectrum as an optical-UV bump (the so called *big blue bump*); this is likely due to a superposition of black body emissions, each produced by a different annulus of the accretion disk. On the other hand, the non-thermal emission is mainly due to indirect reprocessing of the thermal one: The IR spectrum is mainly caused by the dust, which absorbs radiation from the disk and then reradiates it at lower wavelengths; the X-ray one is likely to be originated through inverse-Compton scattering by the hot electrons above or around the accretion disk.

The broad emission lines are due to high-velocity gas clouds orbiting the BH relatively near the accretion disk. Beyond the broad emission line region is located a dusty torus, which can hide the accretion disk if the line of sight is roughly perpendicular to the disk axis. Gas clouds orbiting in regions far away from the central BH are instead responsible for the emission of the narrower lines.

Apart from the loudness or quietness, the AGNs are divided into 3 taxonomical classes according to the features of their emission lines and of their continuum output. The first group (Type 1) is composed by sources with strong continuum and broad emission lines. Radio-quiet sources of this kind are the type 1 Seyfert galaxies, which show low luminosities $L < 10^{45}$ erg s^{-1} and are easily observed only at modest redshifts; and the optically-selected quasars, which can produce powers up to 10^{48} erg s^{-1} and populate the distant Universe. Type 1, radio-loud sources are instead the broad line radio galaxies, which feature low optical luminosities; and the radio quasars, further divided into flat and steep spectrum ones.

The second group (Type 2) is composed by low-power-continuum and narrow-emission-line sources. Radio-quiet objects belonging to this category are the Seyfert

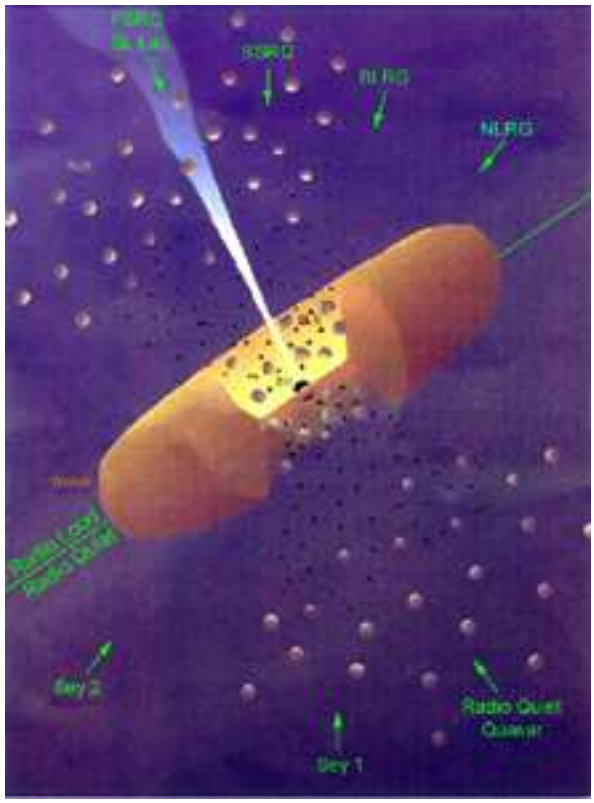

Fig. 4.2 The unified scheme of AGNs. Figure taken from [200].

2 galaxies and the narrow line X-ray galaxies. Among the radio-loud sources, we find the narrow line radio galaxies, that are further divided into two subclasses: The Fanaroff-Riley I that show extended radio lobes reaching Mpc distances from the galactic center; and the Fanaroff-Riley II that feature collimated radio jets ending in small-volumes, high-power radio lobes. To the third group belong sources with very peculiar spectral features, rapid variability, high polarization, and apparent superluminal motions of the compact clouds that produce strong radio emission. This group is made up of BL Lacertae (BL Lac) sources that are radio-loud objects showing no emission lines at all, and by flat spectrum radio quasars. We remark that this classification in not always sharp, and that a numbers of transitional members have been increasingly found in the recent years.

By the mid 1990s it was understood that some of the differences among the AGN classes are due to the geometrical orientation of the accretion disk axis relative to the line of sight (see Fig. 4.2; [200]). This unification is a fundamental step toward the comprehension of how the main physical parameters (such as mass, accretion rate, angular momentum) of a BH may be responsible for the electromagnetic emission

and the jet formation.

If a source is observed at large viewing angles with respect to the disk axis the presence of the dusty torus can obscure the accretion disk itself and the broad line region. For smaller viewing angles, the broad line region becomes more and more visible; thus, among the radio-quiet AGNs an observer would switch from Seyfert II galaxies to Seyfert I ones and to optical quasars.

Geometrical effects are even sharper for radio-loud sources; decreasing the viewing angle we encounter the narrow-line radio galaxies, the broad-line radio galaxies and the steep spectrum radio quasars. Furthermore, for viewing angles smaller than 10° the apparent emitted power increases owing to relativistic beaming. BL Lacs and flat spectrum radio quasars are thought to be radiosources with their jet pointing closely toward the observer, hence the name "Blazars".

Finally, another important feature of almost all AGN classes (with the BL Lacs constituting a notable exception) is their strong cosmological evolution. In particular, the recent detections out to $z \approx 6.4$ [76] have significantly improved the statistics of high-redshift quasars, and confirmed that their population undergoes the most sharp and non-monotonic of evolutions. The comoving density of the bright sources rises on a scale of few Gyrs from the big-bang (actually, from the end of the "Dark Ages") to peak around $z \approx 2.5$; later on, it turns over and falls down by two orders of magnitudes or more to the present.

The optical luminosity function of quasars is plotted in Fig. 4.3 for different redshift bins. A good fit for $z \lesssim 3$ is provided by [57]

$$\Psi(L,z)\,L = \frac{\dfrac{2\times 10^3}{\mathrm{Gpc}^3}}{\left(\dfrac{L}{L^\star}\right)^{\alpha-1} + \left(\dfrac{L}{L^\star}\right)^{\beta-1}}\,, \tag{4.4}$$

in terms of

$$L^\star(z) = L^\star(0)\,10^{k_1\,z + k_2\,z^2} \tag{4.5}$$

and of the parameters $\alpha = 1.1$, $\beta = 3.3$, $k_1 = 1.2$, $k_2 = -0.2$ and $L^\star(0) = 1.9\times 10^{44}$ erg s^{-1}.

At higher redshifts only the bright end is easily observable; this is well fitted by [75]

$$\Psi(L,z)\,L = \frac{3\times 10^{-3}}{\mathrm{Gpc}^3}\left(\frac{L}{L^\star}\right)^{1-\beta}\,, \tag{4.6}$$

in terms of the quantity

$$L^\star(z) = L^\star(3)\,10^{k\,(z-3)} \tag{4.7}$$

and of the parameters $\beta = 2.6$, $k = 0.3$, and $L^\star(3) = 1.6\times 10^{46}$ erg s^{-1}.

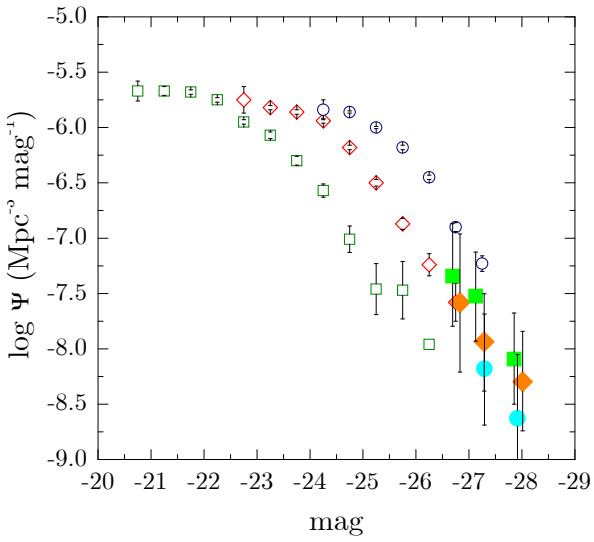

Fig. 4.3 The optical luminosity function of quasars. Redshift binned data from [57]: $0.4 < z < 0.68$ *open squares*; $0.97 < z < 1.25$ *open diamonds*; $1.81 < z < 2.1$ *open circles*. Redshift binned data from [75]: $3.6 < z < 3.9$ *filled squares*; $3.9 < z < 4.4$ *filled diamonds*; $4.4 < z < 5$ *filled circles*.

To explain such an articulated evolution is a difficult task, not completely performed yet. However, a clear point is that the BH paradigm is not enough, and that an equally important role must be played by the environmental conditions in which the BH feeding occurs. These are mainly set by the hierarchical cosmogony, which drives the formation of increasingly large DM halos, wherein the galaxies constitute smaller baryonic cores. Such a scenario implies strong dynamical events to occur: At early epochs mainly through "major" merging events of comparable subgalactic units [86]; later on as milder interactions of member galaxies in groups [40]. All these events tend to break the axial symmetry of the galactic gravitational potential on kpc scales; the specific angular momentum of the gas that provides its support in the galactic host is not conserved, rather it is transferred to the massive DM component. Thus, a sizeable gas fraction is destabilized and funnelled inward; at small scales, dissipative processes take over to redistribute the angular momentum, and cause the gas to reach the nuclear accretion disk, growing new BHs or refuelling an old one (see also [42]).

4.2 Hierarchical preheating from AGNs

In this § we extend the hierarchical preheating model elaborated in the previous chapter to include the AGN contribution.

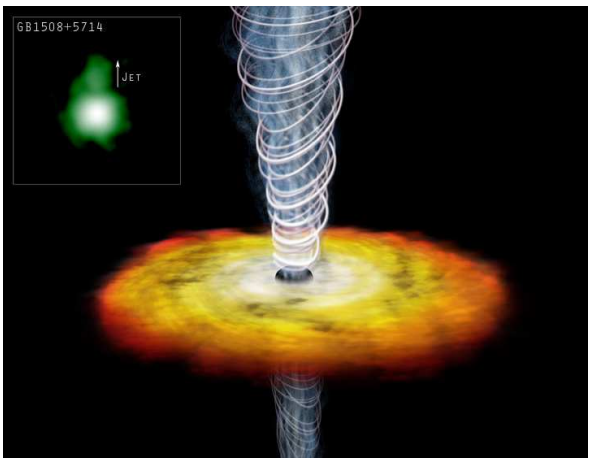

Fig. 4.4 The Chandra image of the quasar GB1508+5714 at $z \approx 4.3$ reveals a jet of high-energy particles that extends more than 10^5 light years from the central supermassive black hole. Credit: X-ray: NASA/CXC/A. Siemiginowska - Ill.: CXC/M. Weiss.

4.2.1 *Energetics*

In the recent years AGNs have been widely established as natural sources of strong feedback (see [201]; [210]; [24]; [213]; [137]; [176]; [172]). The AGN emissions are kindled when the cold galactic gas that mainly forms circumnuclear starbursts partly reaches down to accrete onto a central supermassive BH [131].

Next we evaluate the actual, integrated energy input $\Delta E_\bullet$ originated by AGNs per solar mass condensed into stars, as this quantity is easily compared with the SN contribution. It comes to

$$\Delta E_\bullet = f_\bullet \, \eta_\bullet \, c^2 \, \frac{M_\bullet}{M_{\rm bulge}} \, \frac{M_{\rm bulge}}{M_{\rm IMF}} \, \Delta m_\star \approx 1.2 \times 10^{50} \, f_\bullet \, \frac{\Delta m_\star}{M_\odot} \, {\rm ergs} \; ; \qquad (4.8)$$

here $M_\bullet / M_{\rm bulge} \approx 2 \times 10^{-3}$ is the ratio between the BH mass and its host galactic bulge (see [82]; [77]), and $M_{\rm bulge}/M_{\rm IMF} \sim 1/3$ accounts for the bulge mass observed in blue light compared to that integrated over the star formation history ([72]; [74]).

Therefore AGNs potentially provide a huge energy output, but the effective fraction $f_\bullet$ coupled to the surrounding baryons is considerably more uncertain than for SNae, though likely lower. A number of points, however, stand out. The (10%) radio-loud quasars provide large kinetic energies in the form of relativistic jets (see Fig. 4.4; [87]; [181]); but small covering factors and inefficient thermalization lead to $f_\bullet \sim 10^{-1}$ for these sources. Note that recent X-ray observations of galaxy clusters provide evidence for the role of intermittent activity by radiosources in suppressing cooling flows (see [128]; [191]; [214]; [16]).

For the 90% radio-quiet AGNs a small coupling $f_\bullet \sim 10^{-2}$ is expected if the output is mainly radiative. Indeed, radiation pressure can affect the gas via elec-

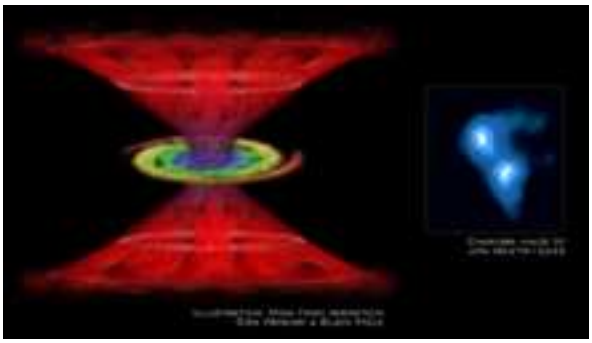

Fig. 4.5 Chandra's X-ray observations reveal evidence of high-speed winds blowing gas away from the supermassive BH that powers the quasar APM 08279+5255, at redshift $z \approx 3.91$. Credit: X-ray: NASA/CXC/PSU/G. Chartas - Ill.: CXC/M. Weiss.

tron scattering or atomic-line excitations, but both processes are highly inefficient. The former because the small momentum of the emitted photons hinders effective conversion into particles' one; the latter because the quasar spectra are flat, and so only a fractional energy 1% will fall in the atomic band $1 \div 10$ eV where the absorption cross sections are sizeable. Higher values of $f_\bullet$ are conceivable in systems where the photons are heavily scattered/absorbed within the gravitational reach of the BH, and may escape only in hard X-rays if at all [73].

On the other hand, values of $f_\bullet$ up to 10% may be associated with outflows or winds originated directly from the accretion disk. It is well known by general theoretical arguments that rotating accretion flows must lose mass unless radiation is very efficient in removing the liberated binding energy. This is because in the disk viscous forces transport energy outward; if radiation is not able to remove most of such energy, a substantial fraction of the gas in the flow will become unbound [15]. Also numerical simulations suggest that accretion disks can produce magnetically active coronae [132], which likely generate outflows; the latter may be further boosted by centrifugal force or by radiation pressure, especially in broad absorption line quasars.

Recently there has been increasing observational evidence for the production of substantial outflows by many AGNs (see Fig. 4.5; also, e.g., [140]; [49]; [164]). From the knowledge of the outflow speed v_w one can infer the values of the effective coupling efficiency; in fact, this is given by the ratio between the energies of photons $p_\gamma\, c$ and (non-relativistic) particles $p_p\, v_w/2$ at momentum equality, i.e., when $p_\gamma = p_p$. If the outflow is not spherically symmetric, $f_\bullet$ is further reduced by a covering factor $f_{\rm cov} \gtrsim 10^{-1}$, to read

$$f_\bullet \sim f_{\rm cov}\, \frac{v_w}{2\, c}\ ; \tag{4.9}$$

since the measured wind speed are of order $v_w \sim c/5$ and $f_{\rm cov} \sim 1/2$ (see, e.g., [158])

the coupling may be estimated around $f_\bullet \sim 5\%$. Hereafter this will be adopted as our reference value.

Considering that the AGN activity closely parallels the star formation in spheroids ([79]; also [85], [199]), we add the AGN integrated thermal input to the stellar one, to obtain a total preheating temperature of $k_B\Delta T_\bullet \approx 0.75$ keV per particle.

4.2.2 *X-ray scaling relations: steps forward*

We are ready to study the impact of the combined preheating from SNae and AGNs on the X-ray and SZ observables. We rely on the hierarchical preheating model developed in § 3.1.4, and consider the effect of raising the preheating temperature from the value $k_B\Delta T_\star \approx 0.25$ keV provided by SNae alone up to the total one $k_B\Delta T_\bullet \approx 0.75$ keV including the AGN contribution.

Fig. 4.6 illustrates how the increase of the preheating temperature affects the density jump g, once the average over the DM merging histories has been performed (see § 3.1.4 for details). Compared with the SN result, the higher preheating temperature contributed by AGNs shifts toward larger scales the deviations of $\langle g^2 \rangle$ from the cluster behavior, making them already appreciable around 4 keV (note that at higher T the results from SNae and AGNs are consistent). This is also evident in the $L_X - T$ correlation, now well reproduced especially at the intermediate scales

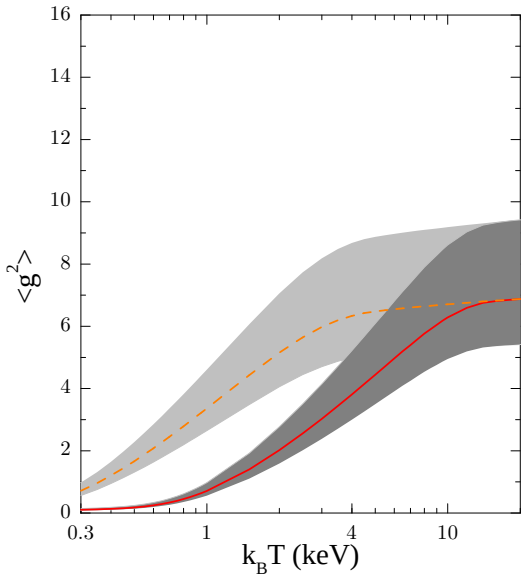

Fig. 4.6 The compression factor averaged over the merging histories. *Dashed* line is for $k_B\Delta T_\star = 0.25$ keV due to stellar preheating alone (the *light shaded* area shows the variance at 99% confidence level), while *solid* line is for the total input $k_B\Delta T_\bullet = 0.75$ keV that includes the quasar contribution (the *heavy shaded* area shows the corresponding variance).

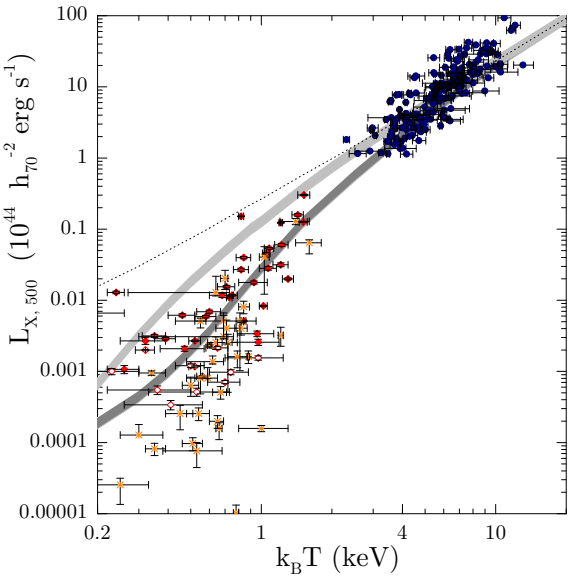

Fig. 4.7 Integrated X-ray luminosity vs. X-ray temperature. Data as in Fig. 2.7. *Light shaded* strip is for SN preheating alone, and *heavy shaded* strip includes the quasar contribution. Variances at 96% confidence level.

(see Fig. 4.7; [110]).

Note, however, that the fit in the poor group range is still marginally consistent with the full data set. Moreover, the variance associated with the DM merging histories is not wide enough to account for the scatter in the data, especially at the smaller scales. The same conclusions apply to the $K-T$ (and the SZ-decrement vs. T) correlation (see Fig. 4.8; 4.9); here, however, the effects are less evident owing to the milder dependence of K and y on the compression factor g. Finally, we remark the preheating from AGNs, although alleviating the energy crisis discussed in § 3.2.1 for SNae, is still subject to the drawback of producing flat entropy profiles in groups.

4.3 Internal Feedback from quasars

But we have not yet considered the internal impact of powerful quasars. The latter discharge energy on timescales comparable to the dynamical time of the gas within the DM halo. So these events are expected to strongly affect the environment by inducing substantial motion of the surrounding medium, especially in the shallower wells of poor groups and galaxies. In this § we address such an internal feedback action by developing a new analytic treatment of quasar-driven blastwaves (see also [45]).

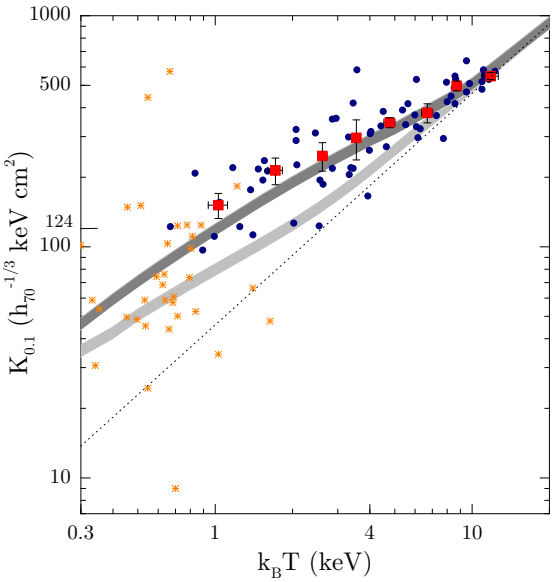

Fig. 4.8 Entropy vs. X-ray temperature. Data as in Fig. 2.8. *Light shaded* strip is for SN preheating alone, and *heavy shaded* strip includes the quasar contribution. Variances at 96% confidence level.

4.3.1 *A new family of self-similar blastwaves*

Sometimes it happens that a physical system exhibits a self-similar behavior; this occurs when its dynamics can be described by a small set of dimensionless numbers, obtained from the original dimensional quantities governing it. Then the number of independent variables can be reduced and simple solutions to otherwise very complicated problems can be found. Although a self-similar solution is only a particular description of the physical problem under consideration, it often constitutes a crucial step toward the comprehension of its overall dynamical evolution.

Self-similar solutions aimed at describing the blastwave originated by a sudden energy discharge in a constant-density medium has been firstly obtained in the 1950s by [177] and applied to a variety of physical problems, including the study of nuclear bomb explosions. Such solutions have then been extended to initial media with power-law density distributions and applied to the theory of SN remnants (see, e.g., [36]). Further generalizations have incorporated time-dependent energy injections and have been used to study, e.g., the propagation of solar-flare-driven shocks (see, e.g., [147]).

All these approaches feature an initial medium with negligible gas pressure so that the resulting blastwave is necessarily strong, in the sense its speed is very large compared to the sound speed of the ambient medium in which the propagation takes place; moreover, they do not include the gravitational effect due to a DM

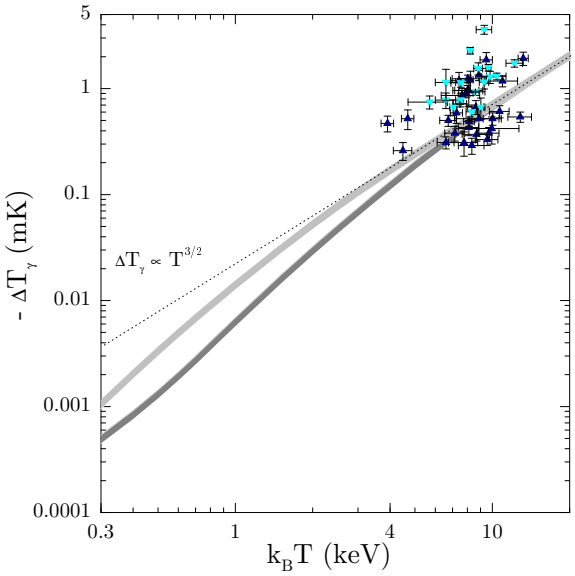

Fig. 4.9 The SZ decrement vs. X-ray temperature. Data as in Fig. 2.10. *Light shaded* strip is for SN preheating alone, and *heavy shaded* strip includes the quasar contribution. Variances at 96% confidence level.

component.

Here we fill in this gap, deriving a new family of self-similar solutions that incorporate DM gravity and a finite initial pressure, adding to a power-law initial density gradient and time-dependent energy injection $\Delta E(t)$. In this § we develop the solutions, and in the next one we will apply them to study the impact of quasar-driven blastwaves on the intergalactic and intracluster media.

Initial conditions

We take the initial configuration to be constituted by a DM profile $\rho_{DM}(r) = \rho_c\,(r_c/r)^\omega$, with power-law index $2 \leq \omega < 5/2$ and core radius $r_c \approx R_v/10$ [1]. The gas is assumed to be in hydrostatic equilibrium within the DM potential well, its density $\rho = f_{\rm gas}\,\rho_{DM}$ being a fraction $f_{\rm gas} \approx 0.15$ of the DM's. The gas pressure

[1] The power-law behavior of the initial density profile is mandatory in order to have self-similar solutions.

and temperature profiles read

$$p = \frac{2\pi G\,(\rho_c r_c^\omega)^2\, f_{\rm gas}}{(\omega-1)\,(3-\omega)}\, r^{2(1-\omega)}$$
$$\frac{kT}{\mu m_p} = \frac{2\pi G\,\rho_c r_c^\omega}{(\omega-1)\,(3-\omega)}\, r^{2-\omega}\ , \tag{4.10}$$

while the thermal, gravitational and total energies are

$$E_{\rm th} = \frac{1}{2}\, m\, c_s^2 \left[\frac{9}{5}\,\frac{3-\omega}{5-2\,\omega}\right]$$
$$E_{\rm grav} = \frac{1}{2}\, m\, c_s^2 \left[-\frac{12}{5}\,\frac{(\omega-1)\,(3-\omega)}{5-2\,\omega}\right]$$
$$E_{\rm tot} = E_{\rm th} + E_{\rm grav} = \frac{1}{2}\, m\, c_s^2 \left[-\frac{3}{5}\,\frac{3-\omega}{5-2\,\omega}\,(4\,\omega-7)\right]\ , \tag{4.11}$$

respectively; here $m = 4\pi\,\rho_c\, r_c^\omega\, r^{3-\omega}/(3-\omega)$ is the gas mass enclosed within r and $c_s = \sqrt{5\,k_B T/3\,\mu m_p} \propto r^{1-\omega/2}$ is the sound speed. The restriction $2 \le \omega < 2.5$ guarantees that the total energy of the system is finite and negative; hereafter we will indicate its modulus with $E(r) \equiv -E_{\rm tot}(< r)$. Our initial configuration is consistent with the virial theorem applied to every sphere of radius $r \le R_v$

$$2\,E_{\rm th} + E_{\rm grav} = 4\pi p\, r^3\ , \tag{4.12}$$

once a surface term is included to account for the non-zero gas pressure at the boundary.

The transient regime

The transient regime is constituted by a blastwave sweeping through the gas, as a result of the energy injections $\Delta E(t)$ by the central source under adiabatic conditions. The ensuing hydrodynamic, unsteady gas flow is described by the system of partial differential equations

$$\partial_t \rho + \partial_r(\rho v) + \frac{2\,\rho v}{r} = 0$$
$$\partial_t v + v\partial_r v + \frac{1}{\rho}\,\partial_r p + \frac{G\,M_{DM}(< r)}{r^2} = 0$$
$$(\partial_t + v\partial_r)\,\frac{p}{\rho^{5/3}} = 0\ , \tag{4.13}$$

supplemented of the Rankine-Hugoniot boundary conditions at the leading shock. These may be derived from the general expressions Eqs. (3.6) and (3.7) specialized to the case of internal shocks, i.e., putting the preshock velocity in the shock rest frame ($\tilde{v}_1$) equal to (minus) the shock speed $(-)\, v_s$. This yields

$$v_2 = \frac{3}{4}\, v_s\, \frac{\mathcal{M}^2 - 1}{\mathcal{M}^2} \qquad p_2 = \frac{p_1}{4}\,(5\,\mathcal{M}^2 - 1) \qquad \rho_2 = 4\,\rho_1\, \frac{\mathcal{M}^2}{\mathcal{M}^2 + 3}\ , \tag{4.14}$$

in terms of the Mach number $\mathcal{M} \equiv v_s/c_s$. Incidentally, the condition for shock propagation $v_s \geq c_s$ may be equivalently written as $p_2 + \rho_2\, v_2^2 \geq p_1$, i.e., the total stress pushing the shock outwards has to overcome the external pressure.

The gas motion described by the above equations will be self-similar if in addition to the spacetime variables r and t the only other two dimensional quantities of the problem are the gravitational constant G and the combination $\rho_c r_c^\omega$. This requirement translates into a constraint on the law of energy liberation, which must be of the form

$$\Delta E(t) \propto G^{(5-\omega)/\omega}\, (\rho_c\, r_c^\omega)^{5/\omega}\, t^{2\,(5-2\,\omega)/\omega}\ ; \tag{4.15}$$

fortunately the resulting time-dependencies are physically acceptable and interesting, because for the considered values of the power-law index $\omega \sim 2 \div 5/2$ they correspond to luminosities going from a constant ($\omega = 2$) to a spike ($\omega = 5/2$). The former case will constitute our fiducial choice, but the models with $\omega > 2$ will also result useful to describe the quasar fading-out due to its own feedback on the accreting gas. Self-similarity implies $\Delta E(t)/E(< R_s)$ to be independent of time and position, as it is simple to see because $E(< R_s) \propto R_s^{5-2\,\omega} \propto t^{2\,(5-2\,\omega)/\omega} \propto \Delta E$; thus $\Delta E/E$ is a good parameter for the description of the solutions. This is even more true because the values of $\Delta E/E$ univocally determine the Mach number, i.e., the strength of the shock, as we shall demonstrate subsequently.

Under the assumption of self-similarity, Eqs. (4.13) may be solved along the following lines. First of all, we define the fundamental parameter $\xi \equiv r/R_s(t)$, where

$$R_s(t) = \left[\frac{5\pi G\, \rho_c r_c^\omega\, \omega^2\, \mathcal{M}^2}{6\,(\omega - 1)\,(3 - \omega)}\right]^{1/\omega}\, t^{2/\omega} \tag{4.16}$$

is the shock radius. The Mach number $\mathcal{M} = v_s(t)/c_s[R_s(t)]$ is independent of time and position, as expected for a self-similar motion. Note that in our fiducial model ($\omega = 2$) the blast moves out with constant speed, while for $\omega > 2$ it decelerates. The latter statement may sound strange because the initial density run is increasingly steeper for larger ω. In fact, the accelerated or retarded propagation of shockwaves in media with density gradient is not solely determined by the law of decay in density; the pressure gradient, the gravitational effects and the time-dependent driving power $L(t) = d\Delta E(t)/dt \propto t^{5\,(-1+2/w)}$ influence the wave motion substantially.

Then we introduce the adimensional functions $V(\xi)$, $R(\xi)$, and $z(\xi)$ through

$$v(r,t) = \frac{r}{t}\,V(\xi) \qquad \rho(r,t) = \frac{1}{G\,t^2}\,R(\xi) \qquad T(r,t) = \frac{3}{5}\frac{r^2}{t^2}\,z(\xi)\ , \tag{4.17}$$

which enable us to convert Eqs. (4.13) into a set of ordinary differential equations

$$\begin{aligned}
&\xi\left[V' + \left(V - \frac{2}{\omega}\right)\frac{R'}{R}\right] = 2 - 3\,V \\
&\xi\left[V'\left(\frac{2}{\omega} - V\right) - \frac{3}{5}\,z\left(\frac{z'}{z} + \frac{R'}{R}\right)\right] = \frac{6}{5}\,z + V^2 - V + \frac{24}{5}\,\frac{\omega-1}{\omega^2\mathcal{M}^2}\,\xi^{-\omega} \\
&\xi\left(V - \frac{2}{\omega}\right)\left(\frac{z'}{z} - \frac{2}{3}\,\frac{R'}{R}\right) = -2\left(V - \frac{1}{3}\right)\ ,
\end{aligned} \tag{4.18}$$

with boundary conditions

$$\begin{aligned}
V_2 &\equiv V(\xi=1) = \frac{3}{2}\,\frac{\mathcal{M}^2-1}{\omega\,\mathcal{M}^2} \\
z_2 &\equiv z(\xi=1) = \frac{1}{4\,\omega^2}\,\frac{(5\,\mathcal{M}^2-1)\,(\mathcal{M}^2+3)}{\mathcal{M}^4} \\
R_2 &\equiv R(\xi=1) = \frac{24\,f_{\rm gas}}{5\,\pi}\,\frac{(3-\omega)\,(\omega-1)}{\omega^2\,(\mathcal{M}^2+3)}\ .
\end{aligned} \tag{4.19}$$

We can lower by 1 the order of the differential problem on using the conservation of entropy, which provides the integral relation

$$\frac{z}{z_2} = \xi^{\omega/(3-\omega)}\,\left[\frac{R}{R_2}\right]^{\frac{4-\omega}{3-\omega}}\,\left[\frac{2-\omega\,V}{2-\omega\,V_2}\right]^{\frac{1}{3}\frac{6-\omega}{7-2\,\omega}}\ . \tag{4.20}$$

It can be easily seen from dimensional arguments that an energy integral does not exist for our problem; nevertheless, the overall energy balance within the blast gives

$$\Delta E(t) - E(<R_s) = 4\pi\int_0^{R_s} dr\,r^2\,\left\{\frac{1}{2}\,\rho\,v^2 + \frac{3}{2}\,p - \frac{G\,M_{DM}(<r)}{r}\,\rho\right\}\ . \tag{4.21}$$

The equation above can be reformulated as

$$\begin{aligned}
\frac{\Delta E}{E} = 1 + \frac{5-2\,\omega}{4\,\omega-7}\,\Bigg\{&\frac{15}{4}\,\frac{(\mathcal{M}^2-1)^2}{\mathcal{M}^2+3}\int_0^1 d\xi\,\xi^4\,\frac{R}{R_2}\left(\frac{V}{V_2}\right)^2 + \\
&+\ \frac{3}{4}\,(5\,\mathcal{M}^2-1)\int_0^1 d\xi\,\xi^4\,\frac{z\,R}{z_2\,R_2} + \frac{4\,\mathcal{M}^2}{\mathcal{M}^2+3}\int_0^1 d\xi\,\xi^{4-\omega}\,\frac{R}{R_2}\Bigg\}\ ,
\end{aligned} \tag{4.22}$$

and shows $\Delta E/E$ to be in one-to-one correspondence with $\mathcal{M}$, as mentioned before; in Fig. 4.10 we plot such a relation for various ω. For strong shocks $\Delta E/E \propto \mathcal{M}^2$ holds; this remark is particularly useful to check that in the formal limit $\mathcal{M} \to \infty$ our new family of self-similar blastwaves converge to the canonical solutions with negligible gravity and null initial gas pressure. E.g., for $\omega = 2$ and constant source luminosity one has $R_s \propto \mathcal{M}\, t \propto (\Delta E/E)^{1/2}\, t$; since $E \propto R_s$ one recovers $R_s \propto L^{1/3} t \propto \Delta E^{1/3}\, t^{2/3}$, in accord with the canonical blastwave. As another example consider $\omega = 2.5$ and instantaneous energy liberation, for which one has $R_s \propto \mathcal{M}^{4/5}\, t^{4/5} \propto (\Delta E/E)^{2/5}\, t^{4/5}$; since $E = $ const. one reobtains the standard dependence $R_s \propto \Delta E^{2/5} t^{4/5}$. Another feature worth to mention is that for larger ω the more impulsive energy discharges provide higher energy densities in the initial stages of the blast motion, and cause the shock to move with higher $\mathcal{M}$ for a given $\Delta E/E$.

Finally, we can numerically solve the differential problem on using a standard Runge-Kutta integrator (with adjustable timestep, see [161]). For various shock strengths we show in Figs. 4.11 and 4.12 the distributions of density, pressure, temperature, entropy and cumulative mass in the blast for our fiducial $\omega = 2$ model. The flow begins at a *piston*, the trailing contact surface where the temperature vanishes and the density diverges weakly, so that the pressure is finite and the enclosed mass is null; in fact, the perturbed flow is confined between the outer shock at R_s and the inner piston located at $\lambda\, R_s < R_s$. Self-similarity implies the

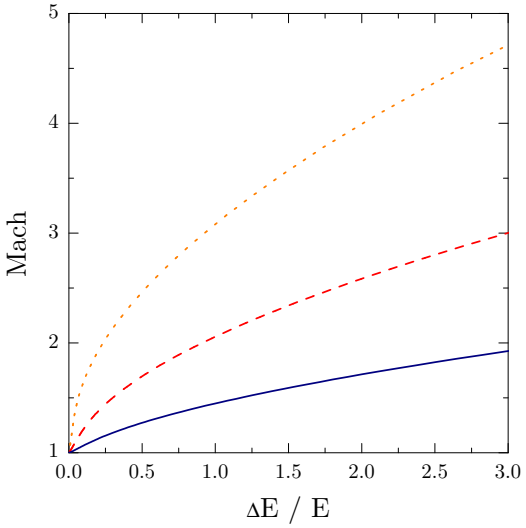

Fig. 4.10 The relation between $\Delta E/E$ and the Mach number set by the global conservation of energy. *Solid* line is for $\omega = 2$, *dashed* line is for $\omega = 2.25$, and *dotted* line is for $\omega = 2.4$.

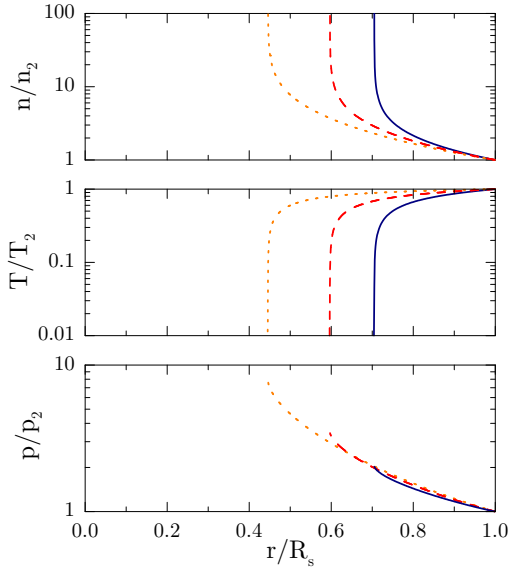

Fig. 4.11 Results for $\omega = 2$. Distributions of density, temperature and pressure within the blast, normalized to their postshock values. *Solid* lines are for a strong shock, *dashed* lines for an intermediate shock and *dotted* lines are for a weak shock.

thickness $1 - \lambda$ of such a shell to depend on the shock strength; in particular, the shell is thinner for larger $\mathcal{M}$, up to the limit $\lambda \approx 0.84$ attained for very strong shock ($\mathcal{M} \gg 1$).

In Fig. 4.13 we represent the piston position as a function of the Mach number, for different values of ω; at a given $\mathcal{M}$ the shell is thicker for larger ω. Finally, Figs. 4.14 and 4.15 represent the distributions of relevant physical quantities inside the flow for different ω; for simplicity and direct comparison, we have plotted only the results for very strong shock ($\mathcal{M} \gg 1$).

Analytic approximations for the limiting behavior of the adimensional variables V, R, z in proximity of the piston may be derived. It turns out that for a given ω such limits are independent of the shock strength, and read

$$V \simeq \frac{2}{\omega} - \frac{6}{5}\left(\frac{7}{\omega} - 2\right)\left[\frac{r - R_p}{R_p}\right] \qquad z \propto \left[\frac{r - R_p}{R_p}\right]^{\frac{1}{3}\frac{6-\omega}{7-2\omega}} \qquad R \propto z^{-1} \ . \quad (4.23)$$

The shell approximation

The presence of the piston leads us to represent our solutions in a simplified manner on using the classic *shell approximation*, known to provide results reliable to better than 15% (see, e.g., [143]).

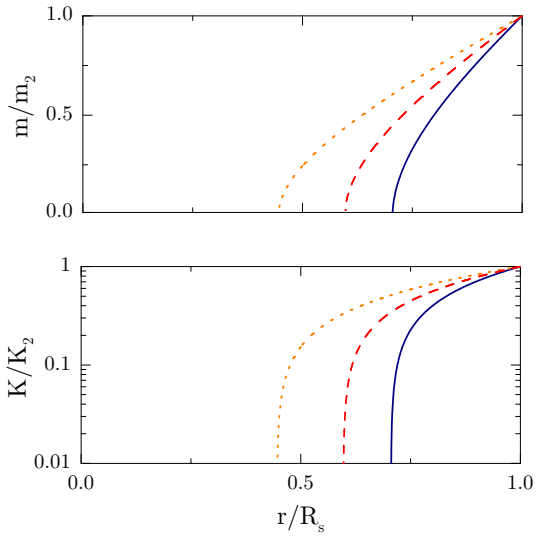

Fig. 4.12 Results for $\omega = 2$. Cumulative mass and entropy distributions within the blast, normalized to their postshock values. *Solid* lines are for a strong shock, *dashed* lines for an intermediate shock and *dotted* lines are for a weak shock.

In this approximation the equation of motion for the shell writes down as

$$\frac{d}{dt}(m\,v_2) = 4\pi\,R_s^2[\langle p\rangle\, - p_1] - \frac{3-\omega}{5-2\,\omega}\,\frac{G\,M_{DM}}{R_s^2}\,m\ , \tag{4.24}$$

in terms of the volume-averaged pressure $\langle p\rangle$, which as function of $\mathcal{M}$ reads

$$\frac{\langle p\rangle}{p_2} = \frac{4}{(3-\omega)\,(5-2\,\omega)\,(5\,\mathcal{M}^2-1)}\,\left[\frac{5}{8}\,(8-3\,\omega)\,(5-2\,\omega)\,(\mathcal{M}^2-1) + 3\,(3-\omega)\right]\ . \tag{4.25}$$

For weak shock with $\mathcal{M} \to 1$ one obtains $\langle p\rangle/p_2 = \langle p\rangle/p_1 = 3/(5-2\,\omega)$ and Eq. (4.25) may be rearranged to recover the virial theorem for the initial equilibrium configuration; in the strong shock limit $\mathcal{M} \gg 1$ the result $\langle p\rangle/p_2 \to (8{-}3\,\omega)/2\,(3{-}\omega)$ matches that valid for classical blastwaves without gravity [36].

Integrating Eq. (4.24) leads to the conservation of energy in the shell approximation, which is

$$\Delta E - E = \frac{1}{2}\,m\,v_2^2 + \frac{3}{2}\,\langle p\rangle\,V - \frac{3-\omega}{5-2\,\omega}\,\frac{G\,M_{DM}\,m}{R_s}\ , \tag{4.26}$$

in terms of the shell volume $V = 4\pi R_s^3(1-\lambda^3)/3$. Eq. (4.26) provides also the

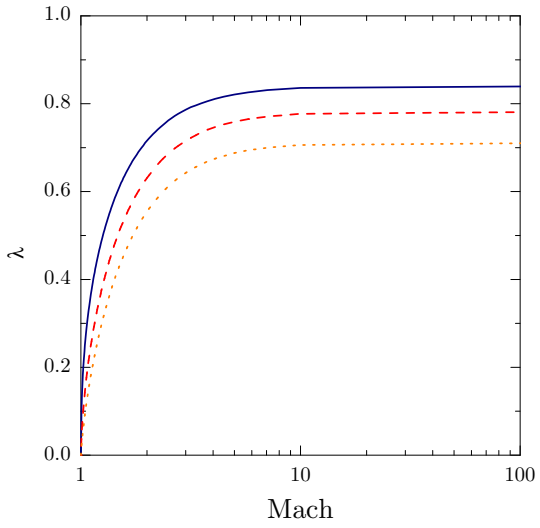

Fig. 4.13 Piston position as a function of the Mach number. *Solid* line is for $\omega = 2$, *dashed* line is for $\omega = 2.25$, and *dotted* line is for $\omega = 2.4$.

relation between $\mathcal{M}$ and $\Delta E/E$ in the shell approximation

$$\frac{\Delta E}{E} = \left\{ \frac{15}{16} \frac{5-2\,\omega}{(3-\omega)\,(4\,\omega-7)} \frac{(\mathcal{M}^2-1)^2}{\mathcal{M}^2} + \frac{1-\lambda^3}{(3-\omega)\,(4\omega-7)} \times \right.$$
$$\left. \times \left[\frac{5}{8}\,(8-3\,\omega)\,(5-2\,\omega)\,(\mathcal{M}^2-1) + 3\,(3-\omega) \right] + \frac{3}{4\omega-7} \right\} \; ; \quad (4.27)$$

A relevant quantity is the ratio between the bulk-motion and thermal energy of the blast, i.e., between the first and second term of the r.h.s. It tends to zero in the weak shock limit ($\mathcal{M} \to 1$) and takes on values $3/(16-6\,\omega)\,(1-\lambda^3)$ for strong shocks with $\mathcal{M} \gg 1$, again consistently with the classic blastwave solutions without gravity.

4.3.2 *Equilibrium recovery and X-ray scaling relations*

The blastwave driven by an active quasar through the surrounding gas will be moderately or strongly supersonic depending on the key parameter $\Delta E/E$.

The (modulus) of the initial, total energy E within R_v is obtained from

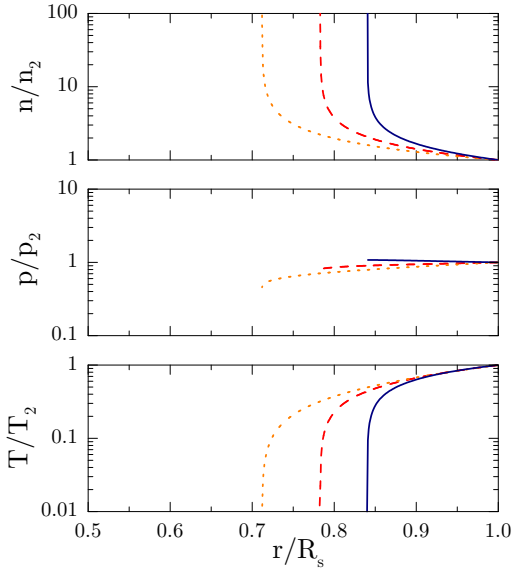

Fig. 4.14 Results for $\mathcal{M} \gg 1$. Distributions of density, pressure and temperature within the blast, normalized to their postshock values. *Solid* lines are for $\omega = 2$, *dashed* lines are for $\omega = 2.25$, and *dotted* lines are for $\omega = 2.4$.

Eqs. (4.11) to read

$$E = \frac{f_{\rm gas}}{\sqrt{2\,\pi\,G^3\,\rho_{DM}}} \left(\frac{k_B T_v}{\mu m_p}\right)^{5/2} (1+z)^{-3/2}\,\mathcal{F}_1(\omega) \approx$$
$$\approx 5.8 \times 10^{60}\,{\rm ergs}\,\frac{f_{\rm gas}}{0.15} \left(\frac{k_B T_v}{\rm keV}\right)^{5/2} h^{-1} \left(\frac{\Delta_{\rm vir}(z)}{18\,\pi^2}\,\frac{\Omega_M}{\Omega_z}\right)^{-1/2} (1+z)^{-3/2}\,\mathcal{F}_1(\omega)\ , \tag{4.28}$$

with $\mathcal{F}_1(\omega) \equiv (4\,\omega - 7)\,[(\omega - 1)\,(3 - \omega)]^{3/2}/(5 - 2\,\omega)$. This has to be compared with the energy ΔE actually injected over the time $t_{\rm dyn,gas}$ the accreting gas takes to dynamically respond. The paradigm of supermassive BHs for the AGNs implies

$$\Delta E = f_\bullet\,\frac{\eta_\bullet\,M_\bullet c^2}{t_S}\,t_{\rm dyn,gas}\,\mathcal{F}_2(\omega) \approx$$
$$\approx 2.5 \times 10^{60}\,{\rm ergs}\,\frac{f_\bullet}{5 \times 10^{-2}}\,\frac{M_\bullet}{10^9\,M_\odot}\,h^{-1} \left(\frac{\Delta_{\rm vir}(z)}{18\,\pi^2}\,\frac{\Omega_M}{\Omega_z}\right)^{-1/2} (1+z)^{-3/2}\,\mathcal{F}_2(\omega) \tag{4.29}$$

here we have defined $\mathcal{F}_2(\omega) \equiv [\omega/2\,(5 - 2\,\omega)]\,(t_{\rm dyn,gas}/t_S)^{5\,(2-\omega)/\omega}$ and adopted

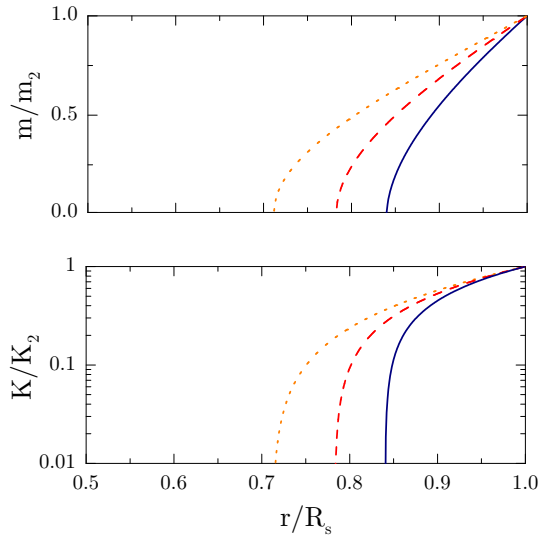

Fig. 4.15 Results for $\mathcal{M} \gg 1$. Cumulative mass and entropy distributions within the blast, normalized to their postshock values. *Solid* lines are for $\omega = 2$, *dashed* lines are for $\omega = 2.25$, and *dotted* lines are for $\omega = 2.4$.

$t_{\rm dyn,gas} \gtrsim 10^{-2}\, t_{\rm dyn}$, as suggested by [133]. Thus the relevant ratio reads

$$\frac{\Delta E}{E} \approx 0.4\, \frac{f_\bullet}{5\times 10^{-2}}\, \frac{M_\bullet}{10^9\, M_\odot}\, \left(\frac{f_{\rm gas}}{0.15}\right)^{-1}\, \left(\frac{k_B T_v}{\rm keV}\right)^{-5/2}\, \mathcal{F}(\omega)\ ; \tag{4.30}$$

the dependence on ω is specified by the quantity $\mathcal{F}(\omega) \equiv \mathcal{F}_2/\mathcal{F}_1 = \{\omega/2\,(4\,\omega - 7)\,[(\omega-1)\,(2-\omega)]^{3/2}\}(t_{\rm dyn,gas}/t_S)^{5\,(2-\omega)/\omega}$. At the scales from clusters to groups $\Delta E/E \lesssim 1$ holds and the leading shock at R_s is not necessarily strong; our self-similar solutions that includes the *restraints* to the blast propagation set by a finite initial gas pressure and by the DM gravity, is required to make realistic predictions.

After the transient and before a major merging reshuffles the DM mass substantially, the gas recovers hydrostatic equilibrium. We assume the renewed equilibrium may be described by a simple distribution $\rho'(r) = \rho'_v\,(r/R_v)^{-\beta'\,\omega}$, but with boundary density ρ'_v and parameter β' altered by the passage of the blast. In particular, the latter heats up the gas so decreasing the value of $\beta' = T_v/\langle T\rangle$, which we reset on using the temperature mass-averaged over the shell, i.e.,

$$\langle T\rangle = \frac{\int dr\, r^2\, \rho'(r)\, T'(r)}{\int dr\, r^2\, \rho'(r)}\ . \tag{4.31}$$

The blast also depletes all densities due to gas ejection; we reset ρ'_v by requiring the volume integral of $\rho'(r)$ to equal the gas mass $m - \Delta m$ left inside R_v by the blast

Table 4.1 Relevant quantities for quasar-driven blasts

	$\omega = 2$				$\omega = 2.4$	
$\mathbf{\Delta E/E}$	$\mathcal{M}$	$\langle \mathbf{p} \rangle / \mathbf{p_1}$	$\mathbf{1 - \Delta m/m}$	β'/β	$\mathcal{M}$	$\langle \mathbf{p} \rangle / \mathbf{p_1}$
0.3.....	1.2	3.6	0.92	0.94	2.1	17.8
1.....	1.5	4.6	0.58	0.86	3.0	21.7
3.....	1.9	6.3	~ 0	0.72	4.7	26.2

at $t \approx t_{\rm dyn}$, to read

$$1 - \frac{\Delta m}{m} = \frac{\int dr\, r^2\, \rho'(r)}{\int dr\, r^2\, \rho(r)}\,. \tag{4.32}$$

It is easily seen that this prescription provides densities $\rho'_v/\rho_v \propto 1 - \Delta m/m$ proportional to the residual gas mass. In Table 4.1 we report the relevant quantities for quasar-driven blastwaves; if compared with preheating, the internal feedback provides poorer thermal affection but much larger dynamical effects leading to blowout.

We compute the X-ray luminosity, the entropy, and the SZ decrement in our fiducial $\omega = 2$ model, assuming as initial values those already affected by the preheating from SNae and AGNs; we plot these quantities as a function of the X-ray temperature in Figs. 4.16, 4.17 and 4.18. At the scales of the clusters $\Delta E/E \ll 1$ holds, and the effects due to internal feedback are negligible because both $1 - \Delta m/m$ and β saturate to the unperturbed values; here hierarchical preheating rules the behaviors of the correlations (see § 3.1.4).

Moving toward poor groups $\Delta E/E \propto T_v^{-5/2}$ rapidly raises and the X-ray luminosity $L_X \propto n^2 \propto (1 - \Delta m/m)^2$ is suppressed strongly due to the increasing contribution of the blowout. The current X-ray data in groups are seen to require coupling levels around $f_\bullet \approx 5 \times 10^{-2}$. In terms of strong, increasingly sporadic quasar impacts we can also understand why the *scatter* of the X-ray data widens toward smaller systems as poor groups or massive galaxies [135]. This we trace back to the increasing *variance* in the occurrence of strong quasar events or even in their coupling $f_\bullet$, that concur to dynamically modulate the plasma ejection $\Delta m/m \propto f_\bullet\, M_\bullet$. As the hierarchical clustering proceeds toward clusters, instead, the evolution of the quasars cuts down most dynamical effects; so impulsive contributions to ΔE hardly can keep pace with the growth of E in such massive and late structures. We stress that nearly *all* data points in Fig. 4.16 are comprised between the upper SN strip and the lower quasar line, except for a few groups with peculiar features under scrutiny ([135]; [142]).

Relatedly, the entropy is enhanced and the SZ is depressed relative to the corresponding initial values. However, while the deficit of $L_X \propto n^2 \sqrt{T}$ is strong already at 1 keV, the entropy $K \propto T\, n^{-2/3}$ is affected only in poor groups because of its milder density dependence; this is even more true in the Comptonization parameter $y \propto n\, T$, where the density depletion is balanced at first by a moderate temperature raise. But eventually, the former dominates and cause long-term entropy excesses

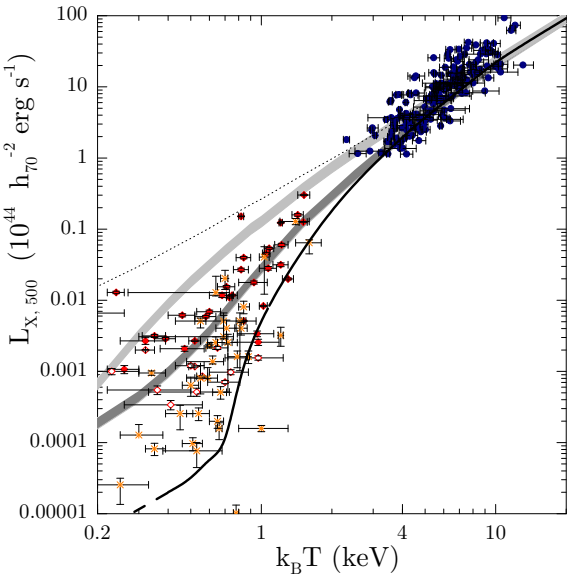

Fig. 4.16 Integrated X-ray luminosity vs. X-ray temperature. Data as in Fig. 2.7. *Light shaded strip* is for SN preheating alone, and *heavy shaded strip* includes the quasar contribution. *Solid line* adds the internal impact from quasars.

and SZ deficits (see also discussion in [108]).

Relatedly, the inner entropy profiles are *far* from flat. They are generated by the adiabatic redistribution of the entropy carried by the blast; we find $K(m) \propto m^{4/3}$ in terms of the perturbed plasma mass increasing from the trailing piston to the leading shock. On requiring this to be also the entropy distribution in the new equilibrium yields $K(r) \propto r^{4/3}$ or $\Gamma \approx 1$; this validates our assumption of isothermality in resetting the new equilibrium, see above Eq. (4.31).

But on approaching galactic scales the luminosity (or SZ) depressions and entropy enhancements saturate because the quasar feedback is self-regulated ([182]; [212]); this implies that $\Delta E/E$ is constrained not to exceed a few, lest the gas contained within kpcs and the accretion it feeds are cut down. The pivotal value $\Delta E/E \approx 1$ recast in terms of the DM velocity dispersion σ_v yields (for $\omega = 2$)

$$M_\bullet \approx 6 \times 10^8 M_\odot \left(\frac{f_\bullet}{5 \times 10^{-2}}\right)^{-1} \left(\frac{f_{\rm gas}}{0.15}\right) \left(\frac{\sigma_v}{300\,{\rm km\,s^{-1}}}\right)^5 . \tag{4.33}$$

Converting to the bulge dispersion $\sigma_\star \propto \sigma_v^{1.2}$ [78] gives $M_\bullet \propto \sigma_\star^4$ (see also [99]). Then for the same values $f_\bullet \approx 5 \times 10^{-2}$ indicated by the X-ray data, the above relation remarkably agrees with the observations of relic BHs in the bulge of many local galaxies (see also [197]); it is also consistent with the mass density in BHs derived from the quasar activity [122]. Finally, we remark that the $M_\bullet - \sigma$ derived

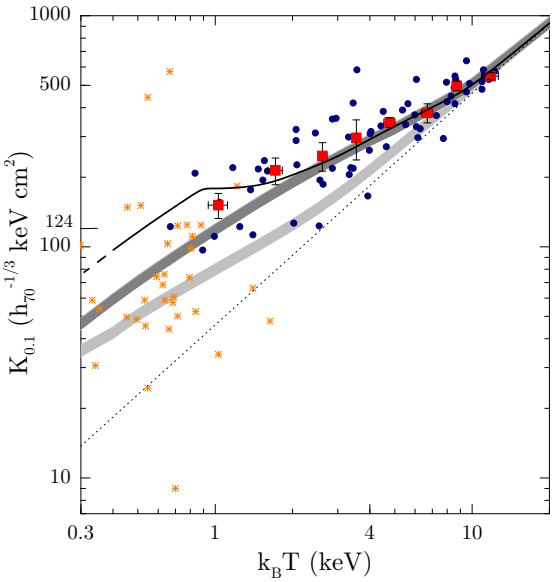

Fig. 4.17 Entropy vs. X-ray temperature. Data as in Fig. 2.8. *Light shaded strip* is for SN preheating alone, and *heavy shaded strip* includes the quasar contribution. *Solid line* adds the internal impact from quasars.

here is independent of the redshift; recent measurements up to $z \sim 3$ seem to confirm this prediction [180].

To sum up, several pieces of data fit together on considering both the external preheating from AGNs and the internal impact from quasars. In particular, the same value $f_\bullet \approx 5 \times 10^{-2}$ that yields agreement with the large-scale X-ray emissions also accords with the mainly optical measurements of nuclear BH masses vs. galactic velocity dispersions.

4.3.3 *Enhanced SZ Effects from quasar feedback*

Although constrained by Eq. (4.33), the energy injections by quasars are large enough to also produce *enhanced* SZ effects during the transient regime (see [109]). This is because during the blast propagation the gas mass is pushed into a shell while its pressure is raised, to the effect of increasing the Comptonization parameter $y \propto p\, R_v$ over the initial, equilibrium value. In the way of a preliminary estimate the latter may be written as $y_{\rm grav} \propto E/R_v^2$ in terms of the gas energy $E \propto p\, R_v^3$ at equilibrium. When a much larger energy $\Delta E \gtrsim E$ is added by a quasar to the ambient medium, we expect SZ signals enhanced at levels $y/y_{\rm grav} \sim \Delta E/E$ (see also [2]; [155]).

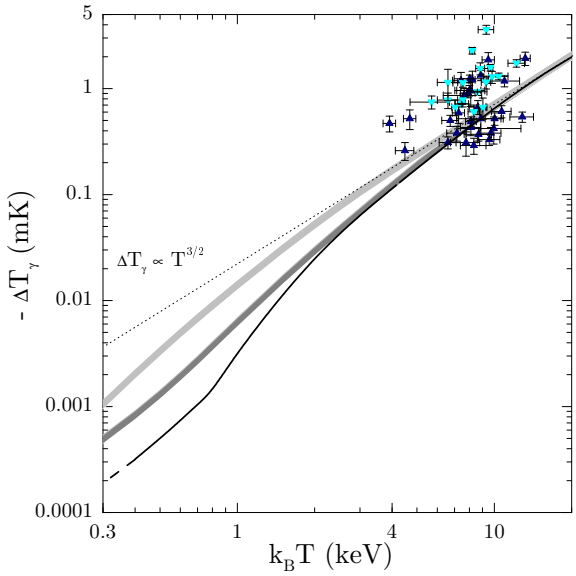

Fig. 4.18 The SZ decrement vs. X-ray temperature. Data as in Fig. 2.10. *Light shaded strip* is for SN preheating alone, and *heavy shaded strip* includes the quasar contribution. *Solid line* adds the internal impact from quasars.

In a more detailed computation, we focus on

$$\bar{y} = \frac{2}{R_v^2} \int_0^{R_v} ds\, s\, \frac{2\, k_B \sigma_T}{m_e c^2} \int_s^{R_v} dr\, \frac{r}{\sqrt{r^2 - s^2}}\, p(r) \ , \tag{4.34}$$

averaged over the area of the structure, since this will subtend small angles $R_v/d_A \lesssim 1'$ for an early group or galaxy (see Fig. 4.19). Normalizing the shock position as $x \equiv R_s(t)/R_v$, we find the full signal

$$\frac{\bar{y}}{\bar{y}_{grav}} = \frac{\langle p \rangle}{3\, p_1} \left(1 - \lambda^3\right) x + \sqrt{1 - x^2} \simeq \frac{\langle p \rangle}{3\, p_1} \left(1 - \lambda^3\right) \ , \tag{4.35}$$

in terms of $\bar{y}_{\rm grav} = (4\, \sigma_T / m_e c^2)\, p(R_v)\, R_v$. The last approximation applies for $x \approx 1$, which maximizes the transit time in the structure and optimizes the observability.

Our results are represented in Fig. 4.20 vs. the depth kT_v of the host potential well [107]. The square illustrates the *minimal* enhancement we expect from an early group at $z = 1.5$ with $kT_v = 1$ keV, $f_\bullet = 5 \times 10^{-2}$ and $M_\bullet = 10^9\, M_\odot$, so with $\Delta E = 0.4\, E$. With radii $R_v \approx 250$ kpc, the angular sizes $2\, R_v/d_A \approx 1'$ are close to their minimum in the Concordance Cosmology (cf. [10]).

The circles in Fig. 4.20 represent our results for a massive ($\sigma_v = 300$ km s^{-1}, $R_v \approx 100$ kpc) and still gas-rich ($f_{\rm gas} = 0.15$) protogalaxy at $z = 2.5$. The open circle refers to $\Delta E \approx E$ or $M_\bullet \approx 6 \times 10^8\, M_\odot$; the filled one to $\Delta E \approx 3\, E$ or $M_\bullet \approx 2 \times 10^9\, M_\odot$, just compatible with the scatter in the $M_\bullet - \sigma$ correlation. The

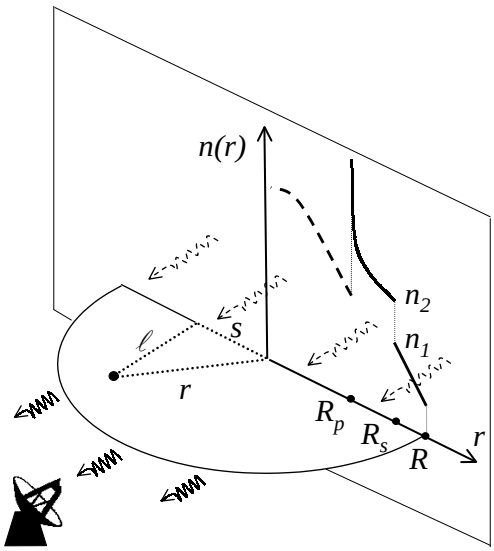

Fig. 4.19 The geometry underlying Eq. (4.34). For a point in the structure r is the radial coordinate, s is its projection on the plane of the sky, and ℓ is the coordinate along the line of sight. On the vertical axis we outline the initial density run, and the flow perturbed by the quasar-driven blastwave.

related angular sizes are around $0.5'$; with resolution fixed at $2\,\theta_b \approx 1'$, the signals will be diluted after $(R_v/d_A\,\theta_b)^2 \approx 1/4$ and scaled down to $\Delta T_\gamma \approx -20\,\mu$K.

Such resolutions will be achieved by several instruments now being built or designed, enabling "blind" sky surveys for SZ signals to μK sensitivities over tens of square degrees (see [33]). In particular, promising perspectives are offered by multi-beam, high frequency radio receivers like OCRA [28], and also by interferometers equipped with wide-band correlators like ATCA, SZA [91], AMI [95], and AMiBA [114]. These SZ enhancements may contribute equally or more than clusters to the excess power detected at high multipoles with BIMA [60] and possibly by CBI ([126]; see also discussion by [63]). In the (sub)millimetric band the SZ signal is positive, and will be accessible to large bolometric arrays like BOLOCAM [127]; these will develop into instruments enabling deep, wide surveys. Eventually, ALMA[2] will provide in selected areas higher resolution for both sides of the SZ effect.

The statistics of these enhanced SZ effects is evaluated on inserting the related blue luminosities $L = \Delta E/10\,f_\bullet\,t_{\rm dyn,gas}$ (with a bolometric correction 10) in the quasar luminosity function Eqs. (4.1). The result is given in the inset of Fig. 4.20 in terms of the cumulative fraction of bright galaxies hosting a type 1 quasar brighter than L. The same luminosity function interpreted in terms of interactions of the

[2]The Atacama Large Millimeter Array will be an interferometer composed of 64 12-meter antennas. It will be able to do imaging in all atmospheric windows between 10 mm and 350 microns, at arcsecond resolution (see also `http://www.alma.nrao.edu/`).

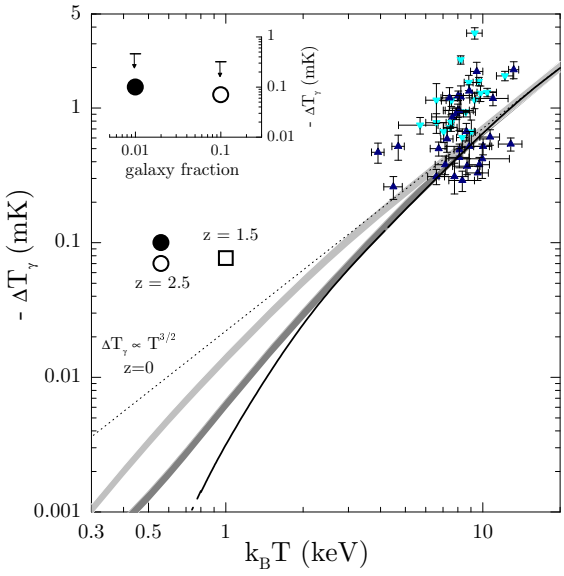

Fig. 4.20 Enhanced SZ effects from quasar feedback. See main text for details.

host galaxy with its group companions [40] yields a few signals per 10 poor groups, with the strength represented by the square in Fig. 4.20.

Detecting 10 such signals will require surveys over 500 arcmin^2 at $1'$ resolution, based on the surface density of 10^2 bright quasars/deg^2 consistent with Eq. (4.1). The candidate peaks are to be followed up with ALMA for higher resolutions; in addition, with optical redshifts, and optical velocities or X-ray temperatures that require current or moderately extrapolated techniques (cf. [170]).

If a galaxy happens to grow a large black hole in times shorter than $t_{\rm dyn}$, the quasar will inject an energy $\Delta E \gtrsim E$ impulsively; we expect this to hinder further accretion and cause the quasar to fade or quench. Such conditions correspond to our models with $\omega \to 2.5$, for which we find (see Table 4.1) strongly enhanced SZ signals during the subsequent transient (see the bars in the inset of Fig. 4.20), but also eventual ejection of a substantial gas fraction $\Delta m/m \to 1$. Then most galactic gas is blown away far outward R_v, so the star formation activity is likely to be terminated early, at $z \sim 2$; such may have been the case in some of the recently discovered EROs (see [3]; [50]).

Enhanced signals as discussed here would constitute *signatures* of strong feedback caught in the act. This is specific of quasars, since SNae feed back at most 0.3 keV per particle over many host dynamical times; on the other hand, extended cooling which depletes n without increasing T hardly could enhance $y \propto n\,T$. Interlopers might be introduced by merging events; however, these primarily govern the growth of the DM halos and set the virial T_v included in our baseline $y_{\rm grav} \propto T_v^{3/2}$.

Only an exceptional major merging may contribute an energy step sizeable but still bound by $\Delta E < E$. Even this produces transonic inflows in the high-T_v partner gas, originating limited warmer features as picked up by highly resolved X-ray studies of clusters. Still smoother inflows are produced by SN preheating (see [205]), while stronger blasts are driven by quasars, in the galaxies and groups that we propose here as primarily SZ objects.

Such signals can provide real time *evidence* of quasars feedback acting on the diffuse baryons in galaxies and groups. The evidence should be looked for primarily in the SZ surveys that will be soon available.

Conclusions

The Road goes ever on and on
Out from the door where it began.
Now far ahead the Road has gone,
Let others follow it who can!
Let them a journey new begin,
But I at last with weary feet
Will turn towards the lighted inn,
My evening-rest and sleep to meet.

- J.R.R. Tolkien: *The Lord of the Rings.* –

Galaxies and their groups and clusters are framed by a skeleton of dark matter particles, contributing in full to long-range gravity but little if anything to localized interactions; but they are also fleshed up by considerable amounts of baryons, which are instead sensitive to short range forces, namely, the weak, the strong, and the (screened) electromagnetic one.

Under the drive of its own *weak* gravity the dark matter clusters hierarchically and tends to produce closely scale-invariant structures of nearly universal shapes; on the contrary, the baryons are driven away from such a simple behavior by several non-adiabatic processes. In particular, they are substantially affected by the bunches of energy fed back when part of them condense under *strong* (self-)gravity. The latter cooperates with other fundamental interactions in the cores of massive stars that eventually explode as prompt, type II supernovae; but in its purest form it acts around the accreting supermassive black holes that are believed to energize the activity of quasars.

Such feedback actions from supernovae and quasars deplete the baryon density by causing thermal *outflow* and dynamical *blowout* from inside the structures; they also *preheat* the gas exterior to the newly forming systems, so hindering its further inflow. These effects are stronger in small structures with shallower gravitational

potential wells, where the nuclear outputs of the baryons compete with the dark matter gravity; the latter instead progressively prevails in larger and larger systems.

However, many details concerning this framework are still unclear, and hotly debated since the late 1980s. A crucial issue concerns how much of the energy discharged by supernovae or quasars actually couples to the ambient medium; conceivable values of the related coupling efficiency for the former sources are up to 50%, while for the latter ones the values are likely to be smaller, ranging from 1% up to 10%.

Whence our interest in probing the physics of the feedback from its overall effects on the baryons pervading galaxies, groups and clusters. To this purpose, in this Thesis we have developed (semi-)analytic modeling of the feedback actions from supernovae and quasars, and have computed their effects on various optical, X-ray and μwave/submm observables; we have also directly compared our findings with the most recent data, and provided specific predictions for future detectability.

The new (semi-)analytic techniques developed for this research, our original results and predictions are briefly summarized below.

• An energetically convenient way of feeding back energy is to preheat the baryons before their virialization in present-day structures, as smaller thermal inputs are required to bring a lower-density medium to a given entropy level.

We develop a semianalytic scheme to show how preheating increasingly modulates the accretion shocks toward smaller systems, to the effect of inducing lower baryon densities and higher entropy levels relative to a pure gravitationally-driven infall.

• Supernovae provide at most 1/4 keV per particle; this mild preheating is not enough to explain the observed X-ray scaling relations, neither in poor clusters nor in groups.

• Including the additional contribution of quasars yields a preheating level around 3/4 keV per particle, a value sufficient to explain the shape of the X-ray scaling relations down to poor clusters. However, the observations in groups and massive galaxies are only marginally fitted; in particular, the wide scatter in the X-ray luminosity vs. temperature correlation at the smaller scales is not accounted for.

Another intrinsic problem with the preheating scenario is that it tends to produce flat entropy profiles in groups; in fact, the latter are expected to have been built up mainly through weak accretion shocks, whereby the gas inflowed adiabatically. However, such a trend is at variance with the current observational evidence, which shows the entropy profiles to increase steeply outward.

• But in going from clusters toward groups and galaxies, the external preheating is progressively overwhelmed by the internal impact of quasar feedback. This consists of a blastwave sweeping throughout the ambient medium, eventually blowing some gas out of the structure. The related density depletions (hence luminosity suppressions) are stronger in groups than in clusters, since the gas is too tightly bound to be substantially ejected from the latter.

To describe this transient regime we have derived a new family of self-similar solutions of the Sedov type, which include dark matter gravity, a steep initial density gradient, and time-dependent energy discharge by the central source. We remark that, differently from the canonical self-similar solutions used to investigate, e.g., the evolution of SN remnants, our approach enables us to treat weak as well as strong internal shocks. This is mandatory to obtain realistic predictions, because the blast propagation is *constrained* by the coupling of the quasar outputs to the surrounding gas, and is *restrained* by initial gas pressure and dark matter gravity; so these blasts are only moderately supersonic even in poor groups or galaxies.

• We find the internal feedback by powerful quasars to eject appreciable gas amounts out of poor groups and massive galaxies so *depressing* the X-ray luminosities while *enhancing* the entropy levels and producing non-isentropic profiles.

We find the current X-ray data in groups and galaxies to require the diffuse baryons to absorb a fraction around 5% of the full energy discharged. Furthermore, we argue that variance of the actual quasar output or even of its coupling level may help to understand the intrinsic scatter shown by the data.

• On approaching the galactic scales no further density depletion takes place, because the internal feedback from quasars is self-regulated. In other words, the energy injection from the black hole cannot exceed by much the binding energy of the gas in the host, lest the energizing accretion is stopped. Pleasingly, with the same value of the coupling indicated by the X-ray data, such a limiting condition yields the steep $M_\bullet - \sigma$ correlation observed mainly in the optical band.

• Although constrained in such a way, the quasar feedback can produce considerably *enhanced* Sunyaev-Zel'dovich signals in and around early galaxies and groups; these arise during the blast transit as the gas is swept in an expanding shell, while its pressure is raised. Searching for such enhanced SZ signals requires either resolutions of order $0'.5$ (galaxies) and $1'$ (poor groups), or must live with some signal dilution. Detecting these signals is challenging at present, but will soon be feasible with large single-dish radiotelescopes equipped with the new multibeam technology, or with the upcoming generation of interferometers.

To sum up, we expect that quasar energy outputs coupled at levels around 5% leave two consistent *relics*: The depressed X-ray luminosities or enhanced entropies in local galaxies and groups; and the steep correlation between black hole masses and host velocity dispersions on subgalactic scales. Relatedly, on intermediate scales we predict *transient* Sunyaev-Zel'dovich signals standing out of a generally depressed landscape. The evidence for the latter should be looked for primarily in the Sunyaev-Zel'dovich surveys that will be soon available; resolved detections will catch the quasar feedback *in the act*, and will highlight its dominant contribution to the energy budget of cosmic baryons.

Bibliography

When I heard the learn'd astronomer,
When the proofs, the figures, were ranged in columns
before me,
When I was shown the charts and diagrams, to add,
divide, and measure them,
When I sitting heard the astronomer where he lectured
with much applause in the lecture-room,
How soon unaccountable I became tired and sick,
Till rising and gliding out I wander'd off by myself,
In the mystical moist night-air, and from time to time,
Looked up in perfect silence at the stars.

- Walt Whitman: *When I Heard the Learn'd Astronomer* –

[1] Abadi, M.G., Bower, R.G., and Navarro, J.F., *MNRAS* **314** (2000), 759.
[2] Aghanim, N., Balland, C., and Silk, J., *A&A* **357** (2000), 1.
[3] Alexander, D.M., Vignali, C., Bauer, F.E., Brandt, W.N., Hornschemeier, A.E., Garmire, G.P., and Schneider, D.P., *AJ* **123** (2002), 1149.
[4] Arnaud, M., and Evrard, A.E., *MNRAS* **305** (1999), 631.
[5] Babul, A., Balogh, M.L., Lewis, G.F., and Poole, G.B., *MNRAS* **330** (2002), 329.
[6] Balbi, A., Ade, P., Bock, J., Borrill, J., Boscaleri, A., De Bernardis, P., Ferreira, P.G., Hanany, S., Hristov, V., Jaffe, A.H., Lee, A.T., Oh, S., Pascale, E., Rabii, B., Richards, P.L., Smoot, G.F., Stompor, R., Winant, C.D., and Wu, J.H.P., *ApJ* **545** (2000), L1.
[7] Balogh, M.L., Babul, A., and Patton, D.R., *MNRAS* **307** (1999), 463.
[8] Balogh, M.L., Pearce, F., Bower, R., and Kay, S., *MNRAS* **326** (2001), 1228.
[9] Bardeen, J., Bond, J., Kaiser, N., and Szalay, A., *ApJ* **304** (1986), 15.
[10] Bennett, C. L., Halpern, M., Hinshaw, G., Jarosik, N., Kogut, A., Limon, M., Meyer, S.S., Page, L., Spergel, D.N., Tucker, G.S., Wollack, E., Wright, E.L., Barnes, C., Greason, M.R., Hill, R.S., Komatsu, E., Nolta, M.R., Odegard, N., Peirs, H.V., Verde, L., and Weiland, J.L., *ApJS* **148** (2003), 1.
[11] Bertschinger, E., *ApJS* **58** (1985), 39.

[12] Birkinshaw, M., *Phys. Rept.* **310** (1999), 97.
[13] Birkinshaw, M., in *Carnegie Observatories Astrophysics Series, Vol. 3: Clusters of Galaxies: Probes of Cosmological Structure and Galaxy Evolution* (2004, Cambridge: Cambridge Univ. Press).
[14] Blanchard, A., Valls-Gabaud, D., and Mamon, G. A., *A&A* **264** (1992), 365.
[15] Blandford, R.D., and Begelman, M.C., *MNRAS* **303** (1999), L1.
[16] Blanton, E.L., Sarazin, C.L., and McNamara, B.R., *ApJ* **585** (2003), 227.
[17] Bond, J. and Szalay, A., *ApJ* **276** (1983), 443.
[18] Bond, J., Cole, S., Efstathiou, G., and Kaiser, N., *ApJ* **379** (1991), 440.
[19] Borgani, S., Governato, F., Wadsley, J., Menci, N., Tozzi, P., Lake, G., Quinn, T., and Stadel, J., *ApJ* **559** (2001), L71.
[20] Borgani, S., Governato, F., Wadsley, J., Menci, N., Tozzi, P., Quinn, T., Stadel, J., and Lake, G. *MNRAS* **336** (2002), 409.
[21] Borgani, S., Murante, G., Springel, V., Diaferio, A., Dolag, K., Moscardini, L., Tormen, G., Tornatore, L., and Tozzi, P., *MNRAS* **348** (2004), 1078.
[22] Bower, R.G., *MNRAS* **248** (1991), 332.
[23] Bower, R.G., *MNRAS* **288** (1997), 355.
[24] Bower, R.G., Benson, A.J., Lacey C.G., Baugh, C.M., Cole, S., and Frenk, C.S. *MNRAS* **325** (2001), 497.
[25] Breitschwerdt, D., and Komossa, S., *Ap&SS* **272** (2000), 3.
[26] Bressan, A, Chiosi, C, and Fagotto, F., *ApJS* **94** (1994), 63.
[27] Brighenti, F., and Mathews, W.G., *ApJ* **553** (2001), 103.
[28] Browne, I.W., Mao, S., Wilkinson, P.N., Kus, A.J., Marecki, A., and Birkinshaw, M., *Proc. SPIE* **4015** (2000), 299.
[29] Bryan, G.L., and Norman, M.L., *ApJ* **495** (1998), 80.
[30] Bryan, G.L., *ApJ* **544** (2000), L1.
[31] Bullock, J.S., Kolatt, T.S., Sigad, Y., Somerville, R.S., Kravtsov, A.V., Klypin, A.A., Primack, J.R., and Dekel, A., *MNRAS* **321** (2001), 559.
[32] Caldwell, R.R., Kamionkowski, M., and Weinberg, N.N., *Phys. Rev. Lett.* **91** (2003), 071301.
[33] Carlstrom, J.E., Holder, G.P., and Reese, E.D., *ARA&A* **40** (2002), 643.
[34] Cavaliere, A., Gursky, H., and Tucker, W.A., *Nature* **231** (1971), 437.
[35] Cavaliere, A., and Fusco-Femiano, R., *A&A* **49** (1976), 137.
[36] Cavaliere, A., and Messina, A., *ApJ* **209** (1976), 424.
[37] Cavaliere, A., Menci, N., and Tozzi, P, *ApJ* **484** (1997), L21.
[38] Cavaliere, A., Menci, N., and Tozzi, P., *MNRAS* **308** (1999), 599.
[39] Cavaliere, A., Giacconi, R., and Menci, N., *ApJ* **528** (2000), L77.
[40] Cavaliere, A., and Vittorini, V., *ApJ* **543** (2000), 599.
[41] Cavaliere, A., and Menci, N., *MNRAS* **327** (2001), 488.
[42] Cavaliere, A., and Vittorini, V., *ApJ* **570** (2002), 114.
[43] Cavaliere, A., Lapi, A., and Menci, N., *ASP Conf. Ser.* **253** (2002), 407.
[44] Cavaliere, A., Lapi, A., and Menci, N., *ASP Conf. Ser.* **268** (2002), 240.
[45] Cavaliere, A., Lapi, A., and Menci, N., *ApJ* **581** (2002), L1.
[46] Cavaliere, A., Bardelli, S., Boschin, W., Lapi, A., and Tormen, G., *MemSAIt* **74** (2003), 335.
[47] Cen, R., and Ostriker, J.P., *ApJ* **519** (1999), L109.
[48] Cen, R., and Bryan, G.L., *ApJ* **546** (2001), L81.
[49] Chartas, G., Brandt, W.N., and Gallagher, S.C., *ApJ* **595** (2003), 85.
[50] Cimatti, A., Daddi, E., Mignoli, M., Pozzetti, L., Renzini, A., Zamorani, G., Broadhurst, T., Fontana, A., Saracco, P., Poli, F., Cristiani, S., D'Odorico, S., Giallongo,

E., Gilmozzi, R., and Menci, N., *A&A* **381** (2002), L68.
[51] Cole, S., and Kaiser, N., *MNRAS* **233** (1988), 637.
[52] Cole, S., Aragon-Salamanca, A., Frenk, C.S., Navarro, J.F., and Zepf, S.E, *MNRAS* **271** (1994), 781.
[53] Cole, S., and Lacey, C., *MNRAS* **281** (1996), 716.
[54] Cole, S., Lacey, C.G., Baugh, C.M., and Frenk, C.S., *MNRAS* **319** (2000), 168.
[55] Colless, M., Peterson, B.A., Jackson, C., Peacock, J.A., Cole, S., Norberg, P., Baldry, I.K., Baugh, C.M., Bland-Hawthorn, J., Bridges, T., Cannon, R., Collins, C., Couch, W., Cross, N., Dalton, G., De Propris, R., Driver, S.P., Efstathiou, G., Ellis, R.S., Frenk, C.S., Glazebrook, K., Lahav, O., Lewis, I., Lumsden, S., Maddox, S., Madgwick, D., Sutherland, W., and Taylor, K., see `http://babbage.sissa.it/html/astro-ph/0306581`.
[56] Croft, R.A.C., Di Matteo, T., Dave, R., Hernquist, L., Katz, N., Fardal, M.A., and Weinberg, D.H., *ApJ* **557** (2001), 67.
[57] Croom, S.M., Smith, R.J., Boyle, B.J., Shanks, T., Miller, L., Outram, P.J., and Loaring, N.S., *MNRAS* **349** (2004), 1397.
[58] Dave, R., Katz, N., and Weinberg, D.H., *ApJ* **579** (2002), 23.
[59] David, L.P., *ApJ* **484** (1997), L11.
[60] Dawson, K.S., Holzapfel, W.L., Carlstrom, J.E., Joy, M., LaRoque, S.J., Miller, A.D., and Nagai, D., *ApJ* **581** (2002), 86.
[61] de Bernardis, P., Ade, P.A.R., Bock, J.J., Bond, J.R., Borrill, J., Boscaleri, A., Coble, K., Crill, B.P., De Gasperis, G., Farese, P.C., Ferreira, P.G., Ganga, K., Giacometti, M., Hivon, E., Hristov, V.V., Iacoangeli, A., Jaffe, A.H., Lange, A.E., Martinis, L., Masi, S., Mason, P.V., Mauskopf, P.D., Melchiorri, A., Miglio, L., Montroy, T., Netterfield, C.B., Pascale, E., Piacentini, F., Pogosyan, D., Prunet, S., Rao, S., Romeo, G., Ruhl, J.E., Scaramuzzi, F., Sforna, D., and Vittorio, N., *Nature* **404** (2000), 955.
[62] De Grandi, S., and Molendi, S., *ApJ* **567** (2002), 163.
[63] De Zotti, G., Burigana, C., Cavaliere, A., Danese, L., Granato, G.L., Lapi, A., Platania, P., and Silva, L., *AIP Conf. Proc.* **703** (2004), 375.
[64] Donahue, M., in *The Riddle of Cooling Flows in Galaxies and Clusters of Galaxies* (2003, see `http://www.astro.virginia.edu/coolflow/`)
[65] Dos Santos, S., and Doré, O., *A&A* **383** (2002), 450.
[66] Edge, A.C., and Stuart, G.C., *MNRAS* **252** (1991), 428.
[67] Efstathiou, G., *MNRAS* **317** (2000), 697.
[68] Efstathiou, G., *MNRAS* **343** (2003), L95.
[69] Eke, V.R., Cole, S., and Frenk, C.S., *MNRAS* **282** (1996), 263.
[70] Ettori, S., and Fabian, A.C., *MNRAS* **305** (1999), 834.
[71] Fabian, A.C., *ARA&A* **32** (1994), 277.
[72] Fabian, A.C., *AIP Conf. Proc.* **599** (2001), 93
[73] Fabian, A.C., Wilman, R.J., and Crawford, C.S., *MNRAS* **329** (2002), L18.
[74] Fabian, A.C., in *Carnegie Observatories Astrophysics Series, Vol. 1: Coevolution of Black Holes and Galaxies* (2004, Cambridge: Cambridge Univ. Press).
[75] Fan, X., Strauss, M.A., Schneider, D.P., Gunn, J.E., L., Robert, H., Becker, R.H., Davis, M., Newman, J.A., Richards, G.T., White, R.L., Anderson, J.E. Jr., Annis, J., Bahcall, N.A., Brunner, R.J., Csabai, I., Hennessy, G.S., Hindsley, R.B., Fukugita, M., Kunszt, P.Z., Ivezic, Z., Knapp, G.R., McKay, T.A., Munn, J.A., Pier, J.R., Szalay, A.S., and York, D.G., *AJ* **121** (2001), 54.
[76] Fan, X., Strauss, M.A., Schneider, D.P., Becker, R.H., White, R.L., Haiman, Z., Gregg, M., Pentericci, L., Grebel, E.K., Narayanan, V.K., Loh, Y.-S., Richards, G.T., Gunn,

J.E., Lupton, R.H., Knapp, G.R., Ivezic, Z., Brandt, W.N., Collinge, M., Hao, L., Harbeck, D., Prada, F., Schaye, J., Strateva, I., Zakamska, N., Anderson, S., Brinkmann, J., Bahcall, N.A., Lamb, D.Q., Okamura, S., Szalay, A., and York, D.G., *AJ* **125** (2003), 1649.

[77] Ferrarese, L., and Merritt, D., *ApJ* **539** (2000), L9.

[78] Ferrarese, L., *ApJ* **578** (2002), 90.

[79] Franceschini, A., Hasinger, G., Miyaji, T., and Malquori, D., *MNRAS* **310** (1999), L5.

[80] Freedman, W.L., Madore, B.F., Gibson, B.K., Ferrarese, L., Kelson D.D., Sakai, S., Mould, J.R., Kennicutt, R.C., Ford, H.C., Graham, J.A., Huchra, J.P., Hughes, S.M.G., Illingworth, G.D., Macri, L.M., and Stetson, P.B., *ApJ* **553** (2001), 47.

[81] Frenk, C.S., White, S.D.M., Bode, P., Bond, J.R., Bryan, G.L., Cen, R., Couchman, H.M.P., Evrard, A.E., Gnedin, N., Jenkins, A., Khokhlov, A.M., Klypin, A., Navarro, J.F., Norman, M.L., Ostriker, J.P., Owen, J.M., Pearce, F.R., Pen, U.-L., Steinmetz, M., Thomas, P.A., Villumsen, J.V., Wadsley, J.W., Warren, M.S., Xu, G., and Yepes, G., *ApJ* **525** (1999), 554.

[82] Gebhardt, K., Bender, R., Bower, G., Dressler, A., Faber, S.M., Filippenko, A.V., Green, R., Grillmair, C., Ho, L.C., Kormendy, J., Lauer, T.R., Magorrian, J., Pinkney, J., Richstone, D., and Tremaine, S., *ApJ* **539** (2000), L13.

[83] Gheller, M., Pantano, O., and Moscardini, L., *MNRAS* **296** (1998), 85.

[84] Ghigna, S., Moore, B., Governato, F., Lake, G., Quinn, T., and Stadel, J., *ApJ* **544** (2000), 616.

[85]Granato, G.L., De Zotti, G., Silva, L., Bressan, A., and Danese, L. *ApJ* **600** (2004), 580.

[86] Haehnelt, M.G., and Rees, M.J., *MNRAS* **263** (1993), 168.

[87] Hardcastle, M.J., Worrall, D.M., Kraft, R.P., Forman, W.R., Jones, C., and Murray, S.S., *ApJ* **593** (2003), 169.

[88] Hawking, S., and Penrose, R., *The Nature of Space and Time* (1996, Princeton: Princeton Univ. Press)

[89] Heckman, T.M., *ASP Conf. Ser.* **254** (2002), 292.

[90] Helsdon, S.F., and Ponman, T.J., *MNRAS* **315** (2000), 356.

[91] Holder, G.P., Mohr, J.J., Carlstrom, J.E., Evrard, A.E., and Leitch, E.M., *ApJ* **544** (2000), 629.

[92] Horner, D.J., 2005, in prep. (see also Horner, D.J., 2001, Ph.D. Thesis, Univ. of Maryland).

[93] Jenkins, A., Frenk, C.S., White, S.D.M., Colberg, J.M., Cole, S., Evrard, A.E., Couchman, H.M.P., and Yoshida, N., *MNRAS* **321** (2001), 372.

[94] Jones, C., and Forman, W., *ApJ* **276** (1984), 38.

[95] Jones, M.E., *ASP Conf. Ser.* **257** (2002), 35.

[96] Kaiser, N., *MNRAS* **222** (1986), 323.

[97] Kaiser, N., *ApJ* **383** (1991), 104.

[98] Kauffmann, G., White, S.D.M., and Guiderdoni, B., *MNRAS* **264** (1993), 201.

[99] King, A.R., *ApJ* **596** (2003), L27.

[100] Kitayama, T. and Suto, Y., *ApJ* **469** (1996), 480.

[101] Knight, P.A., and Ponman, T.J., *MNRAS* **289** (1997), 955.

[102] Knop, R.A., Aldering, G., Amanullah, R., Astier, P., Blanc, G., Burns, M.S., Conley, A., Deustua, S.E., Doi, M., Ellis, R., Fabbro, S., Folatelli, G., Fruchter, A.S., Garavini, G., Garmond, S., Garton, K., Gibbons, R., Goldhaber, G., Goobar, A., Groom, D. E., Hardin, D., Hook, I., Howell, D.A., Kim, A.G., Lee, B. C., Lidman, C., Mendez, J., Nobili, S., Nugent, P.E., Pain, R., Panagia, N., Pennypacker, C.R.,

Perlmutter, S., Quimby, R., Raux, J., Regnault, N., Ruiz-Lapuente, P., Sainton, G., Schaefer, B., Schahmaneche, K., Smith, E., Spadafora, A.L., Stanishev, V., Sullivan, M., Walton, N.A., Wang, L., Wood-Vasey, W.M., and Yasuda, N., *ApJ* **598** (2003), 102.

[103] Kravtsov, A.V., and Yepes, G., *MNRAS* **318** (2000), 227.

[104] Lacey, C. and Cole, S., *MNRAS* **262** (1993), 627.

[105] Lahav, O., Rees, M.J., Lilje, P.B., and Primack, J.R., *MNRAS* **251** (1991), 128.

[106] Landau, L.D., and Lifshitz, E.M., *Fluid Mechanics* (1959, London: Pergamon Press).

[107] Lapi, A., Cavaliere, A., and De Zotti, G., *ApJ* **597** (2003), L93.

[108] Lapi, A., Cavaliere, A., De Zotti, G., and Menci, N., in *Carnegie Observatories Astrophysics Series, Vol. 3: Clusters of Galaxies: Probes of Cosmological Structure and Galaxy Evolution* (2004, see `http://www.ociw.edu/ociw/symposia/series/symposium3/ proceedings.htm/`).

[109] Lapi, A., Cavaliere, A., and De Zotti, G., *AIP Conf. Proc.* **703** (2004), 355.

[110] Lapi, A., Cavaliere, A., and Menci, N., *ApJ* **619** (2005), 60.

[111] Liddle, A.R., Lyth, D.H., Viana, P.T.P., and White, M., *MNRAS* **282** (1996), 281.

[112] Lin, Y.-T., Mohr, J.J., and Stanford, S.A., *ApJ* **591** (2003), 749.

[113] Lloyd-Davies, E.J., Ponman, T.J., and Cannon, D.B., *MNRAS* **315** (2000), 689.

[114] Lo, K.Y., *ASP Conf. Ser.* **257** (2002), 3.

[115] Lokas, E.L., and Mamon, G.A., *MNRAS* **321** (2001), 155.

[116] Luminet, J.-P., Weeks, J., Riazuelo, A., Lehoucq, R., and Uzan, J.-P., *Nature* **425** (2003), 593.

[117] Lupini, F., 1996, Master Thesis, Univ. of Rome "Tor Vergata".

[118] Lynden-Bell, D., *Nature* **223** (1969), 690.

[119] Madau, P., Ferrara, A., and Rees, M.J., *ApJ* **555** (2001), 92.

[120] Mahdavi, A., Boehringer, H., Geller, M.J., and Ramella, M., *ApJ* **483** (1997), 68.

[121] Makino, N., Sasaki, S., and Suto, Y., *ApJ* **497** (1998), 555.

[122] Marconi, A., Risaliti, G., Gilli, R., Hunt, L.K., Maiolino, R., and Salvati, M., *MNRAS* **351** (2004), 169.

[123] Markevitch, M.L., Sarazin, C.L., and Henriksen, M.J., in *X-Ray Imaging and Spectroscopy of Cosmic Hot Plasmas* (1997, Tokio: Univ. Acad. Press), 91.

[124] Markevitch, M., *ApJ* **504** (1998), 27.

[125] Markevitch, M., Gonzalez, A.H., David, L., Vikhlinin, A., Murray, S., Forman, W., Jones, C., and Tucker, W., *ApJ* **567** (2002), L27.

[126] Mason, B.S., Pearson, T.J., Readhead, A.C.S., Shepherd, M.C., Sievers, J., Udomprasert, P.S., Cartwright, J.K., Farmer, A.J., Padin, S., Myers, S.T., Bond, J.R., Contaldi, C.R., Pen, U., Prunet, S., Pogosyan, D., Carlstrom, J.E., Kovac, J., Leitch, E.M., Pryke, C., Halverson, N.W., Holzapfel, W.L., Altamirano, P., Bronfman, L., Casassus, S., May, J., and Joy, M., *ApJ* **591** (2003), 540.

[127] Mauskopf, P., Ade, P., Bock, J., Edgington, S., Golwala, S., Goldin, A., Glenn, J., Haig, D., Hristov, V., Knowles, B., Lange, A., Nguyen, H., and Rownd, B., *AIP Conf. Proc.* **616** (2002), 107.

[128] McNamara, B.R., Wise, M.W., Nulsen, P.E.J., David, L.P., Carilli, C.L., Sarazin, C.L., O'Dea, C.P., Houck, J., Donahue, M., Baum, S., Voit, M., O'Connell, R.W., and Koekemoer, A., *ApJ* **562** (2001), L149.

[129] Menci, N., and Cavaliere, A., *MNRAS* **311** (2000), 50.

[130] Menci, N., Cavaliere, A., and Lapi, A., in *Dark Matter in Astro- and Particle Physics* (2002, Berlin: Springer), 53.

[131] Menci, N., Cavaliere, A., Fontana, A., Giallongo, E., Poli, F., and Vittorini, V., *ApJ* **604** (2004), 12.

[132] Miller, K.A., and Stone, J.M., *ApJ* **562** (2000), 398.
[133] Mo, H.J., Mao, S., and White, S.D.M., *MNRAS* **295** (1998), 319.
[134] Muanwong, O., Thomas, P.A., Kay, S.T., and Pearce, F.R., *MNRAS* **336** (2002), 527.
[135] Mushotzky, R.F., in *Carnegie Observatories Astrophysics Series, Vol. 3: Clusters of Galaxies: Probes of Cosmological Structure and Galaxy Evolution* (2004, Cambridge: Cambridge Univ. Press).
[136] Nakamura, T. and Suto, Y., *Prog. Theor. Phys.* **97** (1997), 49.
[137] Nath, B.B., and Roychowdhury, S., *MNRAS* **333** (2002), 145.
[138] Navarro, J.F., Frenk, C.S., and White, S.D.M., *ApJ* **490** (1997), 493.
[139] Oey, M.S., Clarke, C.J., and Massey, P., in *The Magellanic Clouds and Other Dwarf Galaxies* (2001, Aachen: Shaker Verlag), 181.
[140] Ogle, P.M., Brookings, T., Canizares, C.R., Lee, J.C., and Marshall, H.L., *A&A* **402** (2003), 849.
[141] Oh, S.P., and Benson, A.J., *MNRAS* **342** (2003), 664.
[142] Osmond, J.P.F., and Ponman, T.J., *MNRAS* **350** (2004), 1511.
[143] Ostriker, J.P., and McKee, C.F., *Rev. Mod. Phys.* **60** (1988), 1.
[144] O'Sullivan, E., Ponman, T.J., and Collins, R.S, *MNRAS* **340** (2003), 1375.
[145] Padmanabhan, T., *Structure Formation in the Universe* (1992, Cambridge: Cambridge Univ. Press).
[146] Padmanabhan, T., *Theoretical Astrophysics* **Vol. III** (2003, Cambridge: Cambridge Univ. Press).
[147] Parker, E.N., *Interplanetary Dynamical Processes* (1963, New York: Wiley).
[148] Peacock, J.A., *Cosmological Physics* (1999, Cambridge: Cambridge Univ. Press).
[149] Pearce, F.R., Thomas, P.A., Couchmanm H.M.P., and Edge, A.C., *MNRAS* **317** (2000), 1029.
[150] Peebles, P.J.E., *The Large-Scale Structure of the Universe* (1980, Princeton: Princeton Univ. Press).
[151] Peebles, P.J.E., *Principles of Physical Cosmology* (1993, Princeton: Princeton Univ. Press).
[152] Perlmutter, S., Aldering, G., Goldhaber, G., Knop, R.A., Nugent, P., Castro, P.G., Deustua, S., Fabbro, S., Goobar, A., Groom, D.E., Hook, I.M., Kim, A.G., Kim, M.Y., Lee, J.C., Nunes, N.J., Pain, R., Pennypacker, C.R., Quimby, R., Lidman, C., Ellis, R.S., Irwin, M., McMahon, R.G., Ruiz-Lapuente, P., Walton, N., Schaefer, B., Boyle, B.J., Filippenko, A.V., Matheson, T., Fruchter, A.S., Panagia, N., Newberg, H.J.M., Couch, W.J., and The Supernova Cosmology Project, *ApJ* **517** (1999), 565.
[153] Pettini, M., Shapley, A.E., Steidel, C.C., Cuby, J.G., Dickinson, M., Moorwood, A.F.M., Adelberger, K.L., and Giavalisco, M., *ApJ* **554** (2001), 981.
[154] Pipino, A., Matteucci, F., Borgani, S., and Biviano, A., *NewA* **7** (2002), 227.
[155] Platania, P., Burigana, C., De Zotti, G., Lazzaro, E., and Bersanelli, M., *MNRAS* **337** (2002), 242.
[156] Ponman, T.J., Cannon, D.B., and Navarro, J.F., *Nature* **397** (1999), 135.
[157] Ponman, T.J., Sanderson, A.J.R., and Finoguenov, A., *MNRAS* **343** (2003), 331.
[158] Pounds, K.A., King, A.R., Page, K.L., and O'Brien, P.T., *MNRAS* **346** (2003), 1025.
[159] Pratt, G.W. and Arnaud, M., *A&A* **408** (2003), 1.
[160] Press, W. and Schechter, P., *ApJ* **187** (1974), 425.
[161] Press, W.H., Flannery, B.P., Teukolsky, S.A., and Vetterling, W.T., *Numerical Recipies in Fortran 77* (1992, Cambridge: Cambridge Univ. Press).
[162] Rasmussen, J, and Ponman, T.J., *MNRAS* **349** (2004), 722.
[163] Reese, E.D., Carlstrom, J.E., Joy, M., Mohr, J.J., Grego, L., and Holzapfel, W.L.,

ApJ **581** (2002), 53.
[164] Reeves, J.N., O'Brien, P.T., and Ward, M.J., *ApJ* **593** (2003), 65.
[165] Reimers, D., Baade, R., Hagen, H.-J., and Lopez, S., *A&A* **374** (2001), 871.
[166] Rephaeli, Y., *ARA&A* **33** (1995), 541.
[167] Richstone, D., Ajhar, E.A., Bender, R., Bower, G., Dressler, A., Faber, S.M., Filippenko, A.V., Gebhardt, K., Green, R., Ho, L.C., Kormendy, J., Lauer, T.R., Magorrian, J., and Tremaine, S., *Nature* **395** (1998), A14.
[168] Riess, A.G., Filippenko, A.V., Challis, P., Clocchiatti, A., Diercks, A., Garnavich, P.M., Gilliland, R.L., Hogan, C.J., Jha, S., Kirshner, R.P., Leibundgut, B., Phillips, M.M., Reiss, D., Schmidt, B.P., Schommer, R.A., Smith, R.C., Spyromilio, J., Stubbs, C., Suntzeff, N.B., and Tonry, J., *AJ* **116** (1998), 1009.
[169] Roettiger, K., Stone, J.M, and Mushotzky, R.F, *ApJ* **493** (1998), 62.
[170] Rosati, P., Borgani, S., and Norman, C., *ARA&A* **40** (2002), 539.
[171] Roussel, H., Sadat, R., and Blanchard, A., *A&A* **361** (2000), 429.
[172] Roychowdhury, S., Ruszkowski, M, Nath. B.B., and Begelman, M.C., *ApJ* **615** (2004), 681.
[173] Rybicki, G.B., and Lightman, A.P., *Radiative Processes in Astrophysics* (1979, New York: Wiley).
[174] Sanderson, A.J.R., and Ponman, T.J., *MNRAS* **345** (2003), 1241.
[175] Sarazin, C.L., *X-ray Emission from Clusters of Galaxies* (1988, Cambridge: Cambridge Univ. Press).
[176] Scannapieco, E., and Oh, S.P., *ApJ* **608** (2004), 62.
[177] Sedov, L.I., *Similarity and Dimensional Methods in Mechanics* (1959, London: Academic Press).
[178] Sheth, R.K., Mo, H.J., and Tormen, G., *MNRAS* **323** (2001), 1.
[179] Sheth, R.K., and Tormen, G., *MNRAS* **329** (2002), 61.
[180] Shields, G.A., Gebhardt, K., Salviander, S., Willis, B.J., Xie, B., Brotherton, M.S., Yuan, J., and Dietrich, M., *ApJ* **583** (2003), 124.
[181] Siemiginowska, A., Smith, R.K., Aldcroft, T.L., Schwartz, D.A., Paerels, F., Petric, A.O., *ApJ* **598** (2003), L15.
[182] Silk, J., and Rees, M.J., *A&A* **331** (1998), 1.
[183] Silk, J., *MNRAS* **343** (2003), 249.
[184] Somerville, R.S., and Primack, J.R., *MNRAS* **310** (1999), 1087.
[185] Spergel, D.N., Verde, L., Peiris, H.V., Komatsu, E., Nolta, M.R., Bennett, C.L., Halpern, M., Hinshaw, G., Jarosik, N., Kogut, A., Limon, M., Meyer, S.S., Page, L., Tucker, G.S., Weiland, J.L., Wollack, E., and Wright, E.L., *ApJS* **148** (2003), 175.
[186] Sugiyama, N., *ApJS* **100** (1995), 281.
[187] Sunyaev, R.A., and Zel'dovich, Ya.B., *Comm. Astroph. Sp. Sc.* **4** (1972), 173.
[188] Sunyaev, R.A., and Zel'dovich, Ya.B., *ARA&A* **18** (1980), 537.
[189] Sutherland, R., and Dopita, M.A., *ApJS* **88** (1993), 253.
[190] Takizawa, M., and Mineshige, S., *ApJ* **499** (1998), 82.
[191] Terashima, Y., and Wilson, A.S., *ApJ* **560**, 139.
[192] Thornton, K., Gaudlitz, M., Janka, H.Th., and Steinmetz, M., *ApJ* **500** (1998), 95.
[193] Tormen, G., Moscardini, L., and Yoshida, N., *MNRAS* **350** (2004), 1397.
[194] Tornatore, L., Borgani, S., Springel, V., Matteucci, F., Menci, N., and Murante, G., *MNRAS* **342** (2003), 1025.
[195] Tozzi, P., and Norman, C., *ApJ* **546** (2001), 63.
[196] Tozzi, P., *ASP Conf. Ser.* **268** (2002), 248.
[197] Tremaine, S., Gebhardt, K., Bender, R., Bower, G., Dressler, A., Faber, S.M., Filippenko, A.V., Green, R., Grillmair, C., Ho, L.C., Kormendy, J., Lauer, T.R., Magor-

rian, J., Pinkney, J., and Richstone, D., *ApJ* **574** (2002), 740.
[198] Tripp, T.M., Giroux, M.L., Stocke, J.T., Tumlinson, J., and Oegerle, W.R., *ApJ* **563** (2001), 724.
[199] Umemura, M., in *Carnegie Observatories Astrophysics Series, Vol. 1: Coevolution of Black Holes and Galaxies* (2004, Cambridge: Cambridge Univ. Press).
[200] Urry, C.M., and Padovani, P., *PASP* **107** (1995), 803.
[201] Valageas, P., and Silk, S., *A&A* **350** (1999), 725.
[202] Valageas, P., Schaeffer, R., and Silk, J., *A&A* **388** (2002), 741.
[203] Voit, G.M., and Bryan, G.L., *Nature* **414** (2001), 425.
[204] Voit, G.M., Bryan, G.L., Balogh, M.L., and Bower, R.G., *ApJ* **576** (2002), 601.
[205] Voit, G.M., Balogh, M.L., Bower, G.B., Lacey, C.G., and Bryan, G.L., *ApJ* **593** (2003), 272.
[206] Weinberg, S., *Gravitation and Cosmology* (1972, New York: Wiley).
[207] White, S.D.M., and Rees, M.J., *MNRAS* **183** (1978), 341.
[208] White, S.D.M., and Frenk, C.S., *ApJ* **379** (1991), 52.
[209] White, S.D.M., and Fabian, A.C., *MNRAS* **273** (1995), 72.
[210] Wu, K.K.S., Fabian, A.C., and Nulsen, P.E.J., *MNRAS* **318** (2000), 889.
[211] Wu, X.-P., and Xue, Y.-J., *ApJ* **572** (2002), 19.
[212] Wyithe, J.S.B., and Loeb, A., *ApJ* **595** (2003), 614.
[213] Yamada, M., and Fujita, Y., *ApJ* **553** (2001), L145.
[214] Young, A.J., Wilson, A.S., and Mundell, C.G., *ApJ* **579** (2002), 560.
[215] Zhang, T., and Wu, X., *ApJ* **545** (2000), 141.

Appendix

Numerical constants

Pi	$\pi = 3.1415927$
Euler number	$e = 2.7182818$
Arcsecond	$1'' = 4.8481 \times 10^{-6}$ rad

Physical constants[3]

Speed of light	$c = 2.99792458 \times 10^{10}$ cm s^{-1}
Gravitational constant	$G = 6.67259 \times 10^{-8}$ cm^3 g^{-1} s^{-2}
Planck's constant	$h = 6.6260755 \times 10^{-27}$ erg s
	$\hbar = h/2\pi = 1.05457266 \times 10^{-27}$ erg s
Electron volt	1 eV $= 1.6021772 \times 10^{-12}$ erg
Electron charge	$e = 4.8032068 \times 10^{-10}$ e.s.u.
Electron mass	$m_e = 9.1093897 \times 10^{-28}$ g
Proton mass	$m_p = 1.6727231 \times 10^{-24}$ g
Boltzmann constant	$k_B = 1.380658 \times 10^{-16}$ erg K^{-1}
Thomson cross-section	$\sigma_T = 6.652453 \times 10^{-25}$ cm^2
Stefan-Boltzmann constant	$\sigma = 5.67051 \times 10^{-5}$ erg cm^{-2} K^{-4} s^{-1}
Avogadro's number	$N_A = 6.0221367 \times 10^{23}$
Fine structure constant	$\alpha = 7.29735308 \times 10^{-3}$

[3] Taken from the American National Institute of Standards and Technology, see `http://physics.nist.gov/cuu/index.html`

Astronomical constants

Sidereal year	$1\ \mathrm{yr} = 3.155815 \times 10^7\ \mathrm{s}$
Astronomical unit	$1\ \mathrm{a.u.} = 1.49599 \times 10^{13}\ \mathrm{cm}$
Light year	$1\ \mathrm{l.y.} = 9.4605 \times 10^{17}\ \mathrm{cm}$
Parsec	$1\ \mathrm{pc} = 3.2615\ \mathrm{l.y.} = 3.0856 \times 10^{18}\ \mathrm{cm}$
Solar mass	$M_\odot = 1.989 \times 10^{33}\ \mathrm{g}$
Solar radius	$R_\odot = 6.9598 \times 10^{10}\ \mathrm{cm}$
Solar luminosity	$L_\odot = 3.85 \times 10^{33}\ \mathrm{erg\ s^{-1}}$
Luminosity (L) vs. absolute magnitude (M)	$L = 3.02 \times 10^{35}\ \mathrm{erg\ s^{-1}} \times 10^{-2\,M/5}$
Flux (F) vs. apparent magnitude (m)	$F = 2.52 \times 10^{-5}\ \mathrm{erg\ s^{-1}\ cm^{-2}} \times 10^{-2\,m/5}$

Notation

Defined as	$\equiv$
Equal to	$=$
Approximately equal to	$\approx$
Of order	$\sim$
Proportional to	$\propto$
Different from	$\neq$
Equal up to higher order corrections	$\simeq$
Less than	$<$
Less or equal to	$\leq$
Slightly less than	$\lesssim$
Much less than	$\ll$
Greater than	$>$
Greater or equal to	$\geq$
Slightly greater than	$\gtrsim$
Much greater than	$\gg$
Ranging between	$\div$
Asymptotically equal to	$\rightarrow$
For each	$\forall$
Belonging to	ϵ
Infinity	∞

Index